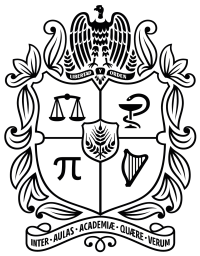

UNIVERSIDAD
NACIONAL
DE COLOMBIA
SEDE MANIZALES

Data-driven modelling of micro and ultra - filtration processes

Luis Humberto López Murillo

Tesis para optar al título de:
Magister en Ingeniería-Ingeniería Química
Director:
Ph.D Oscar Andrés Prado Rubio

Co-director:
Ph.D Víctor Hugo Grisales Díaz

Grupo de Investigación:
Grupo de Investigación en Aplicación de Nuevas Tecnologías
(GIANT)

Universidad Nacional de Colombia
Facultad de Ingeniería y Arquitectura, Departamento de Ingeniería Química
Manizales, Colombia
2022

Lo más importante en la vida es la paz interior, cuídala y protégela como el tesoro más preciado. Ella será tu alegría en todo momento. Ella te guiará por caminos seguros y te aconsejará lo mejor en momentos difíciles. Su presencia es apenas perceptible, pero su ausencia es devastadora. Ella es lo mejor que podrías desear y lo que siempre quisieras tener. Por eso, si quieres vivir contento y dichoso, a ella servirás y para ella vivirás. Por ella lo harás todo y con ella todo lo harás. Que todas tus decisiones sirvan a tu alegría. Aunque te tome tiempo, haz el esfuerzo de pensar: ¿Qué te gratifica más?

Luis H.

"¿Te parece prudente aumentar el ya crecido número de los malos, de los que poco realmente positivo puedes esperar, y desanimar a la minoría de los mejores, que en cambio tanto pueden hacer por tu buena vida? ¿No es más lógico sembrar lo que intentas cosechar en lugar de lo opuesto, aun a sabiendas de que la cizaña puede estropear tu cosecha? ¿Prefieres portarte voluntariamente al modo de tanto loco como hay suelto, en lugar de defender y mostrar las ventajas de la cordura?"

Marco Aurelio

Agradecimientos

Quisiera agradecer a mis padres por el apoyo que me han brindado para llevar a cabo todas mis metas académicas y personales. A mis amigas Laura Andrea Villada Atehortúa y Melissa De La Pava Rodríguez, y a mis amigos Deiber Javier Serna Castaño y Jorge Luis Betancur Bermúdez pues su compañía hizo amena mi existencia durante las extenuantes jornadas de estudio y trabajo. Por último quisiera agradecer a todos mis compañeros de maestría pues me ayudaron a disfrutar de la vida pese a las circunstancias adversas que podamos estar experimentando.

Finalmente quisiera agradecer a mi director de tesis Óscar Andrés Prado Rubio por sus frecuentes enseñanzas sobre la vida y su apoyo emocional a lo largo de nuestra amistad. Además considero en extremo valiosa su influencia en mi formación académica caracterizada por seguir el rigor científico y el análisis exhaustivo de las observaciones realizadas en el transcurso de una investigación.

Content

Modelamiento basado en datos de procesos de micro y ultra - filtración

Resumen

Los procesos de microfiltración (MF) y ultrafiltración (UF) se utilizan ampliamente en varios campos industriales y de investigación, y han surgido diferentes empresas para desarrollar mejoras y nuevos diseños de dichas tecnologías. Sin embargo, algunos inconvenientes relacionados con la operación del proceso, a saber, la polarización de la concentración y el ensuciamiento, impiden que el uso de las membranas se extienda en todos los sectores industriales. La polarización de la concentración y el ensuciamiento son los principales problemas en MF y UF que deben gestionarse para diseñar un proceso de separación. Las estrategias de operación dinámica se utilizan para mitigar los efectos adversos de la polarización y el ensuciamiento y mejorar el rendimiento de la separación. No obstante, existe un equilibrio entre las condiciones operativas para alcanzar los efectos deseados. En esta investigación, se desarrollan y ajustan dos modelos matemáticos híbridos para representar los fenómenos de polarización de la concentración en la UF dinámica de dextrano T500. Dichos modelos arrojan un coeficiente de determinación ajustado de 0.9185 y 0.9626, respectivamente, y pueden predecir la concentración en la superficie de la membrana, el flujo y el rechazo observado. Los resultados muestran el efecto intensificador de la operación dinámica al disminuir el MWCO de la membrana hasta 74 veces sin reducir el flujo. Los datos experimentales de la literatura y los modelos híbridos desarrollados en este documento brindan información sobre el sistema para el diseño de sistemas de membrana donde la selectividad se puede mejorar y ajustar de acuerdo con las condiciones operativas en lugar del tamaño de poro de la membrana. El mejor modelo matemático híbrido se utiliza para explorar el sistema de UF en funcionamiento dinámico en diferentes escenarios con el objetivo de proporcionar una mayor comprensión del sistema. Con este enfoque, se realiza un análisis de sensibilidad para evaluar el desempeño de la separación en términos de flujo y factor de rechazo en función de las variables de entrada: duración del backshock (BS), tiempo entre backshocks (TBBS) y concentración de dextrano (Cb). El análisis de sensibilidad permite encontrar regiones operativas donde se pueden lograr flujos elevados manteniendo un factor de rechazo aceptable. Con el objetivo de resaltar las ventajas de aplicar la operación dinámica en lugar de la filtración convencional, se realiza un análisis comparativo entre una membrana con bajo MWCO en operación convencional de flujo cruzado y una membrana con alto MWCO en operación

dinámica. El efecto de la polarización de la concentración se analiza y explica mediante el módulo de polarización. Este módulo se define como la relación entre la concentración en la superficie de la membrana y la concentración en el seno del fluido. Valores tan altos como 160 para este módulo tienen un impacto negativo en la selectividad, mientras que valores cercanos o inferiores a 34 mejoran la separación. El flujo medio puede aumentarse hasta un 43,8 % con BS = 1 s y TBBS = 5 s. Con respecto al análisis comparativo, los ahorros en costos de membrana alcanzan valores en torno al 50 % al operar una membrana de alto MWCO en condiciones dinámicas. El modelado matemático en ultrafiltración dinámica es una herramienta clave, desde la perspectiva de la ingeniería de sistemas de procesos, para evaluar el rendimiento de la separación en diferentes condiciones operativas. El modelo matemático híbrido desarrollado en esta investigación permite la optimización de la operación a través del análisis de sensibilidad y permite diseñar el proceso de separación dado un objetivo de concentración definido, en el contexto de la ultrafiltración de dextrano.

Palabras clave: Ultrafiltración dinámica, intensificación de membranas, MWCO, modelamiento híbrido.

Data-driven modelling of micro and ultra - filtration processes

Summary

The microfiltration (MF) and ultrafiltration (UF) processes are widely used in several industrial and research fields, and different enterprises have emerged to develop enhancements and new designs of such technologies. Nevertheless, some drawbacks related to process operation, namely concentration polarization and fouling, keep membranes from spreading in all industrial sectors.

Concentration polarization and fouling are the main problems in MF and UF to be managed in order to design a separation process. Dynamic operation strategies are used to mitigate adverse effects of polarization and fouling and improve the separation performance. Nevertheless, there is a balance among the operational conditions to reach the desired effects.

In this research, two hybrid mathematical models are developed and tuned to represent the concentration polarization phenomena in dynamic UF of dextran T500. Such models yield an adjusted determination coefficient of 0.9185 and 0.9626, respectively, and can predict the concentration at the membrane surface, the flux and the observed rejection. The results display the intensifying effect of dynamic operation by decreasing the Molecular Weight Cut-Off (MWCO) of the membrane up to 74 times without reducing the flux. The experimental data from literature and herein developed hybrid models provide system insights for membrane systems design where the selectivity can be enhanced and tunned according to operating conditions rather than the membrane pore size.

The best hybrid mathematical model is used to explore the UF system under dynamic operation at different scenarios aiming to provide further system understanding. With this focus, a sensitivity analysis is accomplished in order to evaluate the separation performance in terms of flux and rejection factor as a function of input variables: backshock time (BS), time between backshocks (TBBS), dextran bulk concentration (C_b). The sensitivity analysis allows finding operational regions where high fluxes can be achieved while keeping acceptable rejection factor. Aiming to highlight the advantages of applying dynamic operation instead of conventional filtration, a comparative analysis is performed between a membrane with low

MWCO under conventional cross-flow operation and a membrane with high MWCO under dynamic operation. Concentration polarization effect is analyzed and explained by concentration polarization modulus. This modulus is defined as the ratio between concentration at the membrane surface and the bulk concentration. Values as high as 160 for this modulus have a negative impact on selectivity, while values close or lower than 34 improve separation. Average flux can be enhanced up to 43.8 % with BS = 1 s and TBBS = 5 s. With respect to the comparative analysis, membrane cost savings reach values around 50 % by operating a membrane of high MWCO under dynamic conditions.

Mathematical modeling in dynamic ultrafiltration is a key tool, from a process system engineering perspective, to assess the separation performance under different operating conditions. The hybrid mathematical model developed in this research allows optimization of operation through sensitivity analysis, and allows designing of the separation process given a definite concentration target, in the context of dextran ultrafiltration.

Keywords: Dynamic ultrafiltration, membrane intensification, MWCO tuning, hybrid modeling.

1. Introduction

Membrane technologies have drawn great attention in the last 60 years because of their remarkable performance in terms of selectivity, throughput, product purity, reduction in chemical usage, mild operating conditions, compactness, carbon footprint reduction, energy saving and process safety (Charcosset, 2006; Abels et al., 2013; Wei et al., 2014; Prado-Rubio et al., 2016). These benefits have led to an increasing research on this topic, thus, a big membrane market has emerged and several companies have been working extensively in the prototype development that can be used industrially. The industrial interest in the membranes is creating scale economies that is helping to decrease the prices of membrane systems. Membrane technologies include several fields such as microfiltration, ultrafiltration, nanofiltration, reverse osmosis, electrodialysis, gas separation, pervaporation, carrier-facilitated transport, membrane contactors, piezodialysis (Baker, 2012), and other integrated systems like hybrid distillation and membrane bioreactors, among others (Prado-Rubio et al., 2019). From the possibilities, the focus of this thesis is on micro- and ultrafiltration processes.

Micro- and ultrafiltration (MF and UF) are processes used to separate and/or concentrate particulate matter, macromolecules and colloids from a fluid stream (Mulder, 1996; Bacchin et al., 2006). These particles and solutes are aimed to be removed by means of a physical barrier so called membrane. The membranes in MF and UF systems are made of a porous material which can retain the particles or the solute with a specific range of size (Baker, 2012) and they mainly differ in the pore size distribution (Scott, 1995).

Some of the applications of MF and UF are summarized in table **1-1**.

Table 1-1.: Application fields of micro- and ultrafiltration processes (Scott, 1995; Mulder, 1996; Baker, 2012).

Application field	Examples
Beverage industry	Clarification of juices, wines and beer. Cold sterilization without sacrificing flavor.
Automotive industry	Removal of electro-coat paintings in water streams.
Dairy sector	Protein concentration (e.g. whey). Cheese production.

Continuation of Table **1-1**

Application field	**Examples**
Petrochemical industry	Refining of oils and petroleum. Oil/water emulsions separation.
Drinking water industry	Microorganisms removal.
Wastewater treatment	Microorganisms and organic matter removal.
Pharmaceutical industry	Sterilization with no thermal damage.
Seawater desalination	Removal of organic matter, microorganisms and oil as a pretreatment or reverse osmosis.
Biotechnology	Metabolite purification and enzyme extraction.
Microelectronic industry	Ultrapure water production.

MF and UF technologies are interesting since they operate at low temperatures, present high product quality and selectivity, have low operating costs when it is compared with conventional separation processes like distillation (Prado-Rubio et al., 2016). Besides, it is a compact technology, and it is easy to scale up and automate (Baker, 2012; Díaz et al., 2017).

Among the application fields of MF and UF, the most interesting and active nowadays is the water (Association, 2005) and wastewater treatment (Schrotter and Bozkaya-Schrotter, 2010), because there is an increasing concern about the conservation of the natural resources and the human health (Knops and Franklin, 2000; Singh, 2015). This concern has been evident through more strict environmental regulation and policies relating to water quality for consumption (Hillis, 2000; Singh, 2015; Sikdar and Criscuoli, 2017) and final disposal (Sikdar and Criscuoli, 2017). The water industry has made major advances in MF and UF technologies due to the imperative necessity to supply water for the population considering the fresh water scarcity around the world (Baker, 2012). Hence, MF and UF are under constant optimization to make membrane technology more competitive. In this regard, it is believed that a deep understanding of the underlying dynamic nature of the phenomena involved in MF and UF could lead to overcome the problems associated to this technology: concentration polarization and fouling. This idea is based on a process system engineering perspective (PSE) which has proven to be a powerful tool in the synthesis, design, control, optimization and intensification of industrial production processes.

According to Pistikopoulos et al. (2021a), “PSE is the scientific discipline of integrating scales and components describing the behavior of a physicochemical system, via mathematical

modelling, data analytics, design, optimization and control". They stated that PSE can be understood at three different layers. The inner layer is related to design, building and operation of manufacturing processes aiming to transform some raw materials into the desired products. The middle layer involves a deep understanding of the process and its underneath phenomena allowing higher efficiencies in resource usage. The outer layer is focused on addressing environmental and social challenges making the process more sustainable.

PSE strongly relies in mathematical models in its core layer, so a deep understanding of the phenomena is required through the development of models based on first principles or system identification (Keil, 2018; Pistikopoulos et al., 2021a).

Different factors have imposed new challenges for the industrial production processes, such as resource limitations, climate change, growing global population, required smarter, flexible and sustainable manufacturing processes and demand of high quality and versatile products (United-Nations, 2015; Pistikopoulos et al., 2021a). In this regard, PSE offers different tools and applications as a way to satisfy these evolving needs of society (Tian et al., 2018).

Process Intensification (PI) is one of the research fields of PSE and aims to decrease significantly the energy consumption and reduce the operational and capital costs of a chemical process by improving the transfer rates of mass, heat and momentum. (Tian et al., 2018). These goals can be achieved if the following outcomes are obtained: smaller equipment size for a given throughput, higher throughput for a given equipment size or a given process, less holdup in equipment or less inventory in process for the same throughput, less usage of utility materials and feedstock for a given throughput, and higher performance for a given unit size (Ponce-Ortega et al., 2012; Tian et al., 2018; Stankiewicz and Moulijn, 2018). Some strategies have been identified and proven to be successful in achieving these outcomes. They can be summarized as: merging various operations or processes into a single equipment, research on new materials with better properties, process integration, design of smaller equipments, operating at different conditions, enhancing the driving forces, applying new operational strategies such as periodic operation or dynamic modes (Tian et al., 2018). These PI activities are grouped by other authors into three levels: (a) equipment, (b) methods, and (c) plant design (Keil, 2018).

PI is applied in several fields of chemical and process engineering such as separation, reaction, combined reaction separation processes, and alternative energy sources (Tian et al., 2018). One successful technology in achieving PI goals is the integration of membrane processes with conventional technologies in separation and reaction fields (Tian et al., 2018; Keil, 2018). Integration of membranes allows yielding high product quality, requiring less space by plant compactness, a minor environmental impact, and an efficient use of energy (Tian et al., 2018; Keil, 2018).

As mentioned before, membrane processes are already used in PI, however, their design and operation is rather far from being optimal. Thus, this thesis is focused on using PSE methods and tools, such as mathematical modeling and simulation, in order to: (1) find appropriate operating conditions for membrane separations in MF and UF processes, (2) increase the MF and UF membrane economic potential and (3) overcome one of the main drawbacks in membrane functioning: concentration polarization.

1.1. Motivation

Membrane technologies are very attractive from an industrial, academic, research and environmental perspective. They offer promising results in the efficient usage of resources, energy consumption and environmental impact. Nevertheless, some drawbacks related to process operation, namely concentration polarization and fouling, keep membranes from spreading in all industrial sectors (Baker, 2012). Besides, it has been shown that the design and optimal operation of the MF and UF systems are limited by the low understanding (translated into little development of principles-based mathematical models) of the underlying dynamic physiochemical phenomena: concentration polarization and fouling (Díaz et al., 2017). The complexity of the membrane process dynamics and the time-variant properties of the feed stream and membrane have made of the membrane separation processes a challenge for being designed, optimized and further intensified (Skiborowski, 2018).

From a process system engineering perspective (PSE), to carry out a design and operation of these processes it is necessary to rely on mathematical models that can represent and predict their behavior in a robust manner (Prado-Rubio and von Stosch, 2017; Tian et al., 2018; Pistikopoulos et al., 2021a).

Although membranes are already considered an equipment for separation intensification or an element to be integrated with other units by intensifying the process (Pistikopoulos et al., 2021b), membrane-based separation can be further intensified through implementation of intensifying methods in the category of new operational strategies such as periodic operation or dynamic modes. For instance, reversing the permeate flow periodically can contribute to the membrane cleaning and mitigation of concentration polarization. Nonetheless, an optimal configuration of the dynamic operation has been made according to extensive experiments and is dependent on the type of membrane, the nature of the solute, transmembrane pressure and other operating conditions (Jonsson and Rubio, 2011; Rosinha, 2011; Díaz et al., 2017; Prado-Rubio and von Stosch, 2017). So, there is a need to develop mathematical models aiming to get a deep understanding of the involved multiscale phenomena and to predict the filtration behavior under different conditions in order to further intensify membrane technologies. These achievements in PI goals allows contributing to the actual challenges such as

sustainability, efficiency in energy and resource usage, high quality products and mitigation of climate change.

Hence, the present thesis is focused in the development of mathematical tools, through PSE, that allow modelling and simulation of dynamic MF and UF systems, such that better operational conditions can be found in order to increase its economic potential. It is expected that such models will allow developing improved process design and optimizing both the performance and the operation conditions for dynamic MF and UF systems.

1.2. Background

1.2.1. Summarized membrane time-line

The industrial application of the membrane technology had its origin in the 1960s and went through four broad phases (Baker, 2012). The first one was characterized by the following features: (1) New processes based on the Loeb-Sourirajan technique to develop high performance membranes. (2) Reduction in the selective layer thickness of the membrane in the order of 0.1 µm was achieved by several companies. (3) Different membrane modules were developed such as plate and frame, capillary, hollow fine fiber and spiral wound. (4) It was very important the support offered by the US Department of Interior, Office of Saline Water (OSW) for the development of reverse osmosis, microfiltration, ultrafiltration and electrodialysis. The second phase was marked by the economic support of OSW. Thanks to the OSW, the results obtained in the research were applied on commercial products. In addition to this, the microfiltration, ultrafiltration, reverse osmosis and electro-dialysis became processes well established commercially. In the third phase, membranes for gas separation processes were developed and used in industrial systems such as nitrogen separation from air, and hydrogen separation. Another process, that began in this phase but has had a slow growth since then, is the pervaporation system for dehydration of solvents.

The attention was focused on water treatment in the last phase. The objective in this stage is to build systems based on microfiltration and ultrafiltration for the treatment of wastewater and municipal water sources. The timeline of these four phases is represented in figure **1-1**.

1.2.2. Market and potential of MF and UF membranes

Economic data about the market of membranes offer a good idea of the dimension and importance that the industry has assigned to the membrane technology in separation processes.

BCC Research has published a report entitled “Ultrafiltration Membranes: Technologies and Global Markets” where it is revealed that “The global ultrafiltration (UF) membranes mar-

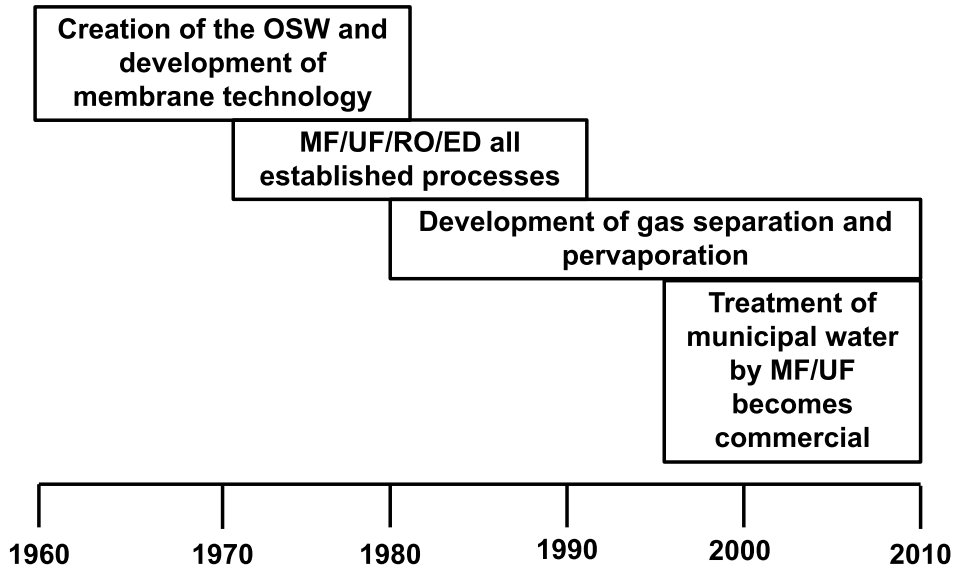

Figure 1-1.: The development of the membrane separation industry, 1960-2010. Reprinted from (Baker, 2012).

ket should reach \$5.5 billion by 2025 from \$4.2 billion in 2020 at a compound annual growth rate (CAGR) of 5.7 % for the forecast period of 2020 to 2025" (BCC-Research, nda). Previously, in 2016, BCC Research had highlighted that the global market for UF membranes had grown to about \$3.3 billion from \$ 3.1 billion in 2015 and that the expected CAGR was of 6.9 % for the period 2016 - 2021, increasing to about \$ 4.6 billion in 2021 (BCC-Research, nda). According to this information, UF market is expected to keep growing in spite of the slighty decrease of the CAGR from 2016 to 2020.

Regarding microfiltration membranes market, BCC Research mentioned that it should reach \$3.7 billion by 2023 from \$ 2.4 billion in 2018 at a CAGR of 9.0 % for the period 2018 to 2023 (BCC-Research, ndb). Previously, the CAGR was estimated in 8 %, 10 % and 6.7 % for 2010, 2013 and 2015, respectively (BCC-Research, ndb). Although there are variations in the growth rate, it is sure that MF market is expected to keep rising for the coming years.

According to Markets and Markets analysts, the main drivers for ultrafiltration systems developments are: (1) the increasing awareness regarding water and wastewater treatment, (2) selective separation technology, and (3) stringent regulatory and sustainability policies concerning the environment (Markets and markets, nd).

Therefore, it is evident the increasing interest in the development of membranes technologies. This allows finding new fields of application and improvements in current processes. The in-

terest in this topic is because of the high reached efficiencies in systems using membranes, and the achievement of separations that before were expensive, difficult, or not still possible. It seems that the objective with membrane technologies is to push reaction and purification systems beyond their limits (Escobar and der Bruggen, 2011).

1.2.3. Basic concepts of membrane processes

"A membrane is nothing more than a discrete, thin interface that moderates the permeation of chemical species in contact with it" (Baker, 2012). According to structure, membranes can be classified into: a) Isotropic and b) Anisotropic.

Isotropic membranes consist of a material layer homogeneous in composition and structure and can be microporous, dense (nonporous) or electrically charged. The thinner is the layer the better is the flux through the membrane. Therefore, a new design was created with the aim of achieve high fluxes without losing mechanical strength and that is the anisotropic membrane. This consists of a porous support material over which a thin layer performs the separation. The support material has a structural function to offer mechanical strength and the thin layer is usually made of some kind of polymer and determines the separation properties and permeation rates (Mulder, 1996; Baker, 2012). Some of the materials used to construct membranes are: polymeric, ceramic, metallic and liquid.

The separation processes with membranes can be grouped according to the driving force as follows (Calabrò and Basile, 2011):

- Pressure driven operations (Microfiltration, ultrafiltration, nanofiltration, reverse osmosis, gas separation and pervaporation).
- Concentration driven operations (Dialysis and osmosis)
- Operations in electric potential gradient (Electro-dialysis, membrane electrolysis, and electrophoresis)
- Operations in temperature gradient (membrane distillation)

In separation processes with membranes under pressure driven operation, a pressure difference is applied as the driving force to separate particles or solutes from a stream (Calabrò and Basile, 2011; Baker, 2012). In this sense, a feed solution is forced to flow through the membrane and only the solvent and the solutes smaller than the pores of the membrane can pass through it to the permeate stream. While the particles larger than the pores are retained over the membrane surface. Depending on the application, the desired product can

be the retained solute or the permeate.

Most of the membranes in pressure driven operations are usually characterized by the molecular weight Cut-Off (MWCO) which is a measure of the retention capability. This parameter depends on several factors such as the pore size distribution of the membrane, suspension stability, bulk concentration, solute size, solute molecular weight, salt content, pH, solute shape, cross-flow velocity, among others (Mulder, 1996; Zydney and Xenopoulos, 2007; Wickramasinghe et al., 2009; Baker, 2012). Hence, the membranes in pressure driven operations are differentiated by the particle size capable to separate. Thus, conventional filtration, microfiltration, ultrafiltration, nanofiltration and reverse osmosis remove particles larger than 1µm, 50 nm, 3nm, 1 nm and 0.1 nm, respectively (Calabrò and Basile, 2011). The separation range have diffuse boundaries because a membrane has a pore size distribution and not a unique value of pore size (figure **1-2**).

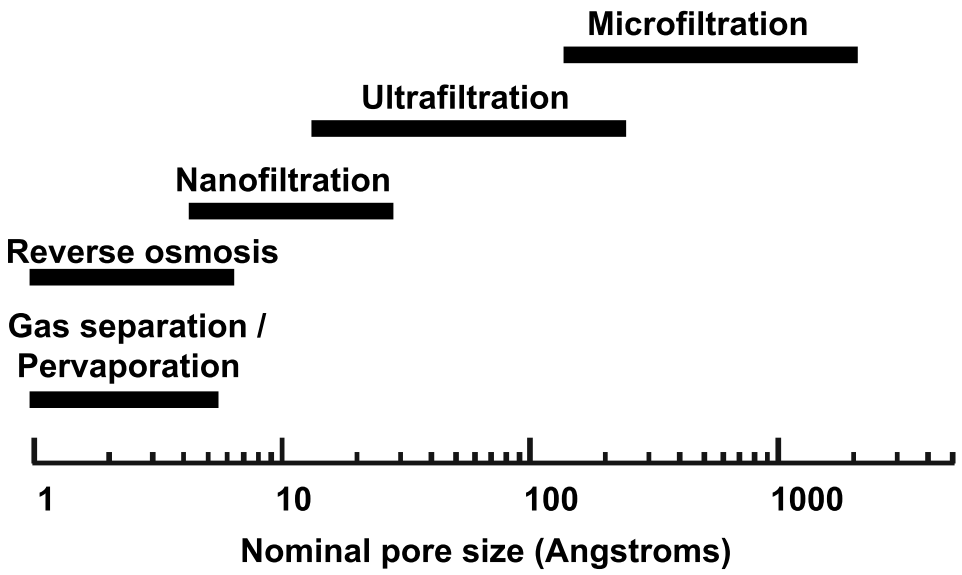

Figure 1-2.: Nominal pore size of membranes used in separations driven by pressure gradients. Reprinted from (Baker, 2012).

The retention capability characterization in UF membranes is carried out by filtrating macromolecules solutions of well defined molecular weight such as polymers (e.g. dextrans, proteins) and viruses (Capannelli et al., 1983; Bakhshayeshi et al., 2011; Yehl and Zydney, 2021), being the dextran retention test the most common for applications where virus removal is not required (Bakhshayeshi et al., 2011). Regarding MF membranes, there are three techniques: bacterial challenge test, bubble point test and, the less common, the latex challenge test (Baker, 2012).

1.2.4. Importance and applications of microfiltration and ultrafiltration

One important feature of MF and UF technologies is that they allow concentration and separation of species while avoiding the thermal damage at the same time (Calabrò and Basile, 2011). This is a very necessary and useful feature that make MF and UF suitable in fields like food, beverage, pharmaceuticals and biotechnology. Additionally, they also find applications in water pretreatment for desalination processes, microelectronic industry, water and wastewater treatment (Leos and Zydney, 2017), automotive industry and medicine (Nunes and Peinemann, 2006).

Regarding water treatment, the environmental legislation is getting more stringent in the last years. This has led to an increase in the utilization of MF and UF systems to achieve satisfactorily the new disinfection standards for drinking water (Kennedy et al., 2008; Peinemann and Nunes, 2010). Examples of the stringent legislation are Giardia and Cryptosporidium removal guidelines of the Surface Water Treatment Rule, USA 1989 and the directive for the quality of water for human consumption, EC 1998. More recent data regarding regulations for drinking water can be found in the federal law "Safe Drinking Water Act (SDWA)" set by the U.S. Environment Protection Agency (EPA, 2021) and in the Guidelines for Drinking-water Quality from the World Health Organization (WHO, 2006).

Desalination of seawater has begun to extend because of the water scarcity. With the aim of supplementing freshwater resources, reverse osmosis (RO) is used to desalinate seawater and brackish water, while MF and UF are used as pretreatment to RO (Kennedy et al., 2008).

1.2.5. Microfiltration (MF)

Particles and biological material with sizes in the range of 0.025 μm to 10 µm can be removed by using MF membranes which usually are made of polymeric or ceramic materials. Although many fibrous media can serve as a filtration media for this same particulate matter, only a MF membrane can guarantee a quantitative retention based on a defined pore size distribution (Calabrò and Basile, 2011). A MF system can be used to clarify and sterilize fluids, trap microorganisms for a later analysis and remove cellular material from a lysate (Mulder, 1996; Association, 2005; Starbard, 2009; Baker, 2012). The membrane configuration depends on the type of module used. The modules normally utilized for MF are the same for UF (Figure **1-3**): hollow fiber, plate and frame, tubular and spiral wound (Association, 2005).

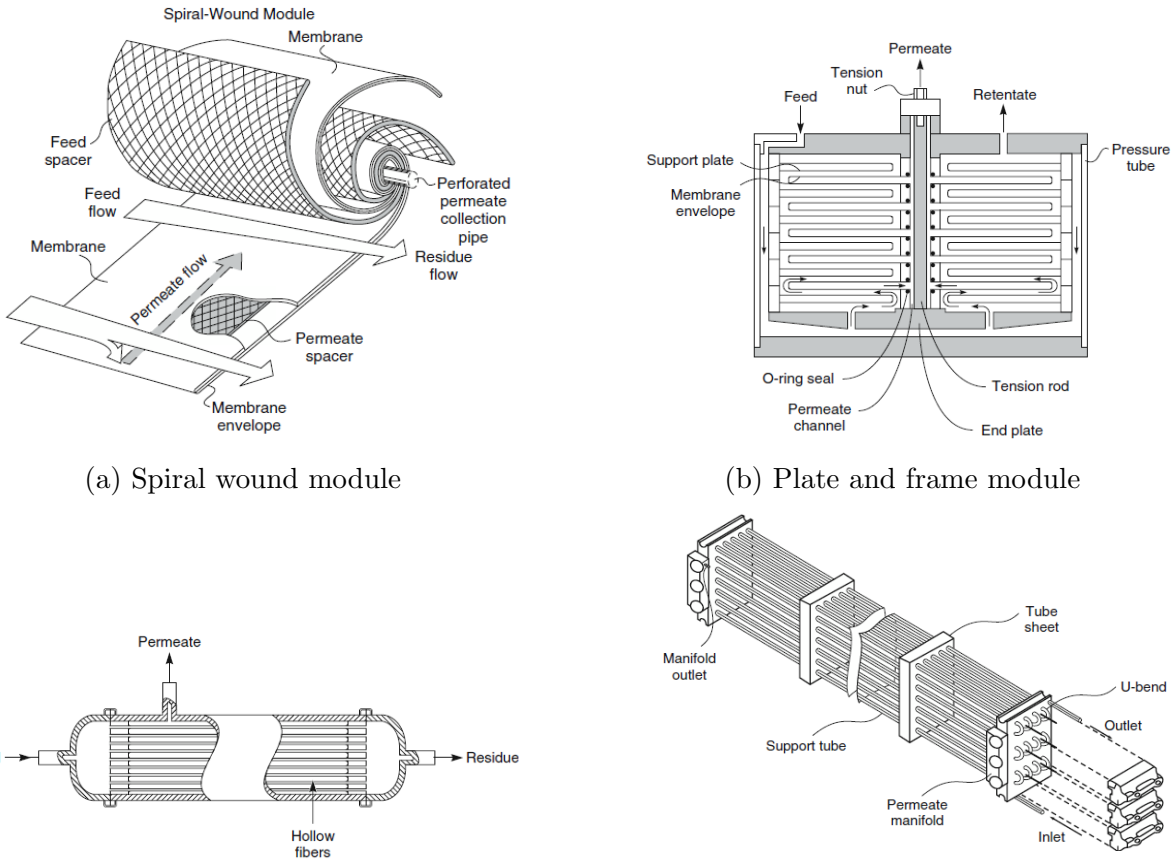

(a) Spiral wound module

(b) Plate and frame module

(c) Hollow fiber module

(d) Tubular module

Figure 1-3.: Types of modules used in microfiltration and ultrafiltration processes. Reprinted from (Baker, 2012)

1.2.6. Ultrafiltration (UF)

Ultrafiltration membranes work like those in MF, the difference lies in the Molecular Weight Cut-Off. Molecules with sizes in the range of 1 -1000 kDa can be retained by UF membranes (Calabrò and Basile, 2011). A membrane used for UF is usually made with an anisotropic structure and its average pore diameter is in the range of 10 – 1000 Å (Baker, 2012).

The main factors affecting the separation and permeability through the UF membranes are (i) Applied pressure difference, (ii) Chemical, molecular and electrostatic interactions between the membrane material and the solute to be retained, (iii) Pore size distribution of the membrane which is related to the MWCO, (iv) pH of the feed stream, (v) Shape of the solute, (vi) Concentration polarization (a concept discussed further in section 1.2.7) and (vii) Fouling (discussed further in section 1.2.7) (Calabrò and Basile, 2011; Baker, 2012).

Characterization of pore size in MF and UF is an important task to classify the membrane in one of the two groups (MF or UF). Traditionally the test consisted in performing some experiments with model molecules such as dextran to evaluate the Molecular Weight Cut-Off of the membrane (Bakhshayeshi et al., 2011; Yehl and Zydney, 2021). Nevertheless, it has arisen the need to evaluate the membrane capability to remove some virus and bacteria from the water. Virus and bacteria removal can not be evaluated with the MWCO because the solutes have different properties like charge, structure and hydrodynamic permeability. For that reason, a virus challenge test is more appropriated to test the performance of the membrane in removal of microorganisms (Peinemann and Nunes, 2010). It is worth mentioning that, although the MWCO had been considered a fixed parameter of membranes, recent research highlight the dependency of MWCO measurement on different factors related to operating conditions (Jonsson and Rubio, 2011; Yehl and Zydney, 2021).

The membrane material in both MF and UF can be polymeric or ceramic. Among the polymeric commonly used compounds are: polypropylene, Polyethersulfone/polyvinylpyrrolidone blends, polysulfone, polyvinyldenefluoride, cellulosic derivatives and polyacrylnitrile (Peinemann and Pereira Nunes, 2010). Common construction materials for the ceramic membranes are: aluminum oxide, titanium dioxide, zirconium dioxide, or a carbon composite (American Water Works Association , 2005). The membrane modules used in UF processes are depicted in Figure **1-3**.

1.2.7. Transport Phenomena and operation types in MF and UF

In order to understand how MF and UF membranes perform separation, it is necessary to discuss the physio-chemical phenomena involved, the driving forces normally used for separation and the operating conditions applied to the membrane modules.

I. Driving Force

The feed stream is forced to cross the MF and UF membrane by means of a pump that applies a pressure difference between the feed-side and the permeate-side of the membrane (Figure **1-4**), so called transmembrane pressure (TMP). Hence, the pressure gradient is the driving force in these processes (pore-flow model). The particulate matter is retained at the membrane by two mechanisms. The first one, corresponds to screen filters in which the particles larger than the membrane pore size are retained in its surface. Usually the screen filters have an anisotropic structure, where a fine micro-porous layer lies on more open micro-porous support. Ultrafiltration membranes are mostly screen filters. The second mechanism is found in the so called depth filters. Here, the particles are not only retained on the external surface of the membrane but also inside the constrictions within the pores or adsorbed in the inner walls of a tortuous path inside the pore. Depth filters have a homogeneous structure, that is, they are isotropic. Microfiltration membranes are mostly depth filters (Baker, 2012). There

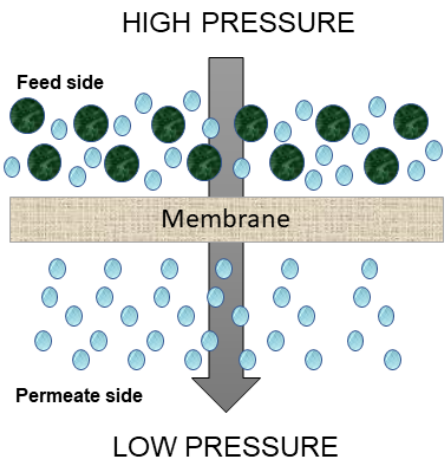

Figure 1-4.: Driving force in microfiltration and ultrafiltration processes (Baker, 2012)

are four mechanisms by which dispersed material gets trapped in a depth filter (Figure **1-5**): (a) simple sieving, (b) inertial impaction, (c) Brownian diffusion, (d) electrostatic adsorption.

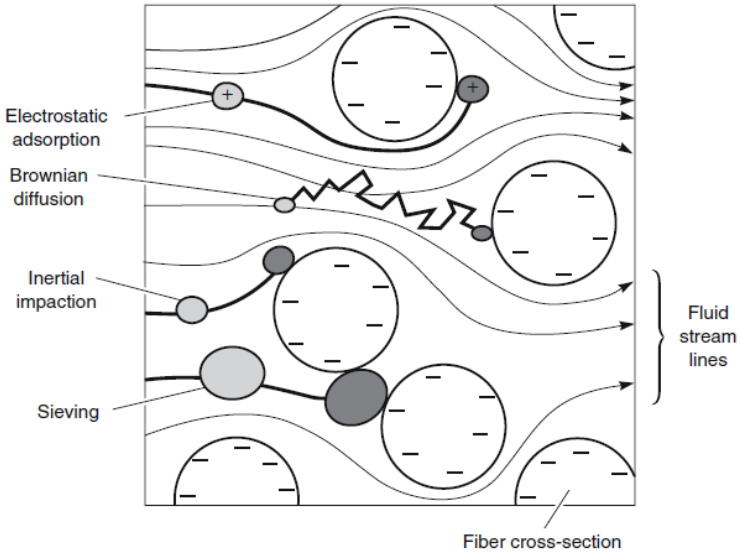

Figure 1-5.: Four mechanisms by which dispersed material is captured in depth filters. Reprinted from (Baker, 2012).

II. Operation modes

The process configuration in UF and MF can be set in multiple forms according to the diagram in figure **1-6**.

Two relevant concepts regarding to the operation of an UF and MF membrane module need to be introduced: constant transmembrane pressure (TMP) operation and constant flux operation (Baker, 2012). Constant TMP refers to a set up where the pressure difference applied to the system (between feed and permeate) is kept constant, thus the flux through the membrane gradually decreases with time because of the fouling (Mulder, 1996; Baker, 2012). In UF processes, most of the constant pressure operation systems work under cross-flow mode in order to keep fouling under control and they have found applications in paint electrocoating systems, food industry, oil-water emulsions, process water, product recycling and biotechnology (Baker, 2012). These applications are usually driven by processes where the components to be separated have enough value to offset the process cost.

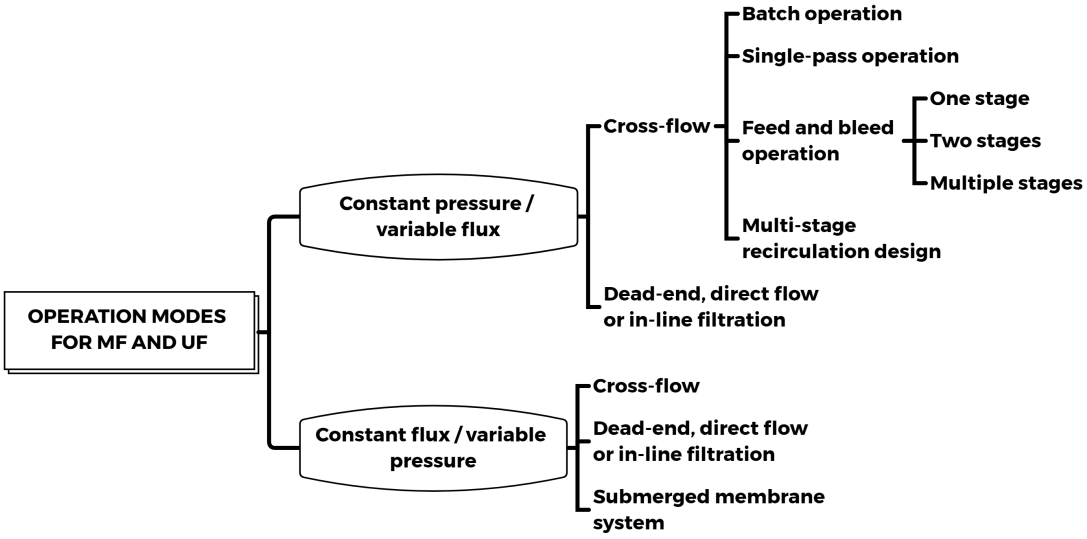

Figure 1-6.: Operation modes in UF and MF (Wagner, 2001; Baker, 2012).

Constant flux consists of membrane system in which the TMP is increased to keep always the same flux, compensating the increasing resistance due to fouling (Mulder, 1996; Baker, 2012). Submerged systems are often the most used in this category by the UF membranes. They find applications where keeping a constant flux is essential for the process, for instance, in drinking water supply and membrane bioreactors (Baker, 2012). Submerged systems are usually coupled with an air sparging system to control the fouling.

In cross-flow mode, the feed stream is pumped in a tangential direction to the membrane surface and the retained stream is recirculated to the system. If the concentration in the recirculation loop is desired to reach a specified concentration level, a bleed stream can be used (Association, 2005; Baker, 2012). Dead-end filtration, also called filtration in deposition

mode or direct filtration, is a configuration where the entire feed stream is forced to cross the membrane in a single step. Hence, all the contaminants, colloids or particulate matter are retained. After some time, a cleaning is necessary to remove this residual cake (Association, 2005; Baker, 2012).

Some of the most commonly used configuration in industries are illustrated in figure **1-7**, and combinations of them are also used, so called, christmas tree design.

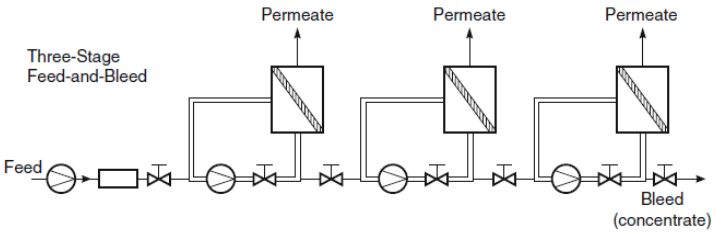

(a) Multiple-stage feed-and-bleed system.

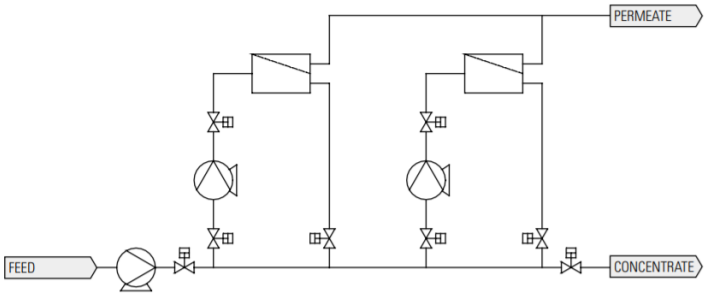

(b) Multi-stage recirculation design

Figure 1-7.: Some of the most commonly used process configurations in UF and MF. Reprinted from (Wagner, 2001; Baker, 2012)

III. Concentration polarization and fouling

It has been observed that the UF and MF membranes undergo a decline in flux with the time (in constant pressure operation) or an increase in the transmembrane pressure (in constant flux operation) and this behavior is caused by two highly coupled phenomena: concentration polarization and fouling (Calabrò and Basile, 2011).

Concentration polarization refers to the generation of a concentration profile at the boundary layer adjacent to the membrane surface. During the ultrafiltration or microfiltration process, a pressure difference is applied to drive the liquid stream plus solutes to flow towards the membrane. A portion of particles or solutes are rejected (retained onto the surface or trapped

in the constrictions inside the pores) due to the selectivity of the membrane. The solutes or particles start to concentrate in the stagnant layers adjacent to the membrane surface in the feed side. The generated concentration profile is considered and additional resistance to the flux and may cause other phenomena. For instance, depending on the nature of the solute, osmotic pressures can be produced, the pressure driving force can be counterbalanced and the membrane performance is negatively affected (Figure **1-8**). Besides, the concentration profile also contributes to counterbalance the flux through the membrane since the solute starts to move against its gradient concentration back to the bulk (so called back-diffusion).

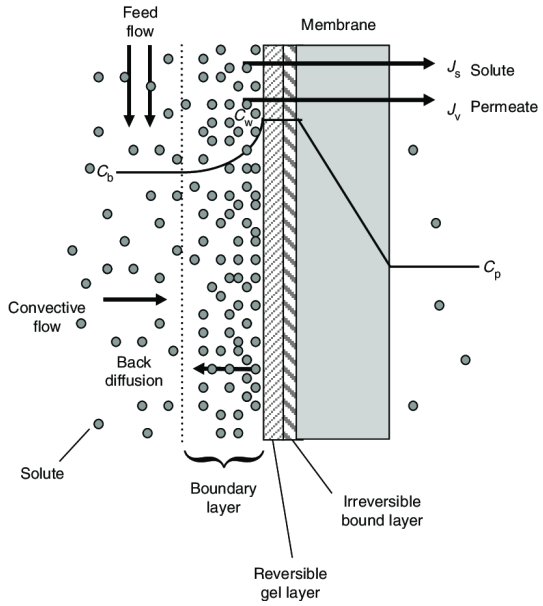

Figure 1-8.: Concentration polarization scheme. Reprinted from (Pabby et al., 2008).

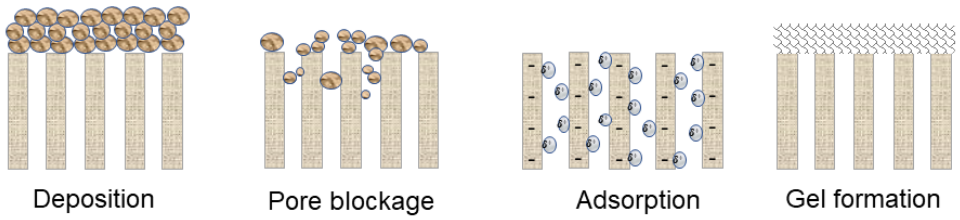

Figure 1-9.: Fouling formation mechanisms in micro- and ultrafiltration membranes (Bacchin et al., 2006).

Due to the high solute concentration in the boundary layer, a second phenomenon is promoted: fouling. Fouling refers to a buildup of material on the membrane pores (Figure **1-9**). For UF and MF, there are various forms in which the fouling can occur:

- Adsorption: occurs when an interaction between the solutes and the membrane material exists. This implies that adsorption is present even when there is no permeation flux.
- Pore blockage: a particle gets trapped in a pore by blocking it totally or partially
- Deposition: this refers to the cake formation at the membrane surface.
- Gel formation: if high values of concentration on the membrane surface are reached due to the concentration polarization, it is possible that some compounds can precipitate or lead to a gel formation. This occurs mainly when the solute involves proteins.

The fouling has serious consequences over the separation performance. For example, in an experimental set up of Hughes and Field (2006) a yeast suspension is filtered under a constant flux operation (Figure **1-10**). The fouling generated by the deposition of the yeast on the membrane surface causes an increase in the TMP during the first hour. This translates into more energy to be supplied by pumping systems and therefore higher operating costs. Additionally, after flushing the membrane (phase II in Figure **1-10**), the TMP can not be restored to its initial value, implying that some of the fouling is irreversibly adhered to the membrane, which negatively affects the separation performance.

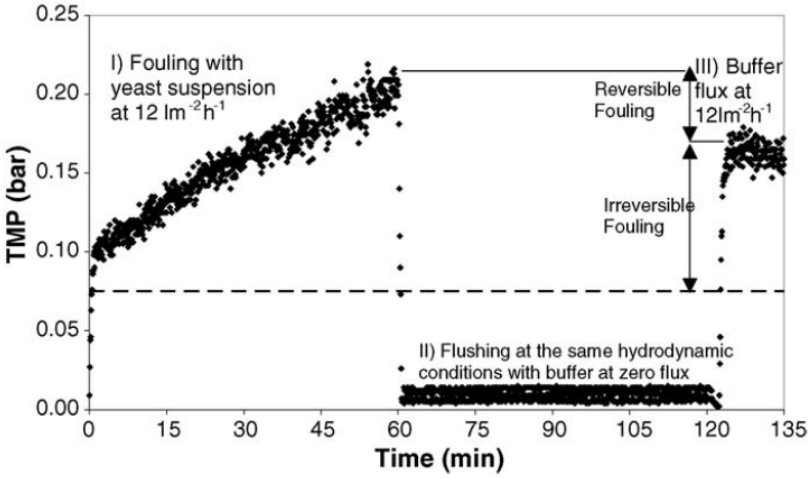

Figure 1-10.: Transmembrane pressure curve in a filtration operation for yeast suspension at constant flux. Reprinted from (Hughes and Field, 2006).

On the other hand, if a separation process is performed under constant pressure, the fouling causes flux decline as the time evolves (Figure **1-11**).

The fouling in the MF and UF membranes is a very important issue to be taken into consideration because it affects directly the membrane replacements costs. Therefore, cleaning

strategies must be applied in order to extend the membrane life-cycle (Calabrò and Basile, 2011).

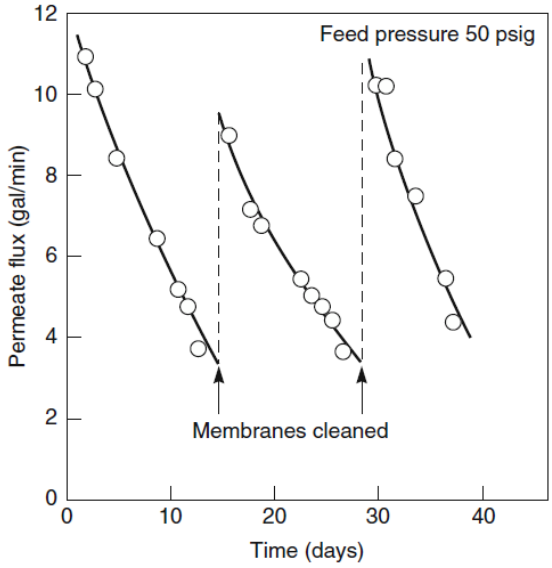

Figure 1-11.: Flux decline in a constant pressure separation process. Reprinted from (Baker, 2012).

IV. Prevention and mitigation of concentration polarization and fouling

There are several strategies for reducing the effect of fouling in separation processes with membranes and they are summarized in Table **1-2**. The techniques categorized as direct methods are those that aim to disturb the hydrodynamic conditions of the boundary layer in order to prevent the solute concentration from achieving high values at the membrane surface. Whilst those strategies grouped under indirect methods utilizes other approaches to mitigate fouling such as modifying the physio-chemical properties of the membrane, adding pre-treatment processes or selecting an appropriate system configuration.

The periodic maintenance cleaning is included in the list of fouling prevention strategies because frequent and short cleanings can diminish the necessity of major cleaning-in-place (CIP) procedures (Peinemann and Pereira Nunes, 2010).

Table 1-2.: Strategies to prevent and reduce fouling in UF and MF membranes. Reprinted from (Peinemann and Nunes, 2010).

Direct Methods	Indirect Methods
Turbulence promoters (e.g., modified membrane spacers)	Pretreatment by filtration
Pulsed or reverse flow	Treatment of the membrane surface

Continuation of Table **1-2**

Direct Methods	Indirect Methods
Rotating or vibrating membranes	Preparation of more hydrophilic membranes
Stirred cells with rotating blades close to the membrane	Selection of appropriated operating mode
Ultrasonic enhancement	Selection of optimum operating conditions
Periodic maintenance cleaning: (1) Chemical cleaning (2) Hydraulic cleaning (3) Mechanical cleaning	
Periodic backwash with permeate or gas	
Generation of a dynamic membrane layer	

1.2.8. Microfiltration/Ultrafiltration modeling

I. Concentration Polarization

A mathematical model for concentration polarization is obtained by applying a mass balance over the boundary layer in the feed side of the membrane. The assumptions in the mass balance are: steady state, Fick law of diffusion, there is no chemical reaction, there is no concentration gradient in a direction parallel to the membrane surface (stagnant layer), density is constant and diffusion coefficient is independent of concentration. After integrating the differential mass balance and reorganizing, the following formula is developed (Baker, 2012):

$$\frac{C_{im} - C_{ip}}{C_{ib} - C_{ip}} = exp\Big(\frac{J_v \cdot \delta}{D_i}\Big) \tag{1-1}$$

Where C_{im} is the concentration of solute in the feed stream at the membrane surface, C_{ip} is the concentration of solute at the permeate side, δ is the boundary layer thickness, J_v is the flux through the membrane and D_i is the Fick diffusion coefficient. This equation predicts the relation of the solute concentration at the membrane surface with the flux. However, this equation does not consider other relevant effects such as the osmotic pressure generated by the solute and the temporal evolution of the concentration profiles over the boundary layer.

II. Fouling

In the absence of fouling, the Darcy's law can be used to establish a relationship between the volumetric flux and the applied transmembrane pressure by means of a proportionality constant referred to as permeability (L_p) (See equation 1-2). Permeability is a property of a porous material for allowing a fluid to pass through it under an applied pressure. Hence, a high permeability indicates high flux through the porous material, while low permeability causes low flux (Popham, 2019).

$$J = L_p \cdot \Delta P \tag{1-2}$$

If the concentration polarization is relevant and the generated osmotic pressure is considerable, hence the model can be rewritten in the following form:

$$J = \frac{1}{\mu \cdot R_m}\Big(\Delta P - \Delta\pi\Big) \tag{1-3}$$

Where R_m is the membrane resistance in the absence of fouling and is measured experimentally. μ is the viscosity of the permeate. $\Delta\pi$ is the osmotic pressure and it is set to zero if the feed does not contain solutes, that is, the feed is pure solvent. An equivalent form of the last equation is:

$$J = \frac{1}{\mu(R_m + R_{cp})}(\Delta P) \tag{1-4}$$

Where R_{cp} is the resistance associated with the concentration polarization layer. Now, if fouling is present in the membrane, the equation can be extended by including extra resistances:

$$J = \frac{1}{\mu(R_m + R_{ads} + R_{rev} + R_{irrev})}(\Delta P - \Delta\pi) \tag{1-5}$$

R_{ads} represents the resistance associated to the adsorption of solute due to interactions with the membrane. R_{rev} corresponds to the reversible resistance that disappears after switching to pure solvent and R_{irrev} corresponds to the resistance that only can be removed when an intensive chemical cleaning procedure is performed.

III. Critical, Threshold and Sustainable Flux

There are some important concepts regarding to the possible operative flux values. The first of them is the critical flux defined as "the flux at which fouling is first observed for a given feed concentration and given cross-flow velocity" (Field and Pearce, 2011). The critical flux can be referred to the strong form, J_{cs} (adsorption is negligible), the weak form, J_{cw} (adsorption is present) or the irreversible form (Bacchin et al., 2006; Beier and Jonsson, 2009). The following expressions assume that the osmotic pressure is small. J_{cs} and J_{cw} are the strong form and the weak form of the critical flux, respectively.

$$J = \frac{1}{\mu \cdot R_m}(\Delta P), \ for\ J < J_{cs} \tag{1-6}$$

$$J = \frac{1}{\mu(R_m + R_{rev} + R_{irrev})}(\Delta P), \ for\ J > J_{cs} \tag{1-7}$$

$$J = \frac{1}{\mu(R_m + R_{ads})}(\Delta P),\ for\ J < J_{cw} \tag{1-8}$$

$$J = \frac{1}{\mu(R_m + R_{ads} + R_{rev} + R_{irrev})}(\Delta P),\ for\ J > J_{cw} \tag{1-9}$$

Critical flux is easily observed in a stationary flux - TMP curve without osmotic pressure effects and corresponds to the point at which the curve starts to deviate from linearity (Figure **1-12**).

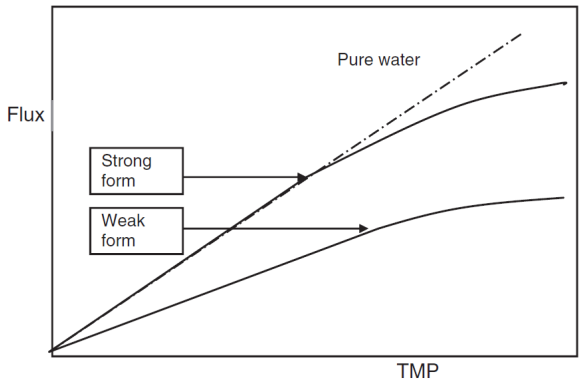

Figure 1-12.: Strong and weak form of the critical flux. Reprinted from (Field and Pearce, 2011).

Nevertheless, the critical flux concept does not apply for a dead-end system in which there is always fouling in some extent. Hence a new concept was introduced: the threshold flux. It consists in a value of the flux above of which the fouling rate increases markedly and below of which the fouling rate is moderate. This is expressed as follows.

$$Rate\ of\ permeability\ loss = a + b \cdot (J - J^*)\ for\ J > J^* \tag{1-10}$$

$$Rate\ of\ permeability\ loss = a\ for\ J < J^* \tag{1-11}$$

In addition to the critical and threshold flux concepts, there is another flux related with the economical aspect of the process. The value of flux at which the operational costs and capital costs are in optimal balance is called sustainable flux. It is referred as a balance because low operational costs are achieved with low fluxes (cleaning procedures are less intensives), but low capital costs are achieved with high fluxes (less membrane area is required). Another definition for sustainable flux is “the net flux that can be maintained using mechanical and

chemical enhancing means to meet an operation cost objective over the projected life of the membrane" (Field and Pearce, 2011).

These concepts of critical, threshold and sustainable flux are very important for specifying the operating conditions of a membrane separation system from techno-economic viewpoint. Therefore, the modelling of the membrane fouling, concentration polarization and/or flux decline is an interesting field of research, since the determination and prediction of the fouling rate could be used to optimize the operational conditions in such a way that the maximum revenues can be achieved. Hence, the following sections deal with possible models that might be used for accomplishing this task.

1.2.9. Mathematical modeling for Process System Engineering

Mathematical modeling is a powerful and useful tool in science and engineering because it can be used for simulation, optimization, process intensification, control, process system engineering, clustering, classification, prediction and monitoring (Hangos and Cameron, 2001; Zendehboudi et al., 2018).

A classification of mathematical models is somewhat difficult because of the rising of a substantial amount of models in the recent years and all of them offer different characteristics and features. However, they can be roughly grouped into three categories: white-box models or first principles models, gray-box models and black-box models, according to their reliability on process knowledge or input-output data inference (Zendehboudi et al., 2018; Azevedo et al., 2019).

The main features of each type of model are summarized in table **1-3** and some examples are sketched in Figure **1-13**.

Purely white or purely black box models are quite rare in process engineering. It is rather common finding models that combine the structure of white box models with some parameters or correlations based on input-output mapping. Hence, grey box models are the models most used in engineering applications. The development of a model can be performed through the seven step modeling procedure sketched in Hangos and Cameron (2001): (1) problem definition by establishing the process description and the modeling goal; (2) identification of the relevant phenomena involved in the process; (3) incorporation of the available process data; (4) development of the model equations; (5) mathematical solution of the model equations; (6) verification of the model solution against reality; (7) validation of the model with new data or experiments. This steps have some return points as shown in figure **1-14**.

The mathematical model development in step four relies on some key components (Hangos

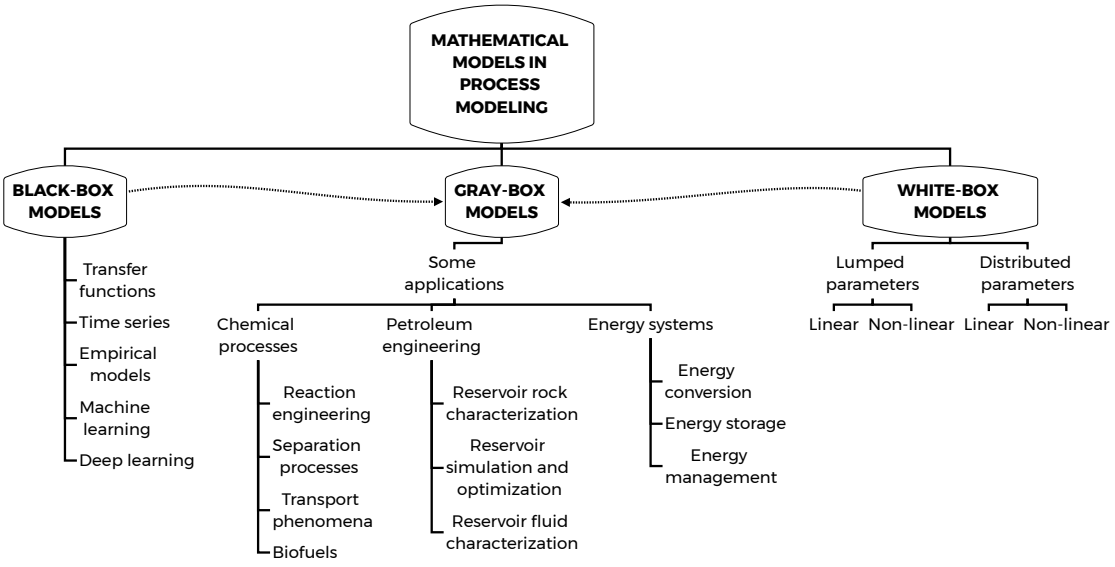

Figure 1-13.: Mathematical model classification. Adapted from Zhang (2010).

and Cameron, 2001):

- Assumptions
- Model equations and characterizing variables: differential equations for mass, energy and momentum balances; constitutive equations for thermodynamic relations, transfer rates and physical constraints.
- Initial conditions (if applicable)
- Boundary conditions (if applicable)
- Parameters. Usually obtained from step three.

As a result of following these steps (Figure **1-14**), a mathematical model is obtained and can be classified in two types: lumped parameter and distributed parameter. The former has variables that do not change spatially, while the latter include variables that vary spatially. Depending on the modeling target, the model can be focused on emulating the dynamic behavior of the process or just its steady state. Hence, the final model can be one of four (Hangos and Cameron, 2001):

Table 1-3.: Features of white, gray and black box models (Zhang, 2010; Zendehboudi et al., 2018; Azevedo et al., 2019).

White box models	Black box models	Gray box models
▪ Rely on the governing equations derived from engineering and nature laws (e.g. mass, energy and momentum conservation laws). ▪ Can be built before the operation of a process. ▪ Provide understanding of the process behavior under the effects of operating conditions. ▪ Have good extrapolation capabilities only limited by the model assumptions. ▪ Feature high computational burden. ▪ Are also called mechanistic, analytical, phenomenological, physical, fundamental and parametric models. ▪ Face several challenges such as high dimensionality, time delay, uncertainties, multi-scale and non-linearity.	▪ Rely on mapping the Input/Output data. ▪ Their parameters do not have physical interpretation. ▪ Their performance is restricted to the range of available data. ▪ Feature low computational burden. ▪ Feature high data demand. ▪ Are also called data-based, non-parametric, empirical and data-driven models.	▪ Combine models from white-box and black-box models. ▪ The well known phenomena is predicted by the white-box part and the unknown part of the process is modeled by the black-box model. ▪ Have the benefits from both white and black box models. ▪ Offer more flexibility because they can be re-calibrated with new dataset. ▪ Reduce the amount of required parameters comapred with black-box models. ▪ Are also called semi-analytical, semi-physical, semi-parametric and hybrid models.

- Lumped parameter dynamic model. Normally represented by a set of ordinary differential equations with initial value problem.
- Distributed parameter dynamic model. Normally represented by a set of partial differential equations.
- Lumped parameter steady state model. Normally represented by a set of algebraic equations.
- Distributed parameter steady state model. Normally represented by a set of ordinary differential equation with boundary value problem.

Most of the parameters used in a model come from empirical correlations. For instance, hydrodynamic properties such as Prandtl number, Reynolds number and mass transfer coefficients are based on equations extracted from several experimental trials (Çengel and Ghajar, 2020). Hence, the parameters can be considered as the black box component in a mathematical model for process engineering applications.

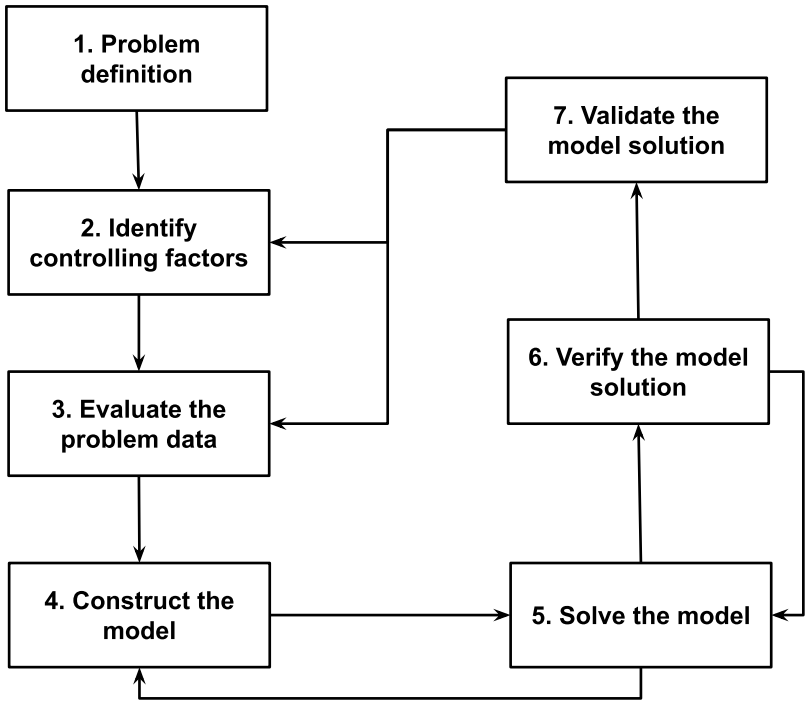

Figure 1-14.: Seven step modeling procedure. Adapted from Hangos and Cameron (2001).

1.3. Hypothesis and Objectives

1.3.1. Hypothesis

Data-driven models can be used in microfiltration and ultrafiltration processes to predict:

- The flux decline and observed rejection in the membrane.
- The best operating conditions for the system in order to accomplish a desired separation performance.

1.3.2. Objectives

I. General Objective

Determine the predictive power of different data driven models in ultrafiltration and microfiltration processes.

II. Specific Objectives

- Identify and analyze different types of data-driven models to predict the behavior of microfiltration and ultrafiltration processes.

- Collect and analyze experimental data of microfiltration and ultrafiltration processes from literature and/or in collaboration with other research groups/enterprises.
- Validate the predictive power of the identified models to reproduce the behavior of microfiltration and ultrafiltration processes.
- Optimize the operational conditions of microfiltration and ultrafiltration processes for water treatment.

1.4. Methodology

This research is focused on model development to improve the operating conditions for dynamic filtration system (MF and UF) towards providing system understanding and best operation scenarios. For achieving that goal, it is required to develop a model that can predict the flux decline, the membrane selectivity and the dynamic behavior of UF and MF membranes under different operation conditions. The overview of the employed methodology is depicted in Figure **1-15**. The main steps for the development of this thesis are sketched as follows:

- The first step consists of collecting experimental data related to MF or UF from literature, research groups and/or enterprises.
- According to the nature of the available data and a previous revision of the mathematical model types, a preliminary selection of the mathematical model is made. Since data come from dynamic ultrafiltration of dextran T500 where some system features are not entirely understood, a hybrid model is proposed in order to capture most of the physico-chemical phenomena by means of deterministic equations. The variability that is not explained by the deterministic relations is managed by black box models.
- The model structural configuration is set. The inputs, outputs and dependencies of the black box model are defined. The mathematical function describing the black box model is then proposed.
- Next, model tuning is performed to adjust the full mathematical model to the experimental data. Some statistical indexes and techniques are used to evaluate the goodness of the fit, such as, adjusted correlation coefficient, parity plots and confidence intervals for the estimated parameters.

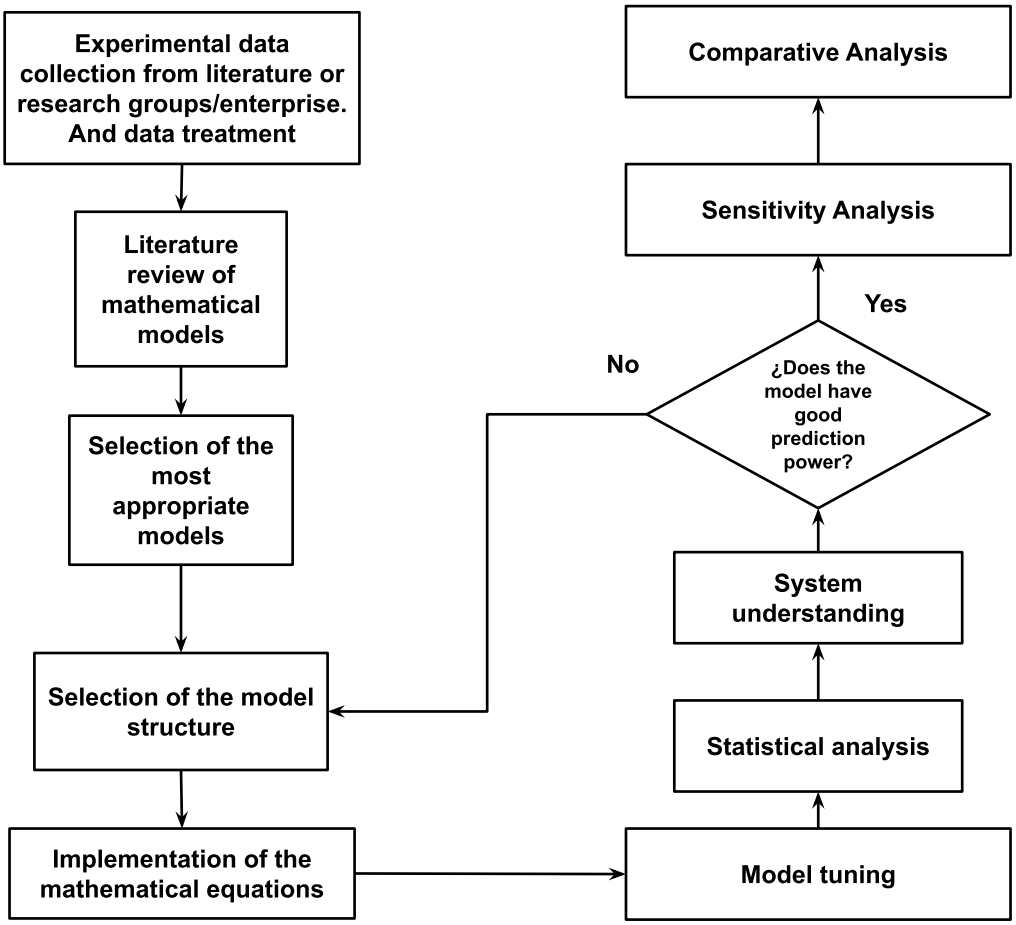

Figure 1-15.: Proposed methodology diagram.

- The output of the model is then analyzed along with the statistic indexes, aiming to assure that parameters are identifiable and lie in physically feasible intervals, and the experimental data are accurately predicted. If the model prediction power is not acceptable, a new structure for the black box model is assumed and the cycle is repeated as shown in Figure **1-15**.

- If the model prediction power is good enough, the model is exploited by performing a sensitivity analysis in order to evaluate the separation performance under different input disturbances, namely, backshock time (BS), time between backshock (TBBS), bulk concentration (C_b) and transmembrane pressure (TMP). The separation performance is analyzed through rejection factor, membrane flux, concentration profiles and concentration polarization modulus.

- Finally, a comparative analysis is accomplished aiming to highlight the benefits of using dynamic operation. Within the comparative analysis, economic savings in terms of required area and membrane costs are highlighted.

1.5. Thesis content

This thesis has been written using each chapter as an article, thus the reader must be aware about potential repetition of information between each chapter. This feature is suitable in order to have chapters with coherence independently of each other.

In order to achieve the proposed objectives of the thesis, the mathematical modeling and analysis of a dynamic ultrafiltration system is performed in two chapters. The chapter entitled "Ultrafiltration intensification by dynamic operation: Insights from hybrid modeling" focuses on the development and identification of the mathematical models aiming to predict the flux and selectivity of a dynamic ultrafiltration system by utilizing experimental data from dextran separation. The content of this chapter was published in a scientific journal article displayed in Appendix A which is recommended to read instead. The chapter entitled "Model-based sensitivity analysis of dynamic ultrafiltration" consists of an analysis of the separation performance in terms of flux, observed rejection and concentration at the membrane surface as a function of the input variables BS, TBBS, C_b and TMP. Besides, a comparative analysis is made at the end of the chapter aiming to highlight the benefits of using dynamic operation versus conventional cross flow operation.

1.6. Impact

1.6.1. Academic

With a developed mathematical model for dynamic MF and UF systems, it is straightforward to establish the operating conditions that allow the filtration process to achieve the desired separation performance. The model also helps to validate if some desired outputs are achievable by the filtration system. This model allows increasing process understanding in dynamic microfiltration and ultrafiltration systems.

1.6.2. Social

Micro and ultrafiltration technologies are spread out across different fields such as: microelectronics, biotechnology, water desalination, pharmaceuticals, dairy sector, automotive sector, beverages, petrochemicals, wastewater and water treatment. According to this, meaningful improvements in the process that involve UF and MF membranes can be highly benefited

as more efficient process are implemented and high quality products are produced. In this way, the life quality of the population can be improved.

1.6.3. Environmental

Further process intensification can be implemented for membrane technologies, especially micro and ultrafiltration processes thanks to this research work. So, the outcomes of the research would help membrane technologies to meet current challenges such as sustainability, efficiency in energy and resource usage and high quality products.

1.7. Contributions

1.7.1. Journal paper

L.H. López-Murillo, V.H. Grisales-Díaz, M. Pinelo, O.A. Prado-Rubio, Ultrafiltration intensification by dynamic operation: Insights from hybrid modeling, Chem. Eng. Process. - Process Intensif. 169 (2021) 108618. https://doi.org/10.1016/j.cep.2021.108618.

L.H. López-Murillo, V.H. Grisales-Díaz, O.A. Prado-Rubio, Model-based sensitivity analysis of dynamic ultrafiltration. Paper under development with a 95 % of progress.

1.7.2. Peer reviewed conference papers

Luis Humberto López- Murillo, Víctor Hugo Grisales Diaz, Manuel Pinelo, Óscar Andrés Prado- Rubio. (2021). Ultrafiltración Dinámica - Modelamiento de la Intensificación de Selectividad. In Proceedings of "XLII Encuentro Nacional de la AMIDIQ – Desafíos actuales de investigación y docencia de ingeniería química" (ISSN: 2683 - 2925). Jorge Ramón Robledo Ortíz (Editor). Pages: PRO 246-251. Academia Mexicana de Investigación y Docencia en Ingeniería Química (AMIDIQ).

1.7.3. Conference presentation

Luis Humberto López- Murillo, Víctor Hugo Grisales Diaz, Manuel Pinelo, Óscar Andrés Prado- Rubio. (2021). Ultrafiltración Dinámica - Modelamiento de la Intensificación de Selectividad. Oral presentation in XLII Encuentro Nacional de la AMIDIQ – Desafíos actuales de investigación y docencia de ingeniería química, 08 - 11 september, 2021. Virtual event.

References

Abels, C., Carstensen, F., and Wessling, M. (2013). Membrane processes in biorefinery applications. *Journal of Membrane Science*, 444:285–317.

Association, A. W. W. (2005). *Microfiltration and Ultrafiltration Membranes for Drinking Water*, volume 53. American Water Works Association.

Azevedo, C. R., Díaz, V. G., Prado-Rubio, O. A., Willis, M. J., Préat, V., Oliveira, R., and Stosch, M. (2019). Hybrid semiparametric modeling: A modular process systems engineering approach for the integration of available knowledge sources.

Bacchin, P., Aimar, P., and Field, R. (2006). Critical and sustainable fluxes: Theory, experiments and applications. *Journal of Membrane Science*, 281:42–69.

Baker, R. W. (2012). *Membrane Technology and Applications*. John Wiley & Sons, 3 edition.

Bakhshayeshi, M., Kanani, D. M., Mehta, A., van Reis, R., Kuriyel, R., Jackson, N., and Zydney, A. L. (2011). Dextran sieving test for characterization of virus filtration membranes. *Journal of Membrane Science*, 379:239–248.

BCC-Research (n.d.a). Ultrafiltration membranes: Technologies and global markets.

BCC-Research (n.d.b). The global market for membrane microfiltration.

Beier, S. P. and Jonsson, G. (2009). Critical flux determination by flux-stepping. *AIChE Journal*, 56:1739–1747.

Calabrò, V. and Basile, A. (2011). 1 - fundamental membrane processes, science and engineering.

Capannelli, G., Vigo, F., and Munari, S. (1983). Ultrafiltration membranes — characterization methods. *Journal of Membrane Science*, 15:289–313.

Charcosset, C. (2006). Membrane processes in biotechnology: An overview. *Biotechnology Advances*, 24:482–492.

Díaz, V. H. G., Prado-Rubio, O. A., Willis, M. J., and von Stosch, M. (2017). Dynamic hybrid model for ultrafiltration membrane processes.

EPA (2021). U.s. environmental protection agency.

Escobar, I. and der Bruggen, B. V. (2011). *Modern Applications in Membrane Science and Technology*, volume 1078. American Chemical Society.

Field, R. W. and Pearce, G. K. (2011). Critical, sustainable and threshold fluxes for membrane filtration with water industry applications. *Advances in Colloid and Interface Science*, 164:38–44.

Hangos, K. M. and Cameron, I. T. (2001). 1 - the role of models in process systems engineering.

Hillis, P. (2000). Membrane case studies, past present and future.

Hughes, D. and Field, R. W. (2006). Crossflow filtration of washed and unwashed yeast suspensions at constant shear under nominally sub-critical conditions. *Journal of Membrane Science*, 280:89–98.

Jonsson, G. E. and Rubio, O. A. P. (2011). Modeling and operation of dynamic membrane processes. International Congress on Membranes and Membrane Processes : ICOM 2011 ; Conference date: 01-01-2011.

Keil, F. J. (2018). Process intensification. *Reviews in Chemical Engineering*, 34:135–200.

Kennedy, M. D., Kamanyi, J., Rodrguez, S. G. S., Lee, N. H., Schippers, J. C., and Amy, G. (2008). Water treatment by microfiltration and ultrafiltration.

Knops, F. N. M. and Franklin, B. (2000). Ultrafiltration for 90 mld cryptosporidium and giardia-free drinking water. a case study for the yorkshire water keldgate plant.

Leos, J. Z. and Zydney, A. L. (2017). *Microfiltration and Ultrafiltration*. Routledge.

Markets and markets (n.d.). Ultrafiltration market by type (polymeric, and ceramic), module (hollow fiber), application (municipal, and industrial (food & beverage processing, chemical & petrochemical processing, pharma processing)), and region - global forecast to 2023.

Mulder, M. (1996). *Basic Principles of Membrane Technology*. Springer Netherlands.

Nunes, S. P. and Peinemann, K.-V. (2006). *Membrane technology: in the chemical industry*. John Wiley & Sons.

Pabby, A. K., Rizvi, S. S. H., and Requena, A. M. S. (2008). *Handbook of membrane separations: chemical, pharmaceutical, food, and biotechnological applications*. CRC press.

Peinemann, K.-V. and Nunes, S. P. (2010). *Membranes for water treatment*. John Wiley & Sons.

Pistikopoulos, E. N., Barbosa-Povoa, A., Lee, J. H., Misener, R., Mitsos, A., Reklaitis, G. V., Venkatasubramanian, V., You, F., and Gani, R. (2021a). Process systems engineering – the generation next? *Computers & Chemical Engineering*, 147:107252.

Pistikopoulos, E. N., Tian, Y., and Bindlish, R. (2021b). Operability and control in process intensification and modular design: Challenges and opportunities. *AIChE Journal*, 67.

Ponce-Ortega, J. M., Al-Thubaiti, M. M., and El-Halwagi, M. M. (2012). Process intensification: New understanding and systematic approach. *Chemical Engineering and Processing: Process Intensification*, 53:63–75.

Popham, N. (2019). Resin infusion for the manufacture of large composite structures.

Prado-Rubio, O. A., Fontalvo, J., and Woodley, J. M. (2019). 8. conception, design, and development of intensified hybrid-bioprocesses.

Prado-Rubio, O. A., Morales-Rodríguez, R., Andrade-Santacoloma, P., and Hernández-Escoto, H. (2016). Process intensification in biotechnology applications.

Prado-Rubio, O. A. and von Stosch, M. (2017). Towards sustainable flux determination for dynamic ultrafiltration through multivariable system identification.

Rosinha, I. P. (2011). High frequency backshock effect on ultrafiltration of selected polysaccharides. master thesis. universidade técnica de lisboa & technical university of denmark.

Schrotter, J.-C. and Bozkaya-Schrotter, B. (2010). Current and emerging membrane processes for water treatment.

Scott, K. (1995). Introduction to membrane separations.

Sikdar, S. K. and Criscuoli, A. (2017). Sustainability and how membrane technologies in water treatment can be a contributor.

Singh, R. (2015). Water and membrane treatment.

Skiborowski, M. (2018). Process synthesis and design methods for process intensification. *Current Opinion in Chemical Engineering*, 22:216–225.

Stankiewicz, A. and Moulijn, J. A. (2018). *Re-Engineering the Chemical Processing Plant*. CRC Press.

Starbard, N. (2009). *Beverage Industry Microfiltration*. Wiley.

Tian, Y., Demirel, S. E., Hasan, M. F., and Pistikopoulos, E. N. (2018). An overview of process systems engineering approaches for process intensification: State of the art. *Chemical Engineering and Processing - Process Intensification*, 133:160–210.

United-Nations (2015). Sustainable development goals.

Wagner, J. (2001). *Membrane Filtration Handbook: Practical Tips and Hints*. Osmonics.

Wei, P., Cheng, L.-H., Zhang, L., Xu, X.-H., lin Chen, H., and jie Gao, C. (2014). A review of membrane technology for bioethanol production. *Renewable and Sustainable Energy Reviews*, 30:388–400.

WHO (2006). Guidelines for drinking-water quality.

Wickramasinghe, S. R., Bower, S. E., Chen, Z., Mukherjee, A., and Husson, S. M. (2009). Relating the pore size distribution of ultrafiltration membranes to dextran rejection. *Journal of Membrane Science*, 340:1–8.

Yehl, C. J. and Zydney, A. L. (2021). Characterization of dextran transport and molecular weight cutoff (mwco) of large pore size hollow fiber ultrafiltration membranes. *Journal of Membrane Science*, 622:119025.

Zendehboudi, S., Rezaei, N., and Lohi, A. (2018). Applications of hybrid models in chemical, petroleum, and energy systems: A systematic review. *Applied Energy*, 228:2539–2566.

Zhang, P. (2010). Industrial control system simulation routines.

Zydney, A. L. and Xenopoulos, A. (2007). Improving dextran tests for ultrafiltration membranes: Effect of device format. *Journal of Membrane Science*, 291:180–190.

Çengel, Y. A. and Ghajar, A. J. (2020). *Heat and Mass Transfer: Fundamentals and Applications*. McGraw-Hill Education.

2. Ultrafiltration intensification by dynamic operation: insights from hybrid modeling

2.1. Abstract

Concentration polarization and fouling are the most important issues to be addressed when designing ultrafiltration (UF) and microfiltration (MF) units for a specific application. Dynamic operation in UF and MF, such as backshock, is a method that allows mitigating adverse effects of polarization and fouling thus enhancing the separation performance. However, there is a trade-off between operational conditions (i.e. backshock duration time BS, the time between backshock TBBS, and flux) to achieve the desired effects. Herein, two hybrid mathematical models are developed and tuned to predict the behavior of the polarization layer in dynamic UF (R^2_{adj} of 0.9185 and 0.9626, respectively). Both hybrid models can estimate the concentration on the membrane surface (e.g. 27 g/L when BS is 1.25 s and TBBS is 5 s). The results illustrate the intensifying effect of dynamic operation by decreasing the Molecular Weight Cut-off up to 74 times without decreasing the membrane flux. The performed experiments and developed models provide system insights for membrane systems design where the rejection could be enhanced and tunned according to operating conditions rather than the membrane pore size.

2.2. Introduction

Ultrafiltration (UF) and microfiltration (MF) are separation technologies widely used in industrial fields such as water treatment (Byhlin and Jönsson, 2003; Jönsson et al., 2006; Verma and Sarkar, 2017, 2018; Chen et al., 2018; Grzegorzek and Majewska-Nowak, 2018; Shi et al., 2019), food (Neggaz et al., 2007), beverage (Macedo et al., 2011), pharmaceutical (Zaidi and Kumar, 2004; KWON et al., 2008; Pu et al., 2012) and biotechnology due to their good performance and selectivity under moderate conditions. Nevertheless, filtration membrane technologies have some drawbacks that limit their performance and efficiency, namely concentration polarization and fouling (Peinemann and Nunes, 2010; Baker, 2012). These phenomena affect membrane performance by reducing the flux and decreasing selectivity (or

rejection factor).

Due to the adverse impact of the aforementioned phenomena, there have been efforts to develop several methods to reduce, control, avoid and correct the effects of concentration polarization and fouling by mechanical, hydraulic, chemical means or their combination (Peinemann and Nunes, 2010; Baker, 2012). Some examples are: turbulence promoters, pulsed or reverse flow (dynamic operation), rotating or vibrating membranes, stirred cells with rotating blades close to the membrane, ultrasonic enhancement, periodic maintenance cleaning, periodic backwash with permeate gas (dynamic operation), generation of a dynamic membrane layer, pre-treatment by filtration, membrane surface treatment, preparation of more hydrophilic membranes, appropriated operating mode selection.

Among the mentioned methods to control concentration polarization and fouling, some could be grouped into the general term "dynamic operation". Particularly, there is a technique in which, every period of time, the flux is reversed across the membrane during a specified amount of time. Then, a pressure is applied in the permeate side and the flux crosses from permeate to the retentate side. Such reversed flux can remove some of the internal and external fouling while disrupting the concentration profile in the boundary layer. There are several variations of this technique with different names: backshock, backpulse and backflush, only differentiating in frequency and duration (Gao et al., 2019). Dynamic operation can be considered as part of process - intensifying methods (Stankiewicz and Moulijn, 2000) since overall performance can be improved significantly by reverting flux in a periodic way (Srijaroonrat et al., 1999; Salladini et al., 2007; Bakhshayeshi et al., 2011b; Borujeni et al., 2015). Nevertheless, further intensification by using dynamic operation only can be achieved for UF and MF if it is performed at the appropriate operating conditions. The appropriate selection of operating conditions is not an easy task for a particular application. Therefore, it is interesting to use a process system engineering approach where mathematical models are used for process design and operation.

Table 2-1.: List of models used for predicting ultrafiltration process behavior.

System	Model type	Model use	Ref
Whey separation process with UF	It includes mass balances and a black box model to predict fouling.	The model is evaluated under different feed stream concentrations and is used for control purposes.	(Saltık et al., 2017)

Continuation of Table **2-1**

System	Model type	Model use	Ref
Cross flow membrane filtration of colloidal suspension	It is an artificial neural network with a radial basis function.	It is used to predict the flux decline under different conditions: particle size, solution pH, ionic strength and transmembrane pressure.	(Chen and Kim, 2006)
Cross flow membrane filtration of colloidal suspension	It is based on Darcy's law integrated with a feed forward artificial neural network	It is used to predict flux and flux resistances.	(Azevedo et al., 2019)
Soy protein production from extracts of deffated soybean flour by using tubular and spiral wound ultrafiltration modules	Darcy's law and film theory.	Flux prediction	(KRISHNAKUMAR et al., 2004)
Cross flow membrane filtration of colloidal suspension	Feedforward back-propagation neural network and a radial basis function network. The architectures of these are found by genetic algorithms.	Flux prediction	(Sahoo and Ray, 2006)
Whey UF process	A data driven differential equation (empiric model).	Flux prediction	(Yee et al., 2009)
Water treatment plant	A hybrid model integrating Darcy's law and artificial neural networks.	Flux prediction in dead-end ultrafiltration process.	(Chew et al., 2017)
Wastewater treatment application	Single Input - Single Output structures and Multiple Input - Single Output structures were evaluated by using system identification techniques.	Flux prediction	(Prado-Rubio and von Stosch, 2017)
Wastewater treatment of a petrochemical process	A hybrid model coupling Darcy's law and artificial neural networks.	Flux prediction	(Grisales Díaz et al., 2017)
Dynamic UF of dextran	Computational fluid dynamics and semi-analytical models	Flux and observed rejetion prediction	(Vinther et al., 2014a,b, 2015; Vinther and Jönsson, 2016a,b)

In literature, different models have been developed for predicting ultrafiltration processes behavior. Some of the latest models are summarized in Table **2-1**. In general, the proposed models have the following limitations to be applied for process intensification:

- Those models based on solution diffusion approach do not include the real phenomena that occurre in UF and MF: the sieving mechanism. Mostly, they are limited to static operation and not dynamic operation.
- Black box models, such as autoregressive models, artificial neural networks, among others, only predict flux and not the permeate concentration, rejection neither selectivity. Additionally, they need extensive experimental data to calibrate the models, and results are particular for the investigated application limiting their use in other fields. Besides, noise from experimental data tends to be captured by the model.
- Development of pure deterministic models is difficult because the phenomena involved are nonlinear and time variant, and there is insufficient process understanding of the mechanistics underneath.
- Recent models using computational fluid dynamics have not been validated with experimental data (Vinther et al., 2014b, 2015; Vinther and Jönsson, 2016a,b).

Therefore, the aim of this research is to analyze the intensifying effect of dynamic operation on UF separation performance, thus develop and tune two hybrid models with different complexity level. Both are intended to predict flux and observed rejection in dynamic UF considering concentration polarization, vital for optimizing process design and operation. The proposed hybrid models merge the flexibility of black box approaches with the interpretability of first principles models, thus they have good extrapolation capabilities and low data requirements [29, 23]. Their structure allows having insights on the phenomena underneath, so they can be used for UF and MF process design and optimization of operating conditions. Compared to previously developed models depicted in table 2, the novel hybrid models proposed in this work are aimed to increase prediction power while providing insights of the dynamic phenomena underneath. Thus, they have enhanced extrapolation capabilities than previous efforts modelling similar systems. Finally, hybrid models can serve as a building block for developing models with phenomena more complicated than concentration polarization.

The paper is structured as follows: the methodology presents the experimental setup, model development, the methods for data treatment and model tuning. The results section shows the models prediction capabilities and the effects of dynamic operation on UF performance. Finally the conclusions are drawn.

2.3. Methodology

All abbreviations and nomenclature used throughout this paper are summarized in table **2-2**.

Table 2-2.: Nomenclature.

	List of symbols
A_m	Membrane area (m^2)
BS	Backshock duration time (s)
c	Total dextran concentration (g/ml)
C	Dextran concentration (kg/m^3 *or* g/L)
D_i	Dextran diffusion coefficient (m^2/s)
F	Cross flow (L/h)
J_s	Dextran flux ($kg/(m^2 \cdot s)$)
J_v	flux through the membrane ($m^3/(m^2 \cdot s)$)
k_1	Coefficients for flux through small pores($-$)
k_2	Coefficients for flux through large pores($-$)
L_p	Membrane permeability ($m^3/(m^2 \cdot s \cdot bar)$)
M_W	Molecular weight (kDa)
MWCO	Molecular weight cut off ($-$)
R_{int}	Intrinsic rejection ($-$)
R_{obs}	Observed rejection ($-$)
RT	Retention time in SE-HPLC (min)
t	time (s)
TBBS	Time between backshocks (s)
TMP	Transmembrane pressure (bar)
v	Volume level in the permeate tank (m^3)
v_{out}	Flow from the permeate tank (m^3/s)
x	Spatial coordinate in the boundary layer (m)
	Greek letters
α	Coefficient in diffusivity expression(m^2/s)
β	Exponent in diffusivity epression ($-$)
δ	Boundary layer thickness (μm)
ΔP_{BS}	Transmembrane pressure during BS (bar)
π	Osmotic pressure (bar)
	Subscripts
i	i^{th} molecular weight interval
p	Permeate
b	Bulk
T	Tank
m	Membrane

2.3.1. Experimental set up

Experiments for conventional and dynamic operation of UF membrane were performed using Dextran T500 (Inês Pereira Rosinha, 2011). Dextrans are commonly used in dextran sieving tests as a standard method for characterizing the pore size distribution of ultrafiltration membranes (Bakhshayeshi et al., 2011a). Additionally, dextrans have very important applications in clinical, pharmaceutical and biomedical field (Song et al., 2012; Gaspar et al.,

2016; Zarrintaj et al., 2020).

The experiments are carried out in an ultrafiltration system used to test cross flow filtration with hollow fibers in continuous, diafiltration or high frequency backshock operation mode. Such equipment is conformed by eight components (see figure **2-1**): hollow fiber module (bore - side feed), pump, feed tank, permeate hold up tank, flowmeter, thermostat, backshock system and a computer.

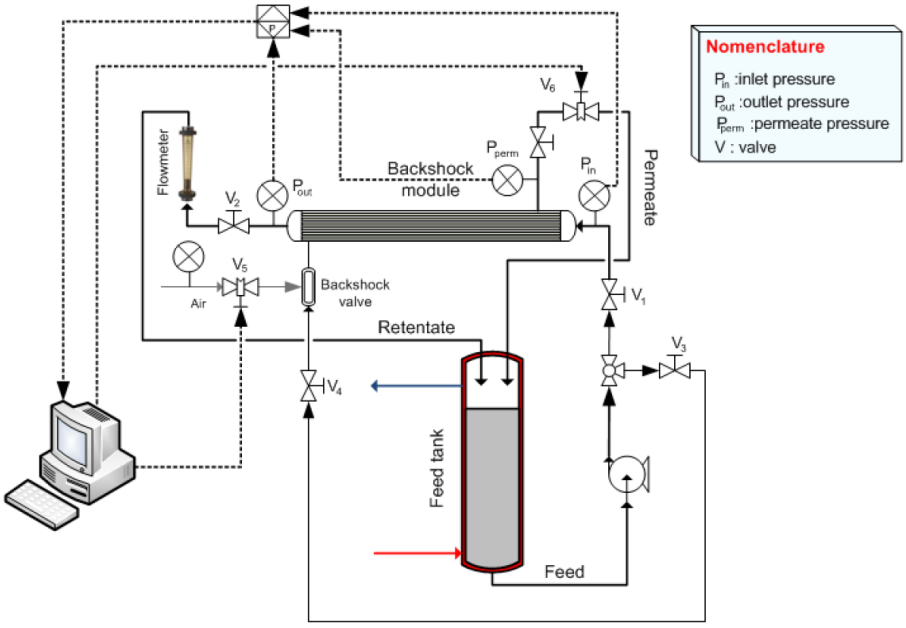

Figure 2-1.: Ultrafiltration system used to test cross flow filtration with hollow fibers in continuous, diafiltration or high frequency backshock operation mode.

The feed solution is dextran T500 (Amersham Pharmacia Biotech AB) in an aqueous solution at 1 g/L. Dextran T500 has an average molecular weight of 500 kDa. The feed tank contains the aqueous solution and is pumped to the membrane module where the stream is divided in two: the retentate and the permeate. The flowmeter is placed in the retentate stream. Both permeate and retentate are returned to the feed tank, closing the system. The permeate stream passes through a tank of 2 L (where samples are taken) before returning to the feed tank. Dextran concentrations are measured by size exclusion high performance liquid chromatography (SE-HPLC) coupled to a refractive index detector as indicated in literature for dextran quantification (Basedow and Ebert, 1979; Tkacik and Michaels, 1991; Zydney and Xenopoulos, 2007; Bakhshayeshi et al., 2011a). A high frequency backshock system is installed to apply pressure in the permeate side to reverse the flow during a time specified by the user in the computer.

The membrane module is a hollow fiber system with poly-ether sulfone (PES) membrane from X-flow Membranes (The Netherland). The module has 54 cm in length, 2.4 cm in shell diameter, 50 tubes and 1.5 mm in tubes diameter corresponding to 0.1 m^2 of membrane area. The operational conditions of the experiment are summarized in Table **2-3**. The dextran solution is fed to the membrane and different backshock times (BS) and times between backshock (TBBS) are evaluated. The reverse flux in dynamic operation allows disruption of the concentration profile at the boundary layer. This strongly modifies concentration polarization phenomenon as concentration at the membrane surface is diluted after each disruption. As consequence, there is a lower probability that solute crosses the membrane through the pores, creating the intensifying effect on membrane rejection (selectivity).

From the experimental perspective, it is necessary to assess which values of BS and TBBS are the best for intensifying the system performance. A total of 9 dynamic experiments are carried out plus a conventional cross flow filtration (without BS). Average permeate and feed concentrations are measured by SE-HPLC, and average flux is also monitored. Chromatograms are mathematically processed to extract the concentration of six molecular weight intervals using an experimental correlation to transform retention time to molecular weight. So, from one single experiment, it can be obtained seven experimental data points: six concentrations (one for each molecular weight interval) and one average flux. Hence, 7 data points per experiment (10 experiments) gives a total of 70 experimental data to perform the model tuning.

Table 2-3.: Operating conditions for the experimental tests in the dynamic ultrafiltration system.

Variable	Value
Transmembrane pressure (TMP)	0.85 bar
Cross flow (F)	162 L/h
Backshock time (BS)	0.25 , 0.75 , 1.25 s
Time between backshock (TBBS)	5, 10, 15 s

2.3.2. SE-HPLC data treatment

Dextran T500 not only contains molecules with 500 kDa, but it presents a molecular weight distribution being 500 kDa the average. Hence, a mathematical procedure is needed to estimate the concentration of each molecular weight intervals from the chromatograms. Eight intervals are constructed but the first and the last are discarded as they do not contribute significantly to the total concentration, so only six intervals are used. To do so, first, a logarithmic relation between retention time and molecular weight is built by analyzing

chromatograms from dextran samples of different average molecular weight (dextran T500, T229, T110, T70, T40 and T10). Then, a linear regression between area under the curve and concentration is developed by performing a calibration curve with samples of dextran T500 at six different concentrations. So, with the logarithmic relation, the elution time is converted to molecular weight and, with the linear regression, the chromatogram signal is divided into intervals and their corresponding areas are transformed to concentration. Thus, the concentration of each molecular weight interval can be computed.

In a previous work, multiple experiments were performed to tune the dynamic operating system, including replicates (Inês Pereira Rosinha, 2011). The best operation performance was selected to investigate in this contribution. The concentration measurements from retentate, permeate and feed streams were made in duplicate. The heights of the replicated chromatograms are averaged before extracting the area under the curve.Once the concentration of each molecular weight interval is computed, the observed rejection factor is calculated (equation 2-1) (Baker, 2012).

$$R_{obs} = 1 - \frac{C_{Ti}}{C_{ib}} \tag{2-1}$$

Where C_{Ti} is dextran concentration of i-th molecular weight interval in the permeate tank, and C_{ib} is dextran concentration of i-th molecular weight interval in feed stream. The observed rejections and fluxes are average quantities since permeate concentrations and fluxes are measured from the permeate tank (which holds up the permeate until sampling) in each experiment.

2.3.3. Model development

Unlike the models reviewed in table 2, the models developed here allow prediction of observed rejection and flux in dynamic ultrafiltration by considering BS and TBBS values.

The models are intended to describe dynamically the phenomena inside the boundary layer formed over the membrane surface in the retentate side (figure **2-2**). So, mass balances are developed for dextran at the boundary layer where diffusive and convective transport are present. Diffusion is modeled by Fick's law and convection is modeled by Darcy's law. Solutes are retained by a membrane sieving action, that is, solutes only can cross the membrane if they pass through larger pores. High dextran concentrations produce osmotic pressures that must be considered in the model. In addition, periodic backshocks are performed, so reverse flux must be part of the model.

The assumptions to be considered in the model construction are:

- There is not chemical reaction at the membrane surface.

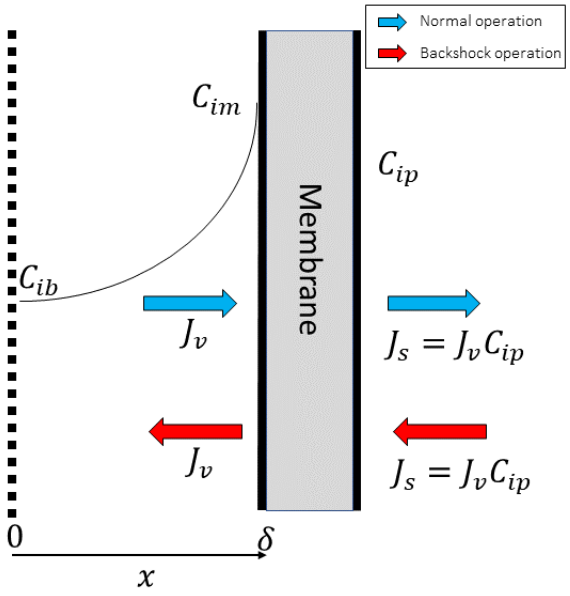

Figure 2-2.: Boundary layer diagram where concentration polarization takes place after achieving steady state. The left side corresponds to feed and the right side to permeate. Adapted from (Baker, 2012)

- Physicochemical properties in the boundary layer are constant.
- There are not velocity components in directions different from the perpendicular one to the membrane surface at the boundary layer.
- The diffusivity coefficients are only dependent on molecular weight and not on the concentration. Interactions between different molecular weight dextrans are ignored. Fick's law is a good representation for describing diffusion of dextrans.
- The tickness of the boundary layer is constant when defining the cross flow velocity. This parameter is estimated using a correlation based on the dimensionless numbers Reynolds and Schmidt (Jonsson, 1984).
- The osmotic pressure generated by high dextran concentration can be modeled by a third degree polynomial (Wijmans et al., 1985).
- The concentration in permeate is much less than in the feed side, so polarization and osmotic pressure is neglected in the permeate side.

A mass balance is performed for each molecular weight interval of dextran over the boundary layer on the membrane surface. Additionally, at the exit of permeate stream, there is a small tank holding up 2 L of retentate from which the samples were taken. For this tank, a simple mass balance is performed to predict its volume and concentration over time.

Both hybrid models share the same phenomena and the same assumptions, only differing in the black box section.

Hybrid model 1

The mass balance for the boundary layer is represented by equation 2-2 (Bird et al., 2002).

$$\frac{\partial C_i}{\partial t} = D_i \frac{\partial^2 C_i}{\partial x^2} - J_v \frac{\partial C_i}{\partial x} \tag{2-2}$$

Where C_i is the solute concentration in the boundary layer, D_i is the solute diffusion coefficient, J_v is the flux trough the membrane and x is the perpendicular direction to the membrane surface. D_i is modeled by equation 2-3 (Vinther et al., 2014a).

$$D = \alpha \cdot (M_W)^{\beta} \tag{2-3}$$

Where α is $2.6804 \cdot 10^{-10}$ and β is -0.4754. The diffusivity expression is considered part of the black box model inside the hybrid model 1.

The partial differential equation (equation 2-2) is coupled with the following boundary condition (Baker, 2012).

$$J_v C_i - D_i \left.\frac{\partial C_i}{\partial x}\right|_{x=\delta} = J_s \tag{2-4}$$

The solute flux through the membrane, J_s, is also expressed as $J_s = J_v C_{ip}$. The flux J_v can be calculated by the Darcy's law (equation 2-5) (Baker, 2012). It is worth mentioning that the flux through the membrane changes when the backshock is taking place, since the inversion of the driving force implies a reverse flux. So, positive transmembrane pressure drives a forward flux during TBBS and the negative transmembrane pressure drives a backward flux during BS.

$$\begin{cases} J_v = L_p(TMP - \Delta\pi) & Forward\ flux \\ J_v = -L_p \cdot \Delta P_{BS} & Backward\ flux \end{cases} \tag{2-5}$$

where, L_p is the membrane permeability, TMP is the transmembrane pressure, $\Delta\pi$ is the osmotic pressure difference across the membrane, ΔP_{BS} is the transmembrane pressure made by the backshock system (being $\Delta P_{BS} = 0.9$ bar from experiments). The second expression in equation 2-5 has a negative sign because, during backshock, the flux is reverted going backwards from permeate to the retentate side. It is important to note that BS, TBBS and ΔP_{BS} have to be carefully chosen for simulations, since the average flux can yield negative values if enough flux is reversed during backshock operation compared to forward operation. BS indicates how long the second expression in equation 2-5 holds, while TBBS - BS indicates how long the first expression in equation 2-5 holds.

The osmotic pressure for dextran is computed by equation 2-6 (Wijmans et al., 1985).

$$\pi = A_1 \cdot c + A_2 \cdot c^2 + A_3 \cdot c^3 \tag{2-6}$$

where, $A_1 = 0.0867$, $A_2 = 2.98$, $A_3 = 89.8$. Equation 2-5 is required in equation 2-2 but it still lacks of information: the boundary condition needs the solute flux, J_s, and therefore the permeate concentration, C_{ip}. The calculation of J_s has already been described for membranes where solution-diffusion model applies (Scott, 1996; Vinther et al., 2014a), e.g. in reverse osmosis (see equation 2-7).

$$J_s = B(C_{im} - C_{ip}) \tag{2-7}$$

where, B is the solute permeability through the membrane and C_{im} is the concentration at the membrane surface. Nonetheless, the solution diffusion model does not describe appropriately the separation mechanism that occurs in ultrafiltration and microfiltration. Hence, it is necessary to develop a more appropriated expression for computing J_s. According to pore flow model, which is more appropriate for ultrafiltration and microfiltration, the solute retention is carried out by the sieving action. It means that the membrane has a pore size distribution, that is, there are pores smaller than the solute size and also pores bigger than solute size. Therefore, the equations 2-8 and 2-9 are used instead (Jonsson, 1980).

$$J_v = k_1(TMP - \Delta\pi) + k_2(TMP - \Delta\pi) \tag{2-8}$$

$$J_s = k_2(TMP - \Delta\pi)C_{im} \tag{2-9}$$

The total flux through the membrane is conformed of two contributions. The first term of equation 2-8 corresponds to the flux through the pores smaller than the solute size, and the second term corresponds to the flux through the pores bigger than the solute size. In equation 2-9 the solute flux is expressed as the flux through the large pores multiplied by the concentration at the membrane surface.

The permeate concentration can be computed with the aid of equations 2-8 and 2-9, as follows.

$$C_{ip} = \frac{J_s}{J_v} = \frac{k_2}{k_1 + k_2} C_{im} \tag{2-10}$$

Recalling the definition of intrinsic rejection (Vinther et al., 2014a).

$$R_{int} = 1 - \frac{C_{ip}}{C_{im}} = 1 - \frac{k_2}{k_1 + k_2} \tag{2-11}$$

So, the permeate concentration can be expressed as a function of the intrinsic rejection and the concentration at the membrane surface (see equation 2-12). Note that R_{int} is specific of the pairing membrane and solute, since k_1 and k_2 are related to the membrane pore size distribution relative to the solute size. It implies that R_{int} is independent of pressure and concentration and only depends on the the solute size relative to the pore size distribution

of the membrane (sieving action). The expression for C_{ip} as a function of R_{int} is considered part of the black box model inside the hybrid model 1.

$$C_{ip} = (1 - R_{int})C_{im} \tag{2-12}$$

The mass balance for the 2 L tank in the permeate stream is in equations 2-13 and 2-14.

$$\frac{dv}{dt} = J_v \cdot A_m - v_{out} \tag{2-13}$$

$$\frac{dC_{Ti}}{dt} = \frac{J_v \cdot A_m \cdot C_{ip} - v_{out} \cdot C_{Ti} - C_{Ti} \cdot \frac{dv}{dt}}{v} \tag{2-14}$$

Where v is the volume level inside the tank, A_m is the membrane area, v_{out} is the outlet flow, being zero when the tank is not full and the same value as the term $J_v \cdot A_m$ when the tank is full, C_{Ti} is the concentration inside the tank for the i^{th} molecular weight interval.

The differential equation 2-2 is solved using the method of lines with 1000 nodes in the boundary layer and ode15s function from Matlab ®. Ode15s function is chosen because of its ability and speed to solve stiff systems.

Hybrid model 2

From preliminary model tuning, it was noticed that still the variance of the experimental data is not fully represented by hybrid model 1. Therefore, an additional gray-box model is proposed to cover the remaining output variance.

If R_{int} from the first hybrid model is plotted against molecular weight, a monotonic ascending curve, that tends to one as molecular weight grows up, is observed. This kind of curve can be modeled by exponentials, sigmoids or rational functions. The latter was proper for modeling R_{int} (equation 2-15a).

$$R_{int} = min\left(1 - \frac{1 + b \cdot (1 + a \cdot M_W)}{1 + a \cdot M_W}, 1\right) \tag{2-15a}$$

This function takes the minimum value between the expression and one, because the rational function can give values greater than one, which is not allowed for the physical interpretation of R_{int}. If a and b are estimated for each operating condition and their dependece on BS/TBBS are analyzed, a Lennard-Jones like function with two parameters could fit the data (equations 2-15b and 2-15c). These last two parameters for a expression are left to depend linearly on TBBS (equations 2-15d and 2-15e).

$$a = \epsilon_1 \cdot \left[\left(\frac{\sigma_1}{BS/TBBS + \sigma_1}\right)^{12} - \left(\frac{\sigma_1}{BS/TBBS + \sigma_1}\right)^{6}\right] + 1.63 \tag{2-15b}$$

$$b = \epsilon_2 \cdot \left[\left(\frac{\sigma_2}{BS/TBBS + \sigma_2} \right)^{12} - \left(\frac{\sigma_2}{BS/TBBS + \sigma_2} \right)^{6} \right] + 2.808 \cdot 10^{-3} \quad \text{(2-15c)}$$

$$\epsilon_1 = P_1 \cdot TBBS + P_2 \quad \text{(2-15d)}$$

$$\sigma_1 = P_3 \cdot TBBS + P_4 \quad \text{(2-15e)}$$

The independet terms in equations 2-15b and 2-15c forces a and b to adopt certain values when there is no backshock. These values are found when a and b were estimated for operation with no backshock.

2.3.4. Parameter estimation and optimization problem

Concentration polarization model in hybrid model 1 (equation 2-2) requires some parameters to be solved, such as intrinsic rejection R_{int} and permeability L_p. Therefore, a parameter estimation must be carried out by using the collected experimental data.

For parameter estimation the model outputs are: fluxes and observed rejection factors for each molecular weight interval, the inputs are: time between backshock (TBBS) and backshock time (BS), and the parameters to be estimated are: intrinsic rejection (R_{int}) and permeability (L_p).

For parameter estimation, a weighted sum of squared residuals is used as objective function (equation 2-16).

$$L = \sum_{n=1}^{N} W_i \cdot (y_{sim} - y_{exp})^2 \quad \text{(2-16)}$$

Where N is the total number of experimental data, W_i are the weights, y_{sim} are the simulated outputs and y_{exp} are the experimental outputs. Using the weigth factor W_i, the observed rejections are scaled to percentages, that is, between 0 and 100 and not in the original range (0 to 1). This is done to provide analogous rejection and flux contributions to the objetive function and have a better trade-off for the model predictions. The model tuning is a non-convex optimization problem, then, it presents multiple local minima, so gradient based algorithms get stuck in there. Thus, a global optimization algorithm is required to find the best parameters that fit the experimental data. The methaheuristic method referred to as particleswarm available in Matlab® is employed with the following parameters: SelfAdjustmentWeight = 1.1 and SocialAdjustmentWeight = 1.8. These values were tunned from preliminary simulation and have shown a faster convergence.

The workflow for the identification of the hybrid model 2 follows the next steps:

- a and b are estimated for each operating condition.

- $P_1, P_2, P_3, P_4, \epsilon_2, \sigma_2$ from equation 2-15 are estimated by using the values of a and b from the previous step. The Matlab function used to find these parameters was lsqcurvefit with the following options: 'StepTolerance' set to $1 \cdot 10^{-10}$ and 'FunctionTolerance' set to $1 \cdot 10^{-10}$.

The chosen statistical indexes for model performance are the adjusted determination coefficient R^2_{adj} plus the parameters and predictor confidence interval of 95 %.

2.4. Results and Discussion

2.4.1. SE-HPLC Data treatment

The concentration of the permeate stream is measured for each operating conditions. For establishing what percentage of the chromatogram is related with each molecular weight interval, the area under the curve is divided into eight regions. The retention time intervals are divided according to [8.3, 9.0, 9.8, 10.7, 11.5, 12.3, 13.2, 14.0, 15] minutes which, through the logarithmic relation, corresponds to [6705, 3636, 1755, 847, 409, 197, 95, 46, 19] kDa. The first and the last divisions are neglected in the analysis due to their relatively low contribution to the total concentration. The divisions between 9 and 14 minutes in retention time are equally spaced.

The experimental results at different BS and TBBS are depicted in table **2-4**. $R_{obs,1}$ corresponds to rejection of dextran with molecular weight between 3636 and 1755 kDa, $R_{obs,2}$ between 1755 and 847 kDa, $R_{obs,3}$ between 847 and 409 kDa, $R_{obs,4}$ between 409 and 197 kDa, $R_{obs,5}$ between 197 and 95 kDa, and $R_{obs,6}$ between 95 and 46 kDa.

Table 2-4.: Experimental data where inputs are BS and TBBS, while outputs are the observed rejection for six molecular weight intervals and flux.

BS	**TBBS**	$R_{obs,1}$ 3636 - 1755 kDa	$R_{obs,2}$ 1755 - 847 kDa	$R_{obs,3}$ 847 - 409 kDa	$R_{obs,4}$ 409 - 197 kDa	$R_{obs,5}$ 197 - 95 kDa	$R_{obs,6}$ 95 - 46 kDa	**Flux [LMH]**
0	-	0.8600	0.7736	0.6885	0.6110	0.5439	0.4729	33.60
0.25	5	0.9646	0.9227	0.8603	0.7807	0.6877	0.5466	39.42
0.75	5	0.9734	0.9636	0.9447	0.9172	0.8760	0.7980	34.67
1.25	5	0.9670	0.9597	0.9477	0.9339	0.9170	0.8799	20.26
0.25	10	0.9363	0.8642	0.7852	0.7028	0.6175	0.5126	38.36
0.75	10	0.9876	0.9714	0.9422	0.8941	0.8189	0.6911	46.35
1.25	10	0.9766	0.9614	0.9437	0.9178	0.8769	0.7888	38.58
0.25	15	0.9323	0.8627	0.7821	0.6941	0.6028	0.4860	37.57
0.75	15	0.9646	0.9481	0.9140	0.8543	0.7592	0.5865	45.98
1.25	15	0.9755	0.9647	0.9407	0.8986	0.8263	0.6800	57.64

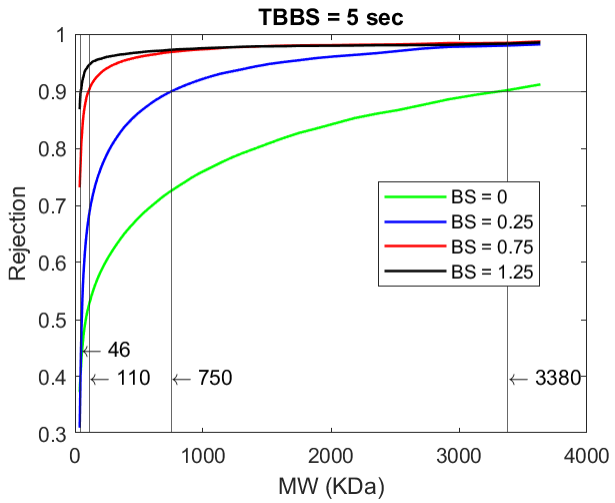

Figure 2-3.: Experimental observed rejection in a continuous spectrum under TBBS = 5 s for four values of BS: 0, 0.25, 0.75 and 1.25 s. The straight lines indicate MWCO in each operating condition. Adapted from (Inês Pereira Rosinha, 2011)

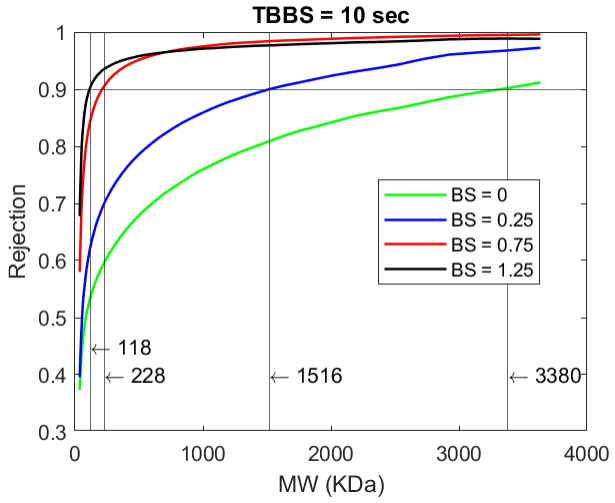

Figure 2-4.: Experimental observed rejection in a continuous spectrum under TBBS = 10 s for four values of BS: 0, 0.25, 0.75 and 1.25 s. The straight lines indicate MWCO in each operating condition. Adapted from (Inês Pereira Rosinha, 2011)

If the absorbance in permeate and feed chromatograms is directly used to compute observed rejection (Zydney and Xenopoulos, 2007; Wickramasinghe et al., 2009), a continuum spectrum is obtained (figures **2-3**, **2-4** and **2-5**). It is observed that increasing BS from 0 to 1.25 seconds, the rejection profiles are higher. It is explained from the fact that backshock system allows the disruption of the profile concentration on the feed side, since the reversed permeate stream dilutes the concentration on the boundary layer (Vinther et al., 2014b; Vinther and Jönsson, 2016a). Dextran concentration at the membrane surface on the feed side is

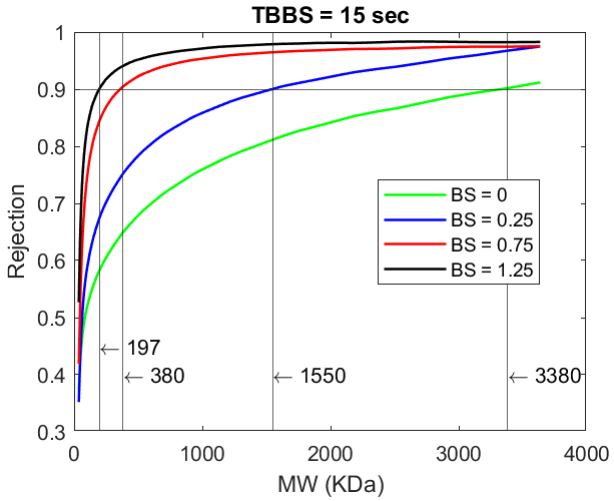

Figure 2-5.: Experimental observed rejection in a continuous spectrum under TBBS = 15 s for four values of BS: 0, 0.25, 0.75 and 1.25 s. The straight lines indicate MWCO in each operating condition. Adapted from (Inês Pereira Rosinha, 2011)

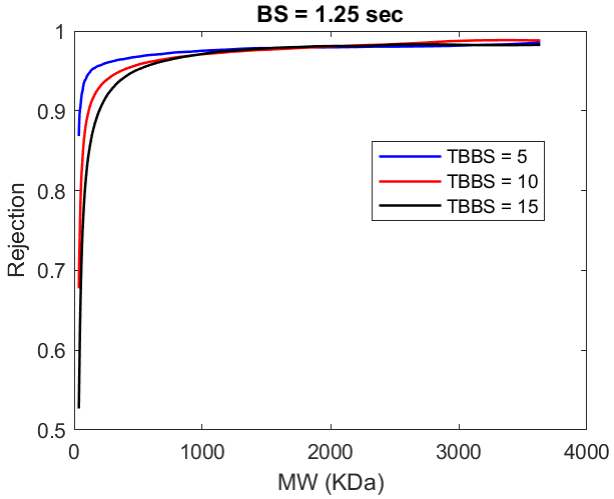

Figure 2-6.: Experimental observed rejection in a continuous spectrum under BS = 1.25 s for three values of TBBS: 5, 10 and 15 s. Adapted from (Inês Pereira Rosinha, 2011)

decreased as BS increases, so there is less probability that solute can cross the membrane and it causes the rejection values to be higher for all molecular weights with respect to static operation (no BS). So, longer times for backschock permit a larger impact on the boundary layer. This is further analzyed with the hybrid models developed in the following sections.

From (figures **2-3**, **2-4** and **2-5**) the membrane molecular weight cut off (MWCO) is reduced substantially from 3380 kDa (without BS) by a factor of 74, 28 and 17, for TBBS of

5, 10 and 15 seconds, respectively. These results disagree with the traditional perspective that separation performance is only defined by the pore size distribution of the membrane, indicating that operating conditions (BS and TBBS) can also influence significantly the separation performance.

Prior reasearch had analogous results showing how operating conditions can affect directly the MWCO of a membrane by disrupting the concentration polarization in the boundary layer by different means (Jonsson, 2008). Investigations on characterization of virus retentive membranes (Grznárová et al., 2006) have shown that the sieving curve (and threfore the MWCO) was highly correlated with important parameters such as stirring speed, TMP and flux. Zydney, A. L. and Xenopoulos, A. found that sieving coefficients and MWCO are highly influenced by changes in filtrate flux, particularly for membranes of high MWCO (Zydney and Xenopoulos, 2007). Wickramasinghe, S.R. and coworkers have stated that the MWCO of a membrane only applies under the test conditions specified by the manufacture, since MWCO is highly dependent on solute species and operating conditions (Wickramasinghe et al., 2009). Yehl, C.J. and Zydney, A.L. have investigated how operating conditions, such as effective wall shear rate and permeate flow rate can influence the MWCO of a hollow fiber membrane during dextran ultrafiltration (Yehl and Zydney, 2021). The MWCO can vary from $<$ 200 kDa to more than 1200 kDa with effective wall shear rates ranging from 2000 s^{-1} to 11000 s^{-1}. Besides, the MWCO can vary between 190 kDa and 1280 kDa for permeate flow rates between 1.7 ml/min and 10 ml/min, respectively. Analogously to the mentioned research, herein it is demostrated that using dynamic operation the separation is highly influenced by disrupting the boundary layer and even could be tuned.

From figures **2-3**, **2-4** and **2-5**, it is interesting to notice the increase of observed rejection for larger dextran molecular weight. This is explanied by the sieving mechanism that allows UF membrane to separate solutes of different size. So, dextrans with high molecular weight are expected to be more retained than the smaller ones. The sieving mechanism can be related to the probability that a solute with a specified size finds a pore large enough to pass through it, considering that the membrane has a pore size distribution.

From figure **2-6** it is evident that lower TBBS values improve substantially rejection factor especially for low molecular weight range. When using low frequency disruptions, polarization generates a reduction on solute rejection since high dextran concentration are maintained longer on the membrane surface. Hence, higher frequencies of backshock allow to keep controlled this by reducing the average solute concentration on the membrane surface, since the backshock times are in the same magnitud order as that of the development of the polarization layer. This point is further discussed in hybrid models section. For this reason, lower TBBS values have a better influence on rejection profiles.

Nevertheless, increasing BS and reducing TBBS does not garantee a better overall performance of the process, considering the trade-off between observed rejection and membrane flux. Table **2-4** indicates that increasing BS from 0.25 to 1.25 seconds, decreases the flux under TBBS of 5, however, increasing the BS under TBBS of 15 increases flux. This is a clear evidence that the effect of BS over flux depends on TBBS value. The flux reduction is generated by two situations: if the BS is too large with respect to TBBS, most of the permeate is used to wash the membrane during backshock causing a decrease in the average flux over a period of time. On the other hand, if the BS is small compared to TBBS, concentration polarization fully develops and flux declines again. For example, the flux of 20.26 LMH in table **2-4** is lower than that of static operation because in such experiment BS represents the biggest proportion of the TBBS, which means that the combination of BS = 1.25 and TBBS = 5 wastes more permeate than the other experiments.

2.4.2. Model calibration and predictive power

Hybrid model 1

The results of the parameter estimation for hybrid model 1 are presented in table **2-5**. An adjusted determination coefficient is computed for the model yielding a value of 0.9185 which is an indicator of good performance for the model.

The values for $R_{int,i}$ are in agreement with their physical interpretation. Note that $R_{int,1}$ corresponds to the highest molecular weight and $R_{int,6}$ to the lowest molecular weight. It is expected that high molecular weight solutes are rejected by the membrane in a higher probability and this is confirmed in table **2-5**. In spite of the high values for the estimated intrinsic rejections, the concentration polarization has such a dramatic impact on the performance that observed rejection is much lower compared to the intrinsic rejections, achieving values of down to 47 %.

The permeability obtained from parameter estimation (table **2-5**) is in agreement with values reported in literature under similar conditions with a membrane made of poly-ether sulfone (García-Molina et al., 2006). There, ultrafiltration of dextran with molecular weight between 36 and 44 kDa was carried out under 1 bar of TMP and a feed concentration of 1g/L. The permeability was found to be between 55 and 65 $L/(m^2 \cdot h \cdot bar)$ corresponding approximately to the confidence interval shown in table **2-5**.

Confidence intervals for each parameter do not include the zero, hence it can be said that such parameters are statistically distinct from zero and contribute to the prediction capability of the model. In addition, the confidence intervals are narrow since their corresponding percentages with respect of the nominal values are below 15 % as shown in the last column

Table 2-5.: Estimated parameters and their confidence intervals for the first hybrid model: intrinsic rejections for six molecular weight intervals and permeability.

Parameter	Value	Confidence interval (at 95 % confidence)	Confidence interval (%)
$R_{int,1}$	0.9990	0.9549 - 1.0431	± 4.41 %
$R_{int,2}$	0.9985	0.9603 - 1.0367	± 3.83 %
$R_{int,3}$	0.9977	0.9627 - 1.0327	± 3.51 %
$R_{int,4}$	0.9965	0.9581 - 1.0349	± 3.85 %
$R_{int,5}$	0.9938	0.9305 - 1.0571	± 6.37 %
$R_{int,6}$	0.9847	0.8435 - 1.1259	± 14.34 %
L_p $L/(m^2 \cdot h \cdot bar)$	56.2211	52.0216 - 60.4206	± 7.47 %

in table **2-5**.

Predictor confidence intervals are computed and illustrated in figure **2-7** for TBBS = 5 s and BS = 1.25 s, and it is observed that they include satisfactorily the experimental data. For the remaining operating conditions, the figures have a similar behaviour (results not shown). However, such intervals include values above 1 and this is not possible for the model since the observed rejections are always lower than the intrinsic rejections. So, although the predictor confidence intervals cover values above 1, the real model outputs for observed rejections are bounded up to the same values as intrinsic rejections.

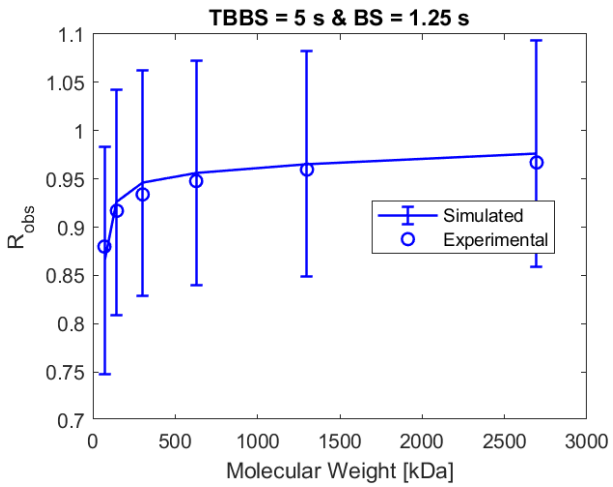

Figure 2-7.: Predictor confidence interval for hybrid model 1.

From parity plots for rejection and flux in figures **2-8** and **2-9**, it is clear that most of the points fall into the ± 15 % , only 4 out of 70 points fall outside. Such differences between the simulated data and experimental data may be due to some assumptions made during model construction, for instance, the membrane is modeled as a barrier perpendicular to the flux and the axial geometry of the hollow fiber is not considered. There are some other

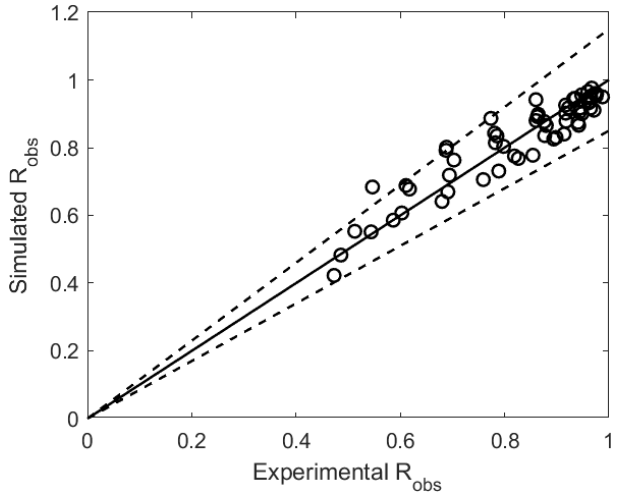

Figure 2-8.: Parity plot for observed rejections (Hybrid model 1). Dashed lines indicate ± 15 %.

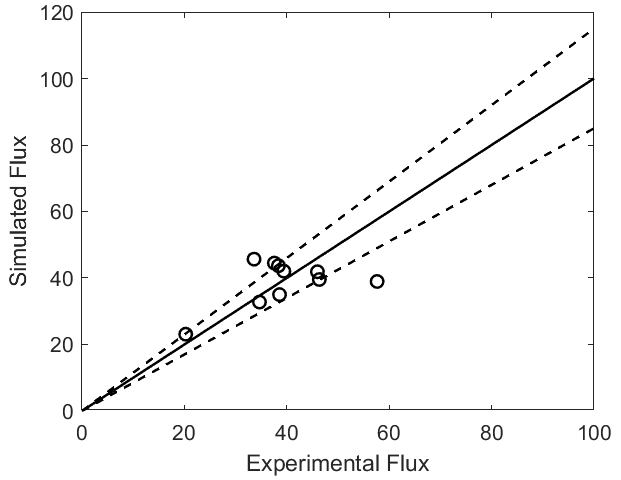

Figure 2-9.: Parity plot for fluxes in LMH (Hybrid model 1). Dashed lines indicate ± 15 %.

factors that could also be influencing such as potential fouling, the membrane asymmetry and changes in the hydrodynamic conditions of the boundary layer.

Although figures **2-8** and **2-9** seem to be a good indicator of model prediction, figures **2-10**, **2-11** and **2-12** clearly indicate that the hybrid model 1 have limitations to capture the variance in observed rejection for TBBS = 10 and TBBS = 15 (for all BS values). This shows the model flaws from a structural or phenomenological perspective. For this reason, a new hybrid model is proposed, intended to be able to predict better the observed rejections.

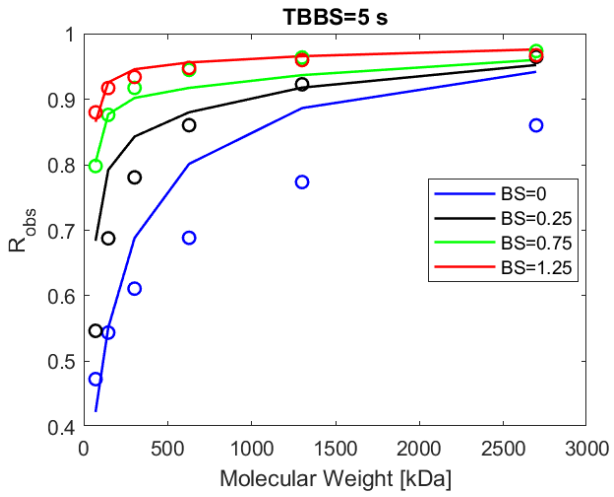

Figure 2-10.: Experimental and simulated observed rejection versus molecular weight under TBBS = 5 s for three values of BS: 0, 0.25, 0.75 and 1.25 s. (Hybrid model 1).

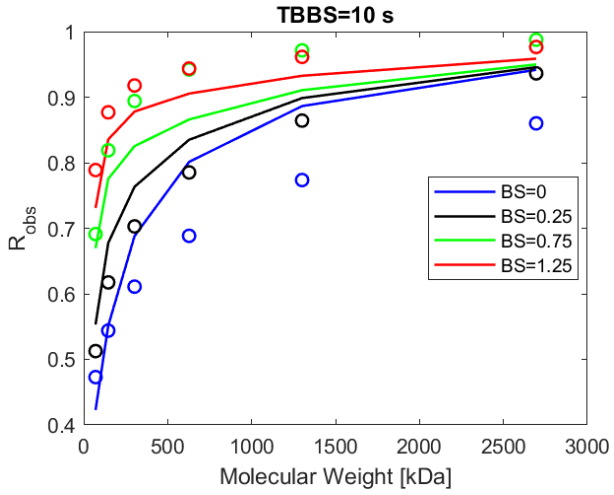

Figure 2-11.: Experimental and simulated observed rejection versus molecular weight under TBBS = 10 s for three values of BS: 0, 0.25, 0.75 and 1.25 s. (Hybrid model 1).

Hybrid model 2

From the previous model, R_{int} can be plotted versus M_W (figure **2-13**). Such a graph points out that R_{int} can be modeled by a rational function like equation 2-15a. The parameters a and b are estimated for each operation condition and they are depicted in figures **2-14** and **2-15**. It is observed that a Lennard-Jones like function can fit the values for a and b. Hence, the black box model used to predict R_{int} is summarized in equation 2-15.

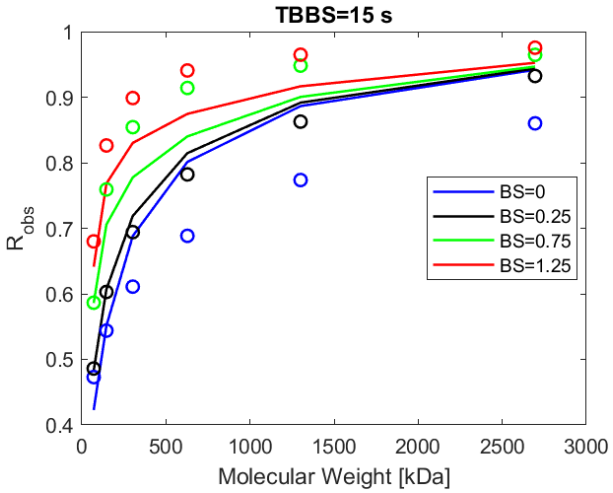

Figure 2-12.: Experimental and simulated observed rejection versus molecular weight under TBBS = 15 s for three values of BS: 0, 0.25, 0.75 and 1.25 s. (Hybrid model 1).

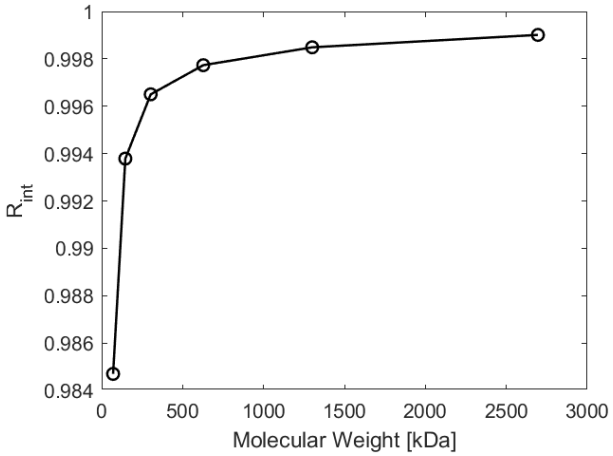

Figure 2-13.: Estimated intrinsic rejection versus molecular weight.

Equations 2-15 have 6 parameters in total to be estimated $P_1, P_2, P_3, P_4, \epsilon_2, \sigma_2$. Table **2-6** summarizes the estimated parameters and their confidence intervals. Since these parameters do not have physical interpretation, they can take any value including negatives. Their confidence intervals show that many of them lie in a wide interval but all of them are statistically different from zero, so they all contribute to the predictive capability of the hybrid model 2.

In figures **2-16** and **2-17** a parity plot for flux and observed rejection are plotted, respectively. The dots in figure **2-17** are more distributed over the 45° line indicating a better prediction for the hybrid model 2 compared to the hybrid model 1. The dots in figure **2-16** seems to be unchanged or the change was imperceptible. It points out that the black box model used to structure the intrinsic rejection in hybrid model 2 only has influence on the

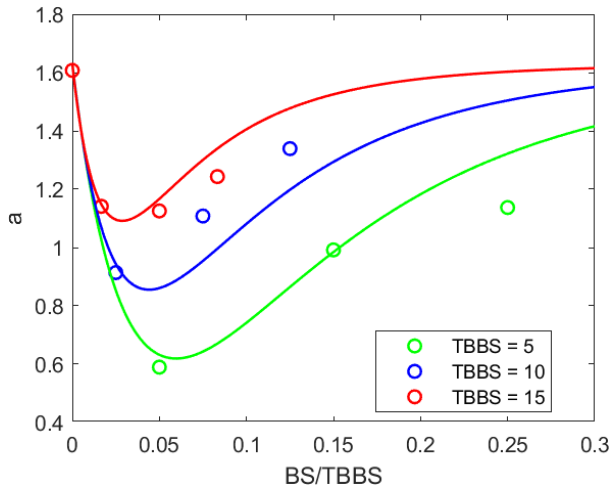

Figure 2-14.: Dependence of a parameter on BS/TBBS and TBBS. Circles represent values from estimation for each operating condition and line represents the fitted equation 2-15b

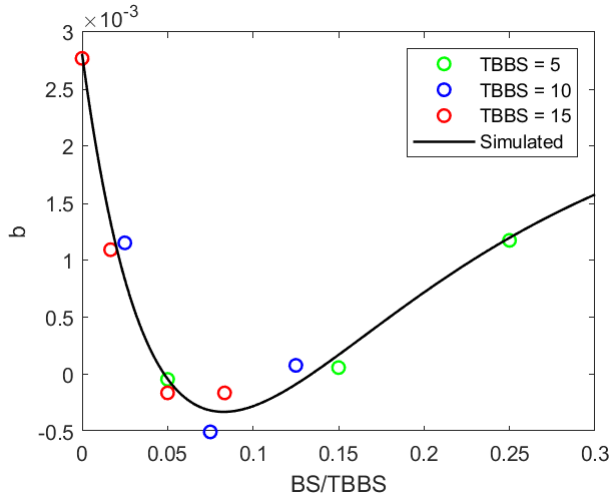

Figure 2-15.: Dependence of b parameter on BS/TBBS. Circles represent values from estimation for each operating condition and line represents the fitted equation 2-15c

observed rejections and not on the fluxes.

Considering that the maximum concentration on the membrane surface, predicted with the hybrid model 2, is almost 30 g/L (figure **2-23**), the osmotic pressure for dextran T500 is negligible compared to the operating transmembrane pressure (TMP = 0.85 bar) for dextran concentration between 0 and 30 g/L (figure **2-18**). Therefore, the flux variance in model predictions is not caused by osmotic pressures. Indeed, the flux variance predicted by the model is due to the different BS and TBBS values. So, the average flux depends on duration

Table 2-6.: Estimated parameters and their confidence intervals for the second hybrid model.

Parameter	**Value**	**Confidence interval (at 95 % confidence)**	**Confidence interval (%)**
P_1	-0.1888	-0.2214 to -0.1562	± 17.27 %
P_2	4.9861	4.8085 to 5.1637	± 3.56 %
P_3	-0.0253	-0.0399 to -0.0106	± 58.10 %
P_4	0.6129	0.4861 to 0.7398	± 20.69 %
ϵ_2	0.0125	0.0110 to 0.0141	± 12.60 %
σ_2	0.6759	0.5629 to 0.7890	± 16.73 %
L_p $L/(m^2 \cdot h \cdot bar)$	56.2211	55.7808 to 56.6614	± 0.78 %

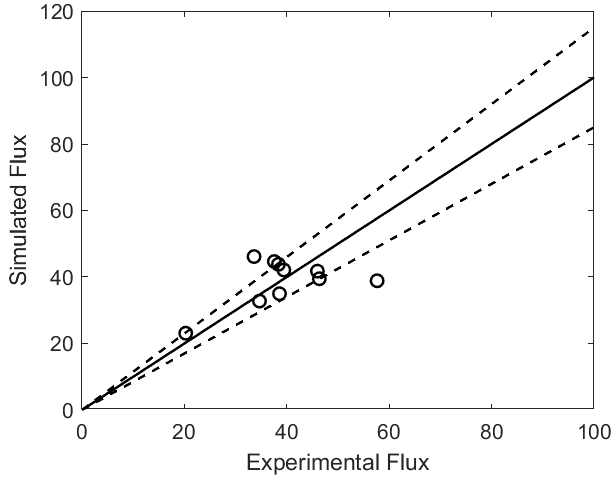

Figure 2-16.: Parity plot for fluxes (Hybrid model 2). Dashed lines indicate ± 15 %.

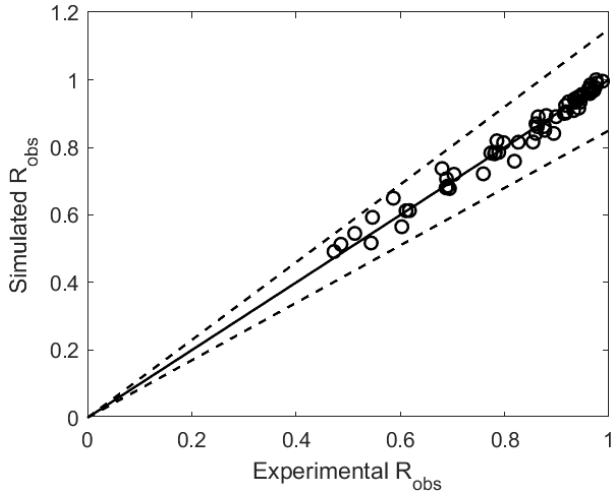

Figure 2-17.: Parity plot for observed rejections (Hybrid model 2). Dashed lines indicate ± 15 %.

and frequency of the backshock as longer BS durations imply wasting more permeate. This analysis conflicts with analysis made in CFD modelling performed by Frank and co-workers (Vinther et al., 2014a,b, 2015; Vinther and Jönsson, 2016a,b) where it is stated that flux variance in UF of dextran T500 is caused by osmotic pressure. There is a subtlety in their analysis, they state that osmotic pressures do not change significantly with molecular weight and for that reason they used the correlation for osmotic pressure of dextran T10. Using experimental data from literature, it can be seen in figure **2-18** that there is a substantial difference between osmotic pressures for dextran T500 and dextran T10, therefore, their properties can not be treated as if they were the same compound.

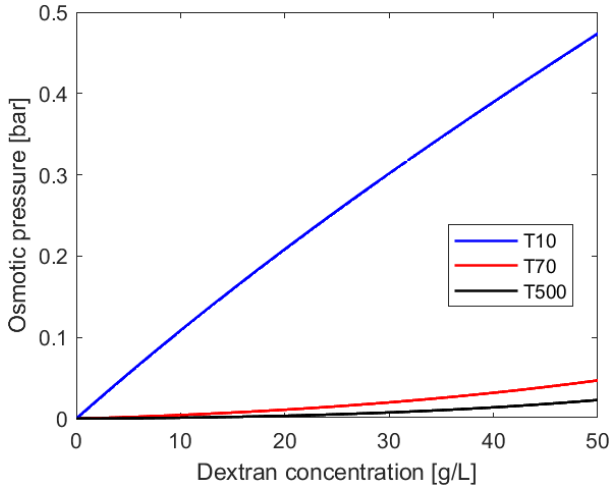

Figure 2-18.: Osmotic pressure for different dextrans: T500, T70 and T10 versus dextran concentration (Jonsson, 1984; Wijmans et al., 1985).

In figures **2-19**, **2-20**, **2-21**, observed rejection are plotted against molecular weight as before. It is evident that the hybrid model 2 has better prediction capabilities than the hybrid model 1 analyzed in the previous section. This better overall performance is confirmed when calculating the adjusted determination coefficient yielding a value of $R^2_{adj} = 0.9626$.

Besides the confidence interval of parameters, the predictor confidence interval was calculated for TBBS = 5 s and BS = 1.25 s and it is illustrated in figure **2-22**. Note that experimental data fall inside the predictor confidence interval which is narrower than the corresponding to hybrid model 1 in figure **2-7**.

A dynamic simulation for dextran concentration profiles in the boundary layer was made by using the hybrid model 2 with BS = 1.25 s and TBBS = 5 s, because it provides an insight of the phenomena occurring there. This simulation allows to know the maximum concentration achieved on the membrane surface predicted by the model and understand the effect of dynamic operation on the concentration profiles over the boundary layer. The results are

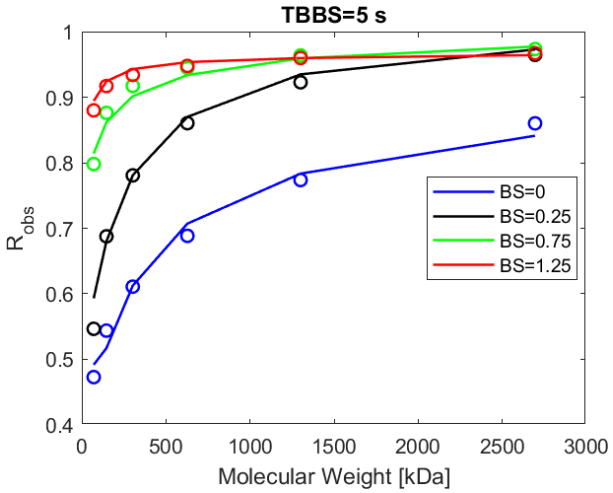

Figure 2-19.: Experimental and simulated (Hybrid model 2) observed rejection versus molecular weight under TBBS = 5 s for different BS = 0, 0.25, 0.75 and 1.25 s.

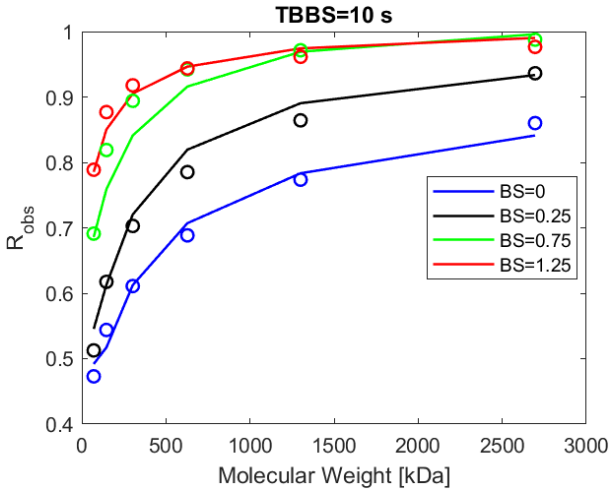

Figure 2-20.: Experimental and simulated (Hybrid model 2) observed rejection versus molecular weight under TBBS = 10 s for different BS = 0, 0.25, 0.75 and 1.25 s.

plotted in figures **2-23** and **2-24**. In figure **2-23** the boundary layer is about 15 μm which is in agreement with the value of 20 μm reported in literature as a typical number for many applications (Baker, 2012). It can be oserved that dextran concentration at the membrane surface can achieved values of almost 30 g/L (figure **2-23**), that is, thirty times the feed concentration. This concentration polarization is mitigated by the backshock system as observed in figure **2-24**. For TBBS of 10 and 15 s, this high concentration value is kept a longer time because the backshock is performed at lower frequency. This result confirms that high dextran concentrations at the membrane surface affect strongly the rejection factors under different operation conditions and that dynamic operation is an efficient method to mitigate concentration polarization as seen before in figures **2-3**, **2-4** and **2-5**.

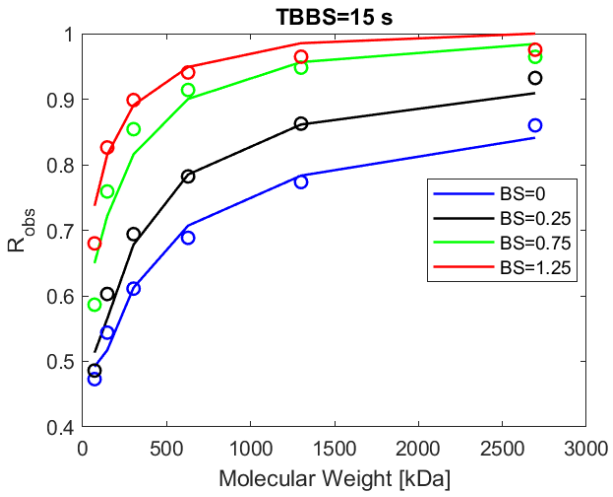

Figure 2-21.: Experimental and simulated (Hybrid model 2) observed rejection versus molecular weight under TBBS = 15 s for different BS = 0, 0.25, 0.75 and 1.25 s.

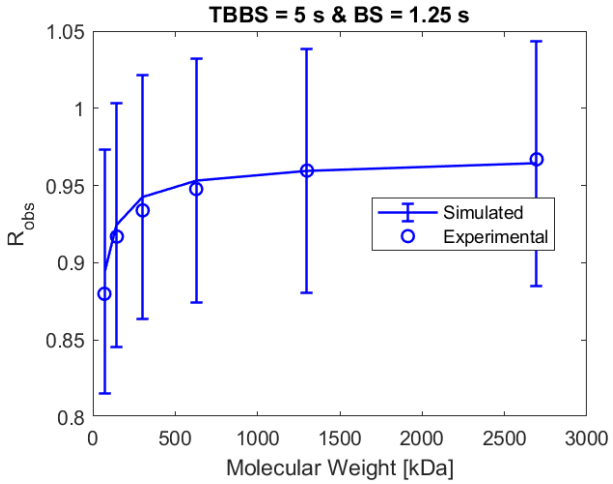

Figure 2-22.: Predictor confidence interval for hybrid model 2.

Since static operation does not use permeate to wash the membrane and dextran T500 has negligible osmotic pressures for concentrations between 0 and 30 g/L, the hybrid model 2 predicts that the maximum flux corresponds to static operation. This fact leads to consider that the concentration on the membrane surface should achieve values higher than 30 g/L, so more significant osmotic pressures can be obtained and maximum flux can correspond to dynamic operation. In fact, it has been reported dextran concentrations (dextran T70) on the membrane surface as high as 177 g/L with a feed concentration of 0.935 g/L under TMP of 2 bar with no BS (Wijmans et al., 1985). Since diffusivity is the main parameter influencing the maximum concentration that dextran can achieve on the membrane surface, the assumption that dextran diffusivity does not depend on concentration is questionable or

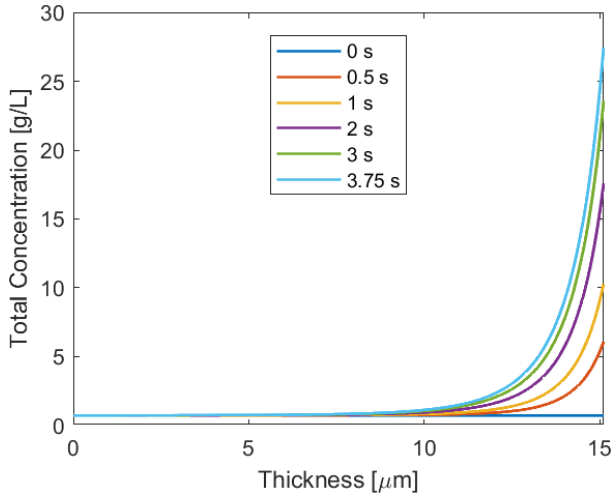

Figure 2-23.: Total dextran concentration in boundary layer during normal operation at 0, 1, 2, 3, 3.75 s.

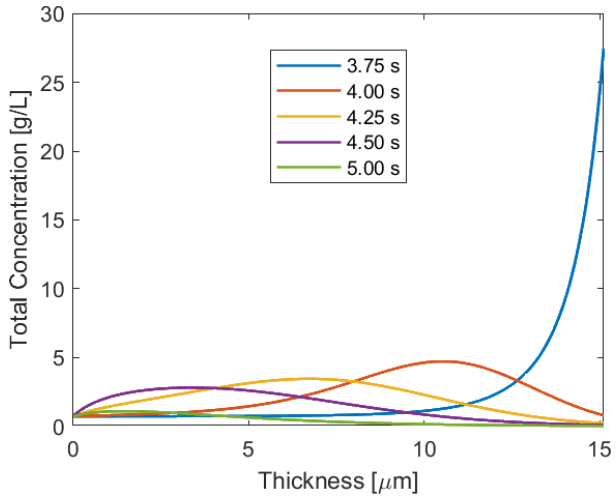

Figure 2-24.: Total dextran concentration in boundary layer during backshock operation at 3.75, 4, 4.25, 4.5, 5 s.

perhaps the correlation itself for diffusivity could be no appropriate for this application or maybe there could be extra phenomena not yet included in the model.

Despite the model limitations, it is evident that most of the variance in experimental data is explained by the model with a high degree of precision.

2.5. Conclusions

Dynamic operation in ultrafiltration, by means of a backshock, have a tremendous effect on the MWCO where it can be tuned from 3380 kDa to values between 46 and 197 kDa, corresponding to a separation intensification in factors of 74 and 17 times, respectively. Two hybrid models were developed with different degree of hybridization. The first achieved an adjusted determination coefficient of 0.9185 while the second 0.9626. This indicates that the modifications introduced into the second hybrid model allow increasing the prediction power significantly.

The results of the present investigation reinforce that separation performance not only depends on physical properties of the membrane and solute but it can also be directly manipulated by means of dynamic operation. The idea that operating conditions can modify the MWCO of a membrane has been recently mentioned in literature but it is not very popularized, so it is necessary that this novel paradigm of separation performance in UF and MF must be spread out in membrane sciences since its applications allow intensifying the UF and MF processes.

The development of hybrid mathematical models for dynamic UF done in this paper open new opportunities for optimization of process design and operation. Additionally, both hybrid models can be used to provide further process insights and can serve as building blocks for developing models including more phenomena beyond concentration polarization. By using the models developed here as building blocks, future research work could include precipitation, gel formation and fouling.

References

Azevedo, C. R., Díaz, V. G., Prado-Rubio, O. A., Willis, M. J., Préat, V., Oliveira, R., and Stosch, M. (2019). Hybrid Semiparametric Modeling: A Modular Process Systems Engineering Approach for the Integration of Available Knowledge Sources. In *Syst. Eng. Fourth Ind. Revolut.*, number January 2020, pages 345–373. Wiley.

Baker, R. W. (2012). *Membrane Technology and Applications*. John Wiley & Sons, 3 edition.

Bakhshayeshi, M., Kanani, D. M., Mehta, A., van Reis, R., Kuriyel, R., Jackson, N., and Zydney, A. L. (2011a). Dextran sieving test for characterization of virus filtration membranes. *J. Memb. Sci.*, 379(1-2):239–248.

Bakhshayeshi, M., Zhou, H., Olsen, C., Yuan, W., and Zydney, A. L. (2011b). Understanding dextran retention data for hollow fiber ultrafiltration membranes. *J. Memb. Sci.*, 385-386:243–250.

Basedow, A. M. and Ebert, K. H. (1979). Production, characterization, and solution properties of dextran fractions of narrow molecular weight distributions. *J. Polym. Sci. Polym. Symp.*, 66(1):101–115.

Bird, R. B., Stewart, W. E., and Lightfoot, E. N. (2002). *Transport phenomena*. J. Wiley, 2nd, wiley edition.

Borujeni, E. E., Li, Y., and Zydney, A. L. (2015). Application of periodic backpulsing to reduce membrane fouling during ultrafiltration of plasmid DNA. *J. Memb. Sci.*, 473:102–108.

Byhlin, H. and Jönsson, A.-S. (2003). Influence of adsorption and concentration polarisation on membrane performance during ultrafiltration of a non-ionic surfactant. *Desalination*, 151(1):21–31.

Chen, H. and Kim, A. S. (2006). Prediction of permeate flux decline in crossflow membrane filtration of colloidal suspension: a radial basis function neural network approach. *Desalination*, 192(1-3):415–428.

Chen, M., Shafer-Peltier, K., Randtke, S. J., and Peltier, E. (2018). Modeling arsenic (V) removal from water by micellar enhanced ultrafiltration in the presence of competing anions. *Chemosphere*, 213:285–294.

Chew, C. M., Aroua, M., and Hussain, M. (2017). A practical hybrid modelling approach for the prediction of potential fouling parameters in ultrafiltration membrane water treatment plant. *J. Ind. Eng. Chem.*, 45:145–155.

Gao, Y., Qin, J., Wang, Z., and Østerhus, S. W. (2019). Backpulsing technology applied in MF and UF processes for membrane fouling mitigation: A review. *J. Memb. Sci.*, 587:117136.

García-Molina, V., Esplugas, S., Wintgens, T., and Melin, T. (2006). Ultrafiltration of aqueous solutions containing dextran. *Desalination*, 188(1-3):217–227.

Gaspar, V. M., Moreira, A. F., de Melo-Diogo, D., Costa, E. C., Queiroz, J. A., Sousa, F., Pichon, C., and Correia, I. J. (2016). Multifunctional nanocarriers for codelivery of nucleic acids and chemotherapeutics to cancer cells. In *Nanobiomaterials Med. Imaging*, pages 163–207. Elsevier.

Grisales Díaz, V. H., Prado-Rubio, O. A., Willis, M. J., and von Stosch, M. (2017). Dynamic hybrid model for ultrafiltration membrane processes. pages 193–198.

Grzegorzek, M. and Majewska-Nowak, K. (2018). The use of micellar-enhanced ultrafiltration (MEUF) for fluoride removal from aqueous solutions. *Sep. Purif. Technol.*, 195:1–11.

Grznárová, G., Viktorin, M., and Lang, A. (2006). Characterization of virus retentive membranes by a tailor-made dextran method. *Desalination*, 200(1-3):297–298.

Inês Pereira Rosinha (2011). High frequency backshock effect on ultrafiltration of selected polysaccharides. Master thesis. Universidade Técnica de Lisboa & Technical University of Denmark.

Jönsson, A.-S., Jönsson, B., and Byhlin, H. (2006). A concentration polarization model for the ultrafiltration of nonionic surfactants. *J. Colloid Interface Sci.*, 304(1):191–199.

Jonsson, G. (1980). Overview of theories for water and solute transport in9 UF/RO membranes. *Desalination*, 35:21–38.

Jonsson, G. (1984). Boundary layer phenomena during ultrafiltration of dextran and whey protein solutions. *Desalination*, 51(1):61–77.

Jonsson, G. (2008). Tuning of the cut-off curves by dynamic ultrafiltration. In *Proc. Int. Conf. Membr. Membr. Process. ICOM2008*, Hawaii.

KRISHNAKUMAR, N., YEA, M., and CHERYAN, M. (2004). Ultrafiltration of soy protein concentrate: performance and modelling of spiral and tubular polymeric modules. *J. Memb. Sci.*, 244(1-2):235–242.

KWON, B., MOLEK, J., and ZYDNEY, A. (2008). Ultrafiltration of PEGylated proteins: Fouling and concentration polarization effects. *J. Memb. Sci.*, 319(1-2):206–213.

Macedo, A., Duarte, E., and Pinho, M. (2011). The role of concentration polarization in ultrafiltration of ovine cheese whey. *J. Memb. Sci.*, 381(1-2):34–40.

Neggaz, Y., Vargas, M. L., Dris, A. O., Riera, F., and Alvarez, R. (2007). A combination of serial resistances and concentration polarization models along the membrane in ultrafiltration of pectin and albumin solutions. *Sep. Purif. Technol.*, 54(1):18–27.

Peinemann, K.-V. and Nunes, S. P. (2010). *Membranes for water treatment*. John Wiley & Sons.

Prado-Rubio, O. A. and von Stosch, M. (2017). Towards Sustainable Flux Determination for Dynamic Ultrafiltration through Multivariable System Identification. In *27th Eur. Symp. Comput. Aided Process Eng.*, volume 3, pages 2719–2724.

Pu, Y., Zou, Q., Liu, L., Han, Z., Wang, X., Wang, Q., and Chen, S. (2012). Clinical dextran purified by fractional ultrafiltration coupled with water washing. *Carbohydr. Polym.*, 87(2):1257–1260.

Sahoo, G. B. and Ray, C. (2006). Predicting flux decline in crossflow membranes using artificial neural networks and genetic algorithms. *J. Memb. Sci.*, 283(1-2):147–157.

Salladini, A., Prisciandaro, M., and Barba, D. (2007). Ultrafiltration of biologically treated wastewater by using backflushing. *Desalination*, 207(1-3):24–34.

Saltık, M. B., Özkan, L., Jacobs, M., and van der Padt, A. (2017). Dynamic modeling of ultrafiltration membranes for whey separation processes. *Comput. Chem. Eng.*, 99:280–295.

Scott, K. (1996). *Handbook of Industrial Membranes*. Elsevier Science, 1st edition.

Shi, L., Huang, J., Zhu, L., Shi, Y., Yi, K., and Li, X. (2019). Role of concentration polarization in cross flow micellar enhanced ultrafiltration of cadmium with low surfactant concentration. *Chemosphere*, 237:124859.

Song, E.-H., Shang, J., and Ratner, D. (2012). Polysaccharides. In *Polym. Sci. A Compr. Ref.*, pages 137–155. Elsevier.

Srijaroonrat, P., Julien, E., and Aurelle, Y. (1999). Unstable secondary oil/water emulsion treatment using ultrafiltration: fouling control by backflushing. *J. Memb. Sci.*, 159(1-2):11–20.

Stankiewicz, A. I. and Moulijn, J. A. (2000). Process intensification: transforming chemical engineering. *Chem. Eng. Prog.*, 96(1):22–34.

Tkacik, G. and Michaels, S. (1991). A Rejection Profile Test for Ultrafiltration Membranes & Devices. *Bio/Technology*, 9(10):941–946.

Verma, S. P. and Sarkar, B. (2017). Rhamnolipid based micellar-enhanced ultrafiltration for simultaneous removal of Cd(II) and phenolic compound from wastewater. *Chem. Eng. J.*, 319:131–142.

Verma, S. P. and Sarkar, B. (2018). Simultaneous removal of Cd (II) and p-cresol from wastewater by micellar-enhanced ultrafiltration using rhamnolipid: Flux decline, adsorption kinetics and isotherm studies. *J. Environ. Manage.*, 213:217–235.

Vinther, F. and Jönsson, A.-S. (2016a). Modelling of optimal back-shock frequency in hollow fibre ultrafiltration membranes I: Computational fluid dynamics. *J. Memb. Sci.*, 506:130–136.

Vinther, F. and Jönsson, A.-S. (2016b). Modelling of optimal back-shock frequency in hollow-fibre ultrafiltration membranes II: Semi-analytical mathematical model. *J. Memb. Sci.*, 506:137–143.

Vinther, F., Pinelo, M., Brøns, M., Jonsson, G., and Meyer, A. S. (2014a). Mathematical modelling of dextran filtration through hollow fibre membranes. *Sep. Purif. Technol.*, 125:21–36.

Vinther, F., Pinelo, M., Brøns, M., Jonsson, G., and Meyer, A. S. (2014b). Predicting optimal back-shock times in ultrafiltration hollow fibre modules through path-lines. *J. Memb. Sci.*, 470:275–293.

Vinther, F., Pinelo, M., Brøns, M., Jonsson, G., and Meyer, A. S. (2015). Predicting optimal back-shock times in ultrafiltration hollow fiber modules II: Effect of inlet flow and concentration dependent viscosity. *J. Memb. Sci.*, 493:486–495.

Wickramasinghe, S. R., Bower, S. E., Chen, Z., Mukherjee, A., and Husson, S. M. (2009). Relating the pore size distribution of ultrafiltration membranes to dextran rejection. *J. Memb. Sci.*, 340(1-2):1–8.

Wijmans, J., Nakao, S., Van Den Berg, J., Troelstra, F., and Smolders, C. (1985). Hydrodynamic resistance of concentration polarization boundary layers in ultrafiltration. *J. Memb. Sci.*, 22(1):117–135.

Yee, K. W., Wiley, D. E., and Bao, J. (2009). A unified model of the time dependence of flux decline for the long-term ultrafiltration of whey. *J. Memb. Sci.*, 332(1-2):69–80.

Yehl, C. J. and Zydney, A. L. (2021). Characterization of dextran transport and molecular weight cutoff (MWCO) of large pore size hollow fiber ultrafiltration membranes. *J. Memb. Sci.*, 622:119025.

Zaidi, S. and Kumar, A. (2004). Experimental studies in the dead-end ultrafiltration of dextran: analysis of concentration polarization. *Sep. Purif. Technol.*, 36(2):115–130.

Zarrintaj, P., Saeb, M. R., Jafari, S. H., and Mozafari, M. (2020). Application of compatibilized polymer blends in biomedical fields. In *Compat. Polym. Blends*, pages 511–537. Elsevier.

Zydney, A. L. and Xenopoulos, A. (2007). Improving dextran tests for ultrafiltration membranes: Effect of device format. *J. Memb. Sci.*, 291(1-2):180–190.

3. Model-based sensitivity analysis of dynamic ultrafiltration

3.1. Abstract

Optimization of design and operation has been a challenging task to implement in microfiltration (MF) and ultrafiltration (UF) systems since there is a lack of robust mathematical models that can predict the time variant behavior of the system under different conditions (input disturbances). In a previous research, a hybrid mathematical model was developed in order to have a high fidelity reproduction of MF and UF systems (López-Murillo et al., 2021). This model also has the ability to predict the behavior of filtration systems under dynamic operation which can intensify the membrane performance in terms of selectivity while keeping high fluxes. Herein, such mathematical model is exploited to explore the UF system under dynamic operation at different scenarios to provide system understanding. In this sense, a sensitivity analysis is performed to evaluate the separation performance in terms of flux and rejection factor as a function of input variables: backshock time (BS), time between backshocks (TBBS), dextran bulk concentration (C_b). The sensitivity analysis allows finding interesting operational regions where high fluxes can be achieved while keeping acceptable rejection factor. The investigated system is the dynamic ultrafiltration of an aqueous solution of dextran T500. In order to highlight the advantages of applying dynamic operation instead of conventional filtration, a comparative analysis is performed between a membrane with low MWCO under conventional cross-flow operation and a membrane with high MWCO under dynamic operation.

From modeling results, concentration polarization is well diagnosed by concentration polarization modulus. Values for this modulus as high as 160 have a negative impact on observed rejection, while values close or lower than 34 improve selectivity. Average flux can be improved up to 43.8 % with BS = 1 s and TBBS = 5 s. Regarding the comparative analysis, membrane cost savings can achieve values around 50 % by using a membrane of high MWCO under dynamic operation.

3.2. Introduction

Ultrafiltration (UF) and microfiltration (MF) are interesting in separation processes where mild conditions are required to achieve high separation performance (Neggaz et al., 2007; KWON et al., 2008; Macedo et al., 2011). Hence, there is a great potential to exploit these technologies for separation of metabolites in bioprocesses to be considered as one of the major applications. MF and UF have a remarkable performance in terms of selectivity, throughput, product purity, reduction in chemical usage, mild operating conditions, compactness, carbon footprint reduction, energy saving and process safety (Charcosset, 2006; Abels et al., 2013; Wei et al., 2014; Prado-Rubio et al., 2016). Nevertheless, the advantages of these membrane technologies can be countered by two coupled phenomena referred to as concentration polarization and fouling (Peinemann and Nunes, 2010; Baker, 2012), where flux and selectivity are mainly affected during operation. These phenomena can be aggravated, if the solute can generate a significant osmotic pressure at the membrane surface. Since concentration polarization allows the formation of concentration profiles over the boundary layer as solute is being retained, the driving force (TMP) can be reduced by the osmotic pressure exerted by the high solute concentration achieved at the membrane surface.

Several techniques have been developed to mitigate concentration polarization and fouling such as turbulence promoters, pulsed flow (dynamic flow), rotating membranes, ultrasonic enhancement, periodic maintenance cleaning, periodic backwash with permeate or gas (dynamic operation), among others (Peinemann and Nunes, 2010). Within the options, the so called "dynamic operation"have the ability of intensifying the separation process and tuning the MWCO of the membrane, which allows a flexible performance adjustment (López-Murillo et al., 2021). During dynamic operation in filtration systems, the flow is periodically reverted from permeate to retentate side during a specified amount of time (backshock time, BS) with a determined periodicity (time between backshocks, TBBS). This strategy allows the disruption of the concentration profiles over the boundary layer. Such disruption is accomplished by diluting the high concentration at the membrane surface and removing some of the retained particles, thus concentration polarization and fouling are mitigated, and separation performance is improved (Jonsson and Prado-Rubio, 2011; López-Murillo et al., 2021).

Due to the inherent complexity of dynamic membrane filtration, mathematical modeling of dynamic MF and UF processes is key for establishing the most appropriate operating conditions for a given target. Several models have been developed in order to predict the behavior of MF and UF systems but most of them are black box approaches with the following limitations: (a) they only predict the flux but neither the rejection factor nor selectivity, (b) their predictions are limited to the range where the data were extracted (i.e. low extrapolation capabilities), (c) they can not be used in other applications, (d) most of the models can only predict the static behavior of the filtration process (expected in crossflow systems below

critical flux operation) (López-Murillo et al., 2021).

Recently, a hybrid mathematical model was successfully developed to predict the dynamic UF process and overcome the limitations from previous models (López-Murillo et al., 2021). This mathematical representation can be used to explore different operating conditions, saving time and economic resources. The case study used in López-Murillo et al. (2021) is the dynamic ultrafiltration of an aqueous solution of dextran T500, since dextran is a biomolecule widely used in the food, clinical and pharmaceutical field, and it is also used for membrane characterization (Bakhshayeshi et al., 2011; Pu et al., 2012; Gaspar et al., 2016; Zarrintaj et al., 2020). Dextran purification and fractionation have been previously investigated (see Table **3-1**). Research has been focused on membrane separation processes such as nanofiltration, ultrafiltration and microfiltration as part of the procedure for separating dextrans with a specified molecular weight. In general terms, microfiltration (MF), ultrafiltration (UF) and nanofiltration (NF) are used to concentrate and purify aqueous dextran solutions. First, high molecular weight dextrans are produced via fermentation by using *Leuconostoc mesenteroides*, and then, concentrated by MF membranes (Díaz-Montes et al., 2020). Dextran molecular weights from $5 \cdot 10^3 - 40 \cdot 10^3$ kDa can be achieved (Mountzouris et al., 2002). By means of an enzymatic hidrolysis procedure, industrial grade dextran can be transformed into oligodextrans with a broad range of M_W and then concentrated with UF or NF membranes (Mountzouris et al., 1999, 2002; Torras et al., 2008; Pinelo et al., 2009; Pu et al., 2012; Su et al., 2018).

Table 3-1.: Dextran separation using membrane technologies.

Title	Process	MWCO	Membrane material	TMP	Flux	Performance	Reference
Microfiltration-mediated extraction of dextran produced by *Leuconostoc mesenteroides SF3*	MF and MDF	0.1 μm	Polysulfone	0.4 - 1.7 bar	8 - 16 $kg\,m^{-2}\,h^{-1}$	Yield: 22.48 $g\,L^{-1}$	(Díaz-Montes et al., 2020)
Modeling and optimal operation of intermittent feed diafiltration for refining oligodextran using nanoporous ceramic membranes	UF and UDF	2 kDa	ZrO_2 and $\alpha - Al_2O_3$	0.7 MPa	25 - 165 LMH	Rejection: 82 % - 94 %	(Qi et al., 2020)
Directing filtration to narrow molecular weight distribution of oligodextran in an enzymatic membrane reactor	UF in enzymatic membrane reactor	20 kDa	Polyether sulfone	3 bar	34- 45 LMH	Yield: 50 %	(Su et al., 2018)

Continuation of Table **3-1**

Title	Process	MWCO	Membrane material	TMP	Flux	Performance	Reference
Clinical dextran purified by fractional ultrafiltration coupled with water washing	Fractional UF	100 kDa 30 kDa 1 kDa	No available	0.2 MPa	42- 82 32 - 40 6- 7 LMH	D value: 5.4, 2.2, 2.5, 3.4	(Pu et al., 2012)
Membrane technology for purification of enzymatically produced oligosaccharides: Molecular and operational features affecting performance	A review that provides an overview of the available knowledge about the behaviour of enzymatically produced carbohydrate-based oligo- and polysaccharides during membrane separation						(Pinelo et al., 2009)
Composite polymeric membranes for process intensification: Enzymatic hydrolysis of oligodextrans	Dextran separation and purification was performed through an enzymatic membrane reactor made of polysulfone and activated carbon loaded with dextranase. Their results are focused on (1) enzyme activity, (2) enzyme adsorption by the activated carbon, (3) characterization of the designed enzyme membrane reactor and (4) average molecular weight of dextran present in product.						(Torras et al., 2008)
Continuous production of oligodextrans via Controlled Hydrolysis of Dextran in an Enzyme Membrane Reactor	UF	10 kDa	No available	100 kPa	No available	Yield: 84.4 % - 98.7 %	(Mountzouris et al., 2002)
Modeling of oligodextran production in an ultrafiltration stirred-cell membrane reactor	UF	10 kDa	No available	200 - 400 kPa	0.01 - 0.11 ml $cm^{-2}min^{-1}$	Yield: 25 %- 84 %	(Mountzouris et al., 1999)

The main purpose of this contribution is to use the previously developed hybrid mathematical model from López-Murillo et al. (2021) to investigate different scenarios of dextran UF separation. This research aims to find interesting operational regions where high fluxes can be obtained while keeping high selectivity. Additionally, modeling results allows designing processes where economic savings can be achieved by using a high MWCO membrane under dynamic operation instead of a low MWCO membrane under conventional cross-flow operation. This approach demonstrates the usefulness and relevance of PSE strategies to screen for operating conditions given a required separation performance. First, dynamic simulations are performed to determine the membrane flux, the time dependent concentration profiles at the membrane surface, the concentration in the permeate stream, and the observed rejection for the UF of an aqueous solution of dextran T500 (section 3.3.2). Such simulations allow understanding how these variables evolve with time under specified values of dextran bulk concentration (C_b), backshock times (BS) and time between backshocks (TBBS). Subsequently, a stationary analysis is made as a function of C_b, BS and TBBS, by extracting some features after the cycles become stationary (section 3.3.3). This analysis is convenient

to summarize the simulation results from different operating conditions in a compact form. Finally, aiming to highlight the benefits of using dynamic operation instead of conventional filtration, a comparative analysis is performed (section 3.3.4) by computing the average flux and observed rejection for two membranes modules with different MWCO, one being operated under dynamic conditions and the other under conventional cross-flow conditions (without backshock).

This contribution is structured as follows. The methodology presents a summary of the hybrid mathematical model, the dynamic operation analysis, the stationary operation analysis and the comparative analysis for dextran separation. The results section shows the models prediction according to the operating conditions defined in methodology. Finally the conclusions are drawn.

3.3. Methodology

Previously, a hybrid model has been developed for a dynamic UF system for an aqueous solution of dextran T500 (López-Murillo et al., 2021). Then, the dextran is concentrated into the retentate stream and a permeate flow passes through the membrane where mainly water is extracted. The permeate is collected in a small tank where part of it is periodically reversed to generate the dynamic operation. The membrane module is a hollow fiber system with poly-ether sulfone membrane from X-flow Membranes (The Netherland). The module has dimensions of 2.4 cm for shell diameter, 54 cm for length, 1.5 mm in tubes diameter and has 50 tubes, corresponding to 0.1 m^2 of membrane area. The cross-flow velocity used for operation is $V_{cross} = 0.509$ m/s (Rosinha, 2011; Jonsson and Prado-Rubio, 2011; López-Murillo et al., 2021).

3.3.1. Hybrid mathematical modeling description

The hybrid model describes the transient behavior of the physico-chemical phenomena at the boundary layer adjacent to the membrane surface in the retentate side. Differential mass balances are formulated for dextran where two transport mechanisms are present: diffusive and convective. Diffusion is represented by Fick's law and convection by Darcy's law. It is assumed that MF and UF membranes retain solutes by means of a sieving action. Additionally, the model considers: (i) the osmotic pressure generated by high dextran concentrations at the membrane surface as a result of concentration polarization, and (ii) the reversed permeate flux during periodic backshocks. The solution of this model displays the temporal evolution of concentration profiles and permeate flux (López-Murillo et al., 2021).

The hybrid model is represented by Equations 3-1 - 3-11 and a brief explanation of each one is presented next. The description of each variable and parameter is displayed in Table **2-2**. The values of the parameters and assumptions used for the simulations are taken from López-Murillo et al. (2021).

Differential mass balance of dextran over the boundary layer adjacent to the membrane surface for each molecular weight:

$$\frac{\partial C_i}{\partial t} = D_i \frac{\partial^2 C_i}{\partial x^2} - J_v \frac{\partial C_i}{\partial x} \tag{3-1}$$

Boundary conditions at the membrane surface and bulk solution:

$$\begin{cases} J_v C_i - D_i \frac{\partial C_i}{\partial x}\big|_{x=\delta} = J_s \\ C_i|_{x=0} = C_{ib} \end{cases} \tag{3-2}$$

Mass balances for the permeate tank:

$$\frac{dv}{dt} = J_v \cdot A_m - v_{out} \tag{3-3}$$

$$\frac{dC_{Ti}}{dt} = \frac{J_v \cdot A_m \cdot C_{ip} - v_{out} \cdot C_{Ti} - C_{Ti} \cdot \frac{dv}{dt}}{v} \tag{3-4}$$

Black box model for dextran diffusivity:

$$D = \alpha \cdot (M_W)^{\beta} \tag{3-5}$$

Total flux expression by modified Darcy's law:

$$\begin{cases} J_v = L_p(TMP - \Delta\pi) & Forward\ flux \\ J_v = -L_p \cdot \Delta P_{BS} & Backward\ flux \end{cases} \tag{3-6}$$

Osmotic pressure correlation:

$$\pi = A_1 \cdot c + A_2 \cdot c^2 + A_3 \cdot c^3 \tag{3-7}$$

Solute flux expression:

$$J_s = J_v C_{ip} \tag{3-8}$$

$$C_{ip} = (1 - R_{int}) C_{im} \tag{3-9}$$

Black box model for R_{int}:

$$R_{int} = min\left(1 - \frac{1 + b \cdot (1 + a \cdot M_W)}{1 + a \cdot M_W}, 1\right) \tag{3-10a}$$

$$a = \epsilon_1 \cdot \left[\left(\frac{\sigma_1}{BS/TBBS + \sigma_1}\right)^{12} - \left(\frac{\sigma_1}{BS/TBBS + \sigma_1}\right)^{6}\right] + 1.63 \tag{3-10b}$$

$$b = \epsilon_2 \cdot \left[\left(\frac{\sigma_2}{BS/TBBS + \sigma_2}\right)^{12} - \left(\frac{\sigma_2}{BS/TBBS + \sigma_2}\right)^{6}\right] + 2.808 \cdot 10^{-3} \tag{3-10c}$$

$$\epsilon_1 = P_1 \cdot TBBS + P_2 \tag{3-10d}$$

$$\sigma_1 = P_3 \cdot TBBS + P_4 \tag{3-10e}$$

Observed rejection expression for each molecular weight interval:

$$R_{obs,i} = 1 - \frac{C_{i,T}}{C_{i,b}} \tag{3-11}$$

Global observed rejection expression:

$$R_{obs} = 1 - \frac{C_T}{C_b} \tag{3-12}$$

The partial differential equations are solved by using the method of lines, discretizing the derivatives by centered finite differences with 1000 nodes in space and solving the remaining ordinary differential equations with a solver for stiff ODE's - ode15s - in Matlab® version 2019b. The relative and absolute tolerance for ode15s are both set as $1 \cdot 10^{-8}$.

3.3.2. Dynamic Operation analysis

The effect of dextran bulk concentration C_b, backshock time BS, and time between backshocks TBBS on the separation performance is shown through the analysis of the dextran concentration achieved at the membrane surface, and its influence on the flux and observed rejection. Therefore, time profiles of these variables are crucial for obtaining insights into the phenomena occurring during filtration. In this regard, two simulation scenarios are performed: one with $C_b = 1$ g/L and the other with $C_b = 10$ g/L. Both of them are evaluated with TMP = 0.85 bar, TBBS = 5 s, BS = 1.25 s. Flux J_v, concentration at the membrane surface C_m and concentration at the permeate tank $C_{i,T}$ are computed for each instant of time. The observed rejection for each molecular weight interval is calculated by using the concentrations at the permeate tank (Equation 3-11).

3.3.3. Stationary Operation analysis

Although dynamic simulations can give some insights of the relevant transport phenomena, there is a limitation in how many degrees of freedom can be depicted. In order to have a wider panorama of operating conditions, a stationary operation analysis is used. Here, stationary operation refers to the stage when the cycles in dynamic operation are stabilized, hence, some static like features can be extracted. For the stationary analysis, the operational variables are depicted in Table **3-2**.

Ten simulations are performed by varying dextran bulk concentration from 1 to 10 g/L while keeping BS, TBBS and TMP at 1.25 s, 5 s and 0.85 bar, respectively. Other eight simulations are accomplished by varying BS from 0.2 s to 1.6 s while keeping C_b, TBBS and TMP at 1 g/L, 1.25 s and 0.85 bar, respectively. This last simulation outline is repeated with $C_b = 10$ g/L. Eleven simulations are implemented by changing TBBS from 5 s to 15 s while keeping C_b, BS and TMP at 1 g/L, 1.25 s and 0.85 bar, respectively. Finally, nine simulations are performed by varying TMP from 1 bar to 3 bar while holding C_b, BS, and TBBS at 1 g/L, 1.25 s and 5 s, respectively. The established ranges for BS and TBBS are set according to normal values utilized in backshock systems (López-Murillo et al., 2021; Rosinha, 2011). The TMP interval is taken from usual values for operation of UF modules. The range for C_b is selected from 1 to 10 g/L since UF is normally used for concentration of oligodextrans after enzymatic hydrolysis of high molecular weight dextrans, and previous research have reported concentrations between 1.5 and 50 g/L (Mountzouris et al., 2002; Torras et al., 2008; Su et al., 2018).

The output features are the average flux, the maximum concentration at the membrane surface and the total observed rejection. In this stationary operation analysis, the concentration at the membrane surface (C_m) is taken in its maximum value achieved during the filtration cycle (corresponding to the time before the backshock is applied), the average flux

Table 3-2.: Operating conditions for the dynamic simulation of dextran separation in the stationary operation analysis.

Variable	Value	units
Bulk concentration (C_b)	1 - 10	g/L
Backshock time (BS)	0.2 - 1.6	s
Time between backshock (TBBS)	5 - 15	s
Transmembrane pressure (TMP)	1-3	bar

is computed by averaging the instantaneous flux over the simulation time, and the observed rejection is calculated with the total dextran concentration in the permeate tank (Equation 3-12). This sensitivity analysis allows finding appropriate operating conditions for a desired filtration performance in terms of flux and rejection as it is done in section 3.3.4.

3.3.4. Comparative analysis for dextran separation

According to experimental evidence and simulation results, BS and TBBS values can be adjusted to accomplish certain membrane rejection, which changes the conventional paradigm that the MWCO is defined by the membrane pore size distribution (Jonsson and Prado-Rubio, 2011; Rosinha, 2011; Yehl and Zydney, 2021; López-Murillo et al., 2021). Hence, high MWCO membranes can be used under dynamic operation to perform separations with similar rejections of low MWCO membranes but with higher fluxes, which in principle will require less membrane area. This emerging paradigm allows saving money in the design of a facility which uses membrane technologies, namely, UF and MF. In this section a comparative analysis is performed to show the benefits of using membranes with high MWCO under dynamic operation with respect to using membranes of low MWCO under conventional cross-flow operation (without backshock). Two UF membranes modules are intended to concentrate dextran from an aqueous solution of dextran T500 at 1 g/L and at 10 g/L. The dextran has the same molecular weight distribution from López-Murillo et al. (2021). The separation process is performed under TMP between 1 and 3 bar since these values are typical for UF processes. Both membranes are under the same TMP values but one has an MWCO of 3380 kDa (membrane 1) and the other 72 kDa (membrane 2). These MWCO values have been selected since certain BS and TBBS values are already known to tune MWCO of membrane 1 to 72 kDa (López-Murillo et al., 2021). Such values are 1.25 s and 5 s for BS and TBBS, respectively.

The estimated mathematical model from López-Murillo et al. (2021) is used for membrane 1, but a modified version is required for simulation of membrane 2. Particularly, only three parameters have to be set: permeability L_p and parameters "a" and "b" from Equations 3-10b and 3-10c. According to data from Pu et al. (2012), as shown in Table **3-1**, a correlation can be obtained for permeability L_p estimation from MWCO in dextran separations. So, a potential equation is adjusted for prediction of L_p as a function of MWCO, by using the mean values for flux from Table **3-1** and the corresponding MWCO. Once L_p is estimated, "a" and "b" are tuned. Since membrane 2 is under conventional cross-flow operation, "a" and "b" are simplified to the independent term in their respective equations. A grid of values is tried for "a" and "b", with ranges from 1 to 100 and $-1 \cdot 10^{-3}$ to $1 \cdot 10^{-3}$, respectively, until a MWCO of 72 kDa is obtained. This tuning approach for "a" and "b" is preferred over parameter estimation through optimization because the latter requires several evaluations of the objective function in order to converge to the result, and the simulation time used for evaluating a single point is significantly high. Besides, the grid evaluation allows guaranteeing to be close to the global optimum because the the response surface is known.

After the model for membrane 2 is adjusted and simulations are performed, fluxes and observed rejections for membrane 1 and 2 are compared. Since flux determines the required area for a specified flow, and rejection measures the separation performance, these two features are key in the comparative analysis.

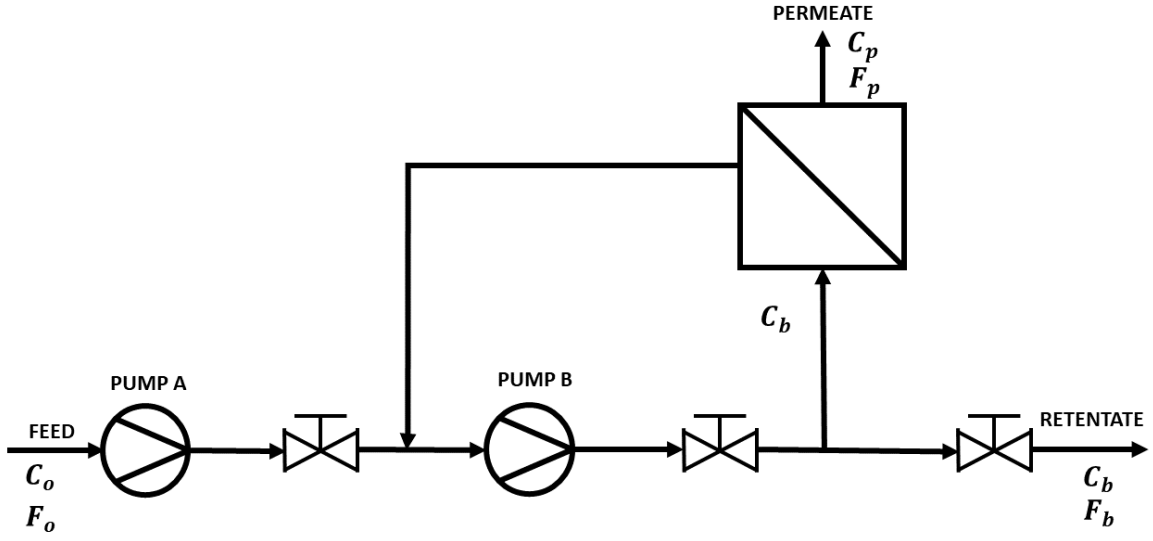

Figure 3-1.: A dynamic ultrafiltration design aimed to take a feed stream of F_o at concentration C_o and concentrate it at C_b.

In order to compare both membranes for a common target, a separation process is sketched in Figure **3-1**. First, the target concentration C_b is varied from 6 g/L to 10 g/L and the cost of the membrane area is computed along with its corresponding retentate flow (F_b). The feed stream flow F_o, TMP, BS and TBBS are hold at 10 000 L/h, 1 bar, 1.25 s and 5 s, respectively. Second, F_o is changed in the range from 4 000 L/h to 10 000 L/h while keeping TMP, C_b, BS and TBBS at 1 bar, 10 g/L, 1.25 s and 5 s, respectively. Membrane costs and retentate flow (F_b) are calculated. And finally, the TMP is varied between 1 and 3 bar, while holding F_o, C_b, BS and TBBS at 10 000 L/h, 10 g/L, 1.25 s and 5 s, respectively. In all the cases, the feed concentration C_o is maintained at 4 g/L. The membrane cost is asummed to be a similar value to $241 £/m^2$ since this is the price per unit area for a membrane made of polysulfone with 2-mm fiber in the year 2020 (Zeynali et al., 2020).

The membrane area is calculated through a global mass balance and a dextran mass balance over the separation system from Equations 3-13 and 3-14. Where F and ρ stands for flow and density, and subscript o, p and b indicates feed, permeate and retentate bulk, respectively. Considering that a dextran solution with a concentration of up to 10 g/L has a density approximately equal to pure water, some simplifications can be made (Mach and Lacko, 1968). Additionally, if permeate flow can be replaced by $F_p = J_v \cdot A_m$, and after some algebra, an expression can be obtained for the required area A_m (Equation 3-15). Using Equations 3-13 and 3-14, an expression is obtained for computing retentate flow (Equation 3-16).

$$C_o \cdot F_o - C_b \cdot F_b - F_p \cdot C_p = 0 \tag{3-13}$$

$$F_o \cdot \rho_o = F_p \cdot \rho_p + F_b \cdot \rho_b \tag{3-14}$$

$$A_m = \frac{F_o \cdot (C_o - C_b)}{J_v \cdot (C_p - C_b)} \tag{3-15}$$

$$F_b = F_o \cdot \frac{C_o - C_p}{C_b - C_p} \tag{3-16}$$

3.4. Results and Discussion

3.4.1. Dynamic Operation analysis

Figure **3-2** depicts the total dextran concentration at the membrane surface over time for dynamic ultrafiltration with bulk concentration (C_b) of 1 and 10 g/L. The concentration profiles show that increasing 10 times C_b causes the maximum concentration on the membrane surface (C_m) to increase in 3.6 times from 43.4 to 158.7 g/L. This is in accordance with previous research, which has estimated that dextran concentration can achieve values from 51 up to 364 g/L at the membrane surface for conventional UF of dextran T70 at $0.43 < C_b < 1.42$g/L,

$2 < \text{TMP} < 6$ bar and cross-flow velocities $1.06\ \text{m/s} < V_{cross} < 2.75\ \text{m/s}$ (Wijmans et al., 1985). In general terms, although this research uses dextran T500, and the TMP, C_b and V_{cross} are different, the maximum values for C_m (Figure **3-2**) are within the range of possible values estimated in Wijmans et al. (1985) to give confidence in the predicted results.

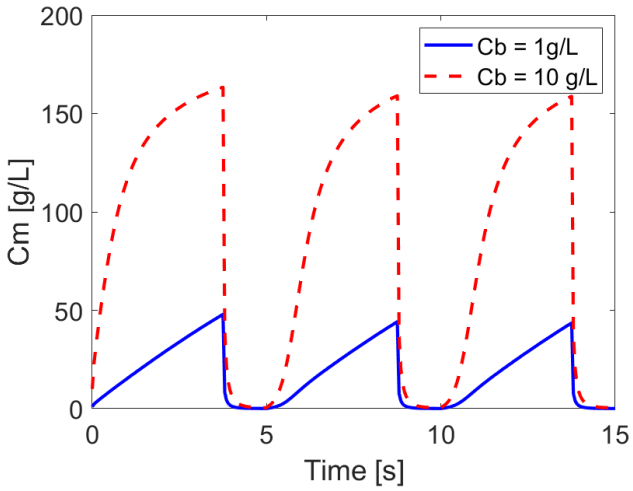

Figure 3-2.: Evolution of total dextran concentration at the membrane surface with TMP=0.85 bar, BS=1.25 s, TBBS=5 s.

In figure **3-3**, the instantaneous membrane flux is illustrated over time. The flux decline is explained since the osmotic pressure, produced by the rise in C_m, plays an important role in the dynamic behavior by reducing the driving force (TMP). C_m values of 43.4 and 158.7 g/L imply an osmotic pressure of 0.016 and 0.4477 bar, respectively. This is equivalent to a reduction of the TMP (0.85 bar) from 1.8 % to 50.3 %. Osmotic pressure has been reported as the main cause for flux decline in dextran filtration (Wijmans et al., 1985; Vinther et al., 2014a,b, 2015; Vinther and Jönsson, 2016a,b). For instance, Wijmans et al. (1985) estimated osmotic pressures as high as 0.73 bar for conventional UF of dextran T70 at $C_b = 0.935$ g/L, TMP = 2 bar and $C_m = 177$ g/L. Although Wijmans et al. (1985) experiment used dextran T70 and herein dextran T500 is investigated, it is clear that omsotic pressure can significantly diminish the driving force in dextran UF. Consistently, in Figure **3-3**, while flux does not decrease significantly at $C_b = 1$ g/L, it does with $C_b = 10$ g/L. Increasing C_b in 10 times, the flux at the end of each cycle declines to almost half, from 46 to 20 LMH.

In Figure **3-4**, the observed rejection of different dextran MW fractions is plotted. It illustrates that filtration process retention of the target molecules is in average 3.5 % higher by increasing C_b. This behavior can be explained through the results from previous research with similar systems. Zuriaga-Agustí et al. (2014) investigated an ultrafiltration of a binary mixture of carboxymethyl cellulose sodium salt and an azo dye. They found comparable rejection values irrespective of the pore size distribution of the membranes used in their

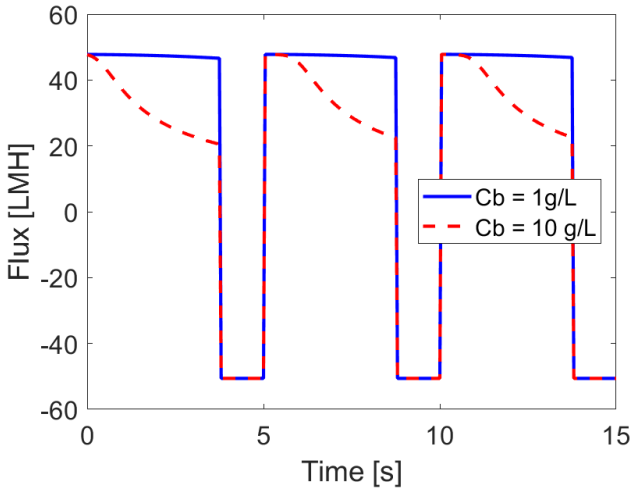

Figure 3-3.: Permeate flux evolution with TMP=0.85 bar, BS=1.25 s, TBBS=5 s.

experiments. They proposed that a dynamic layer helps to filtration during operation and the selectivity is not entirely defined by the membrane pore size distribution. Analogously, other researchers found that membranes of 5 and 10 kDa in MWCO have similar rejections for stevioside and they attributed this behavior to the formation of a dynamic cake layer that helps to retain more solute (Chhaya et al., 2012). Recently, oligodextrans have been concentrated by using a tailor-made ceramic membrane with MWCO of 2 kDa, and they have found that observed rejection for oligodextrans between 1 kDa and 4 kDa incremented from 84 to 92 % by increasing C_b from 15 to 45 g/L at TMP = 0.7 MPa (Qi et al., 2020). This result has been argued to be present in macromolecules filtration, since a dynamic layer is formed at the membrane surface with increasing solute concentration (Qi et al., 2020). Hence, the results predicted by the model simulation are aligned with recent experimental observations associated to the concept of a dynamic layer. Such trend in dextran rejection has been captured through the black box model for intrinsic rejection, R_{int} in equation 3-10a.

From dynamic simulations, it is straightforward to understand that C_b plays an important role in dextran separation with UF membranes as high osmotic pressures can be generated, thus reducing the flux. Nevertheless, plotting every dynamic simulation for each operating condition is not an efficient strategy to analyze the whole behavior of dynamic ultrafiltration of dextran. Thus, several simulations can be summarized in plots, if average quantities are computed.

3.4.2. Stationary Operation analysis

To evaluate different conditions and visualize them all in a single picture, a stationary operation analysis is accomplished in this section. Different values are tested for C_b and the results are plotted in Figure **3-5**. Maximum concentration on the membrane surface $C_{m,max}$,

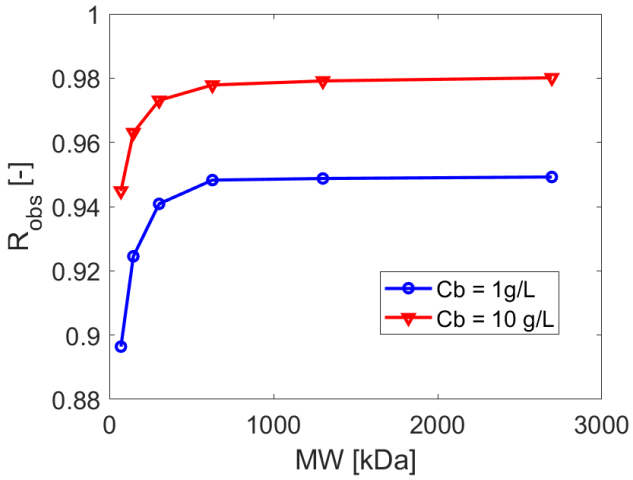

Figure 3-4.: Observed rejection for dextran ultrafiltration with TMP=0.85 bar, BS=1.25 s, TBBS=5 s.

average flux J_{avg} and observed rejection R_{obs} are the output variables shown in the vertical axis. As it was mentioned previously, higher C_b implies a reduction for average flux. From discussion about Figure **3-4**, it is expected that the selectivity performs better at higher C_b and this is evident in Figure **3-5** where the observed rejection increases (from 94.0 % to 97.3 %) at rising C_b values (from 1 to 10 g/L). As C_b is increased, the $C_{m,max}$ also augments through a non-linear relationship, since more dextrans are retained at the membrane surface. The increment in $C_{m,max}$ is reflected by an increase in osmotic pressure. Particularly, for $C_{m,max}$ of 43.4 and 158.7 g/L, the osmotic pressures are 0.0167 and 0.4477, respectively, which affects directly the driving force for the flux. Therefore, an increase in 27 times in the osmotic pressure caused an equivalent reduction of the average flux J_{avg} from 22.96 to 13.89 LMH.

If backshock times (BS) are varied according to Table **3-2**, the results are depicted in Figure **3-6**. At lower BS values, concentration polarization is stronger and observed rejection decreases as $C_{m,max}$ takes higher values. Interestingly, it was mentioned before that macromolecules concentrated at the membrane surface enhance the rejection factor. In order to clarify why $C_{m,max}$ values as high as 160 g/L enhance rejection factor in Figure **3-5** ($R_{obs} = 97.3\,\%$) but not in Figure **3-6** ($R_{obs} = 67.5\,\%$), it is necessary to compute the concentration polarization modulus defined as the ratio C_m/C_b (Baker, 2012). The farther the modulus is from unity the more severe is concentration polarization. In Figure **3-5** this modulus ranges from 43.38 to 15.87, and, in Figure **3-6** ranges from 160.7 to 33.9. From this observation it can be said that two mechanisms are occurring during dextran UF: the formation of a dynamic layer that enhances rejection and the concentration polarization that deteriorates it. When concentration polarization modulus increments, the membrane rejection is decreased by concentration polarization. However, when the modulus declines, the dynamic layer enhances filtration. From Figure **3-6**, it is evident that high BS values allow mitigating more efficiently the polariza-

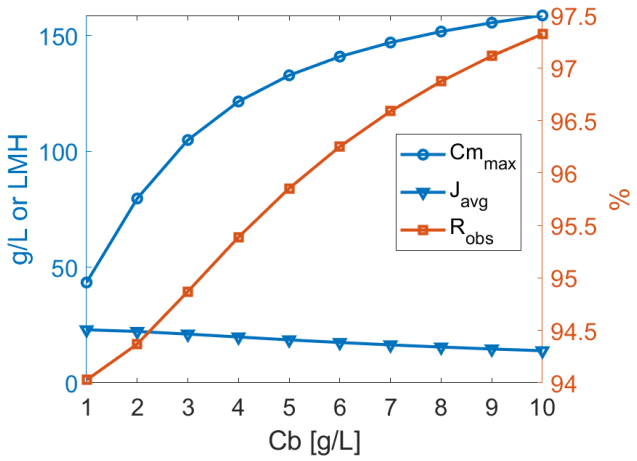

Figure 3-5.: Maximum dextran concentration at the membrane surface, average flux and molecular weight cut off under different bulk concentrations (TMP=0.85 bar, BS=1.25 s, TBBS=5 s).

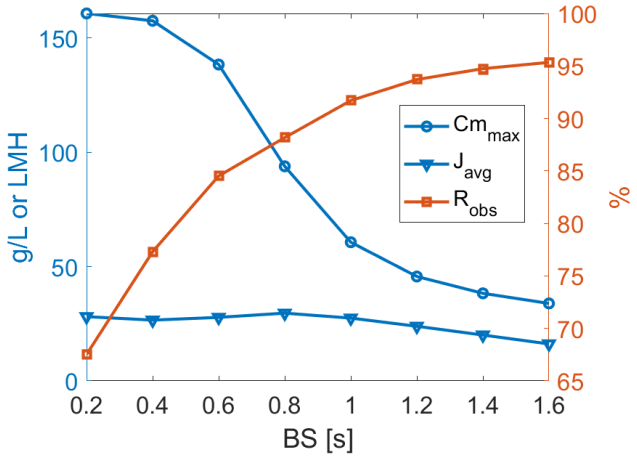

Figure 3-6.: Maximum dextran concentration on the membrane surface, average flux and molecular weight cut off under different backshock time values (TMP=0.85 bar, C_b=1 g/L, TBBS=5 s).

tion effect. This result is in good agreement with research of Vinther et al. (2014b); Vinther and Jönsson (2016a) where fluxes and rejections of dextran dynamic UF are enhanced by using BS from 0.5 to 1 s under TMP = 2 bar and TBBS = 5 s, mitigating concentration polarization phenomena. Nevertheless, BS can not be set arbitrarily large, because at some point BS starts to use more permeate than necessary, wasting it, thus decreasing average flux.

To analyze the influence of BS on J_{avg}, different C_b values were tested (Figure **3-7**). For $C_b = 5$ g/L and $C_b = 10$ g/L, small BS values do not effectively mitigate concentration polarization, thus, the average flux is barely enhanced. When BS is increased up to 1 s, the

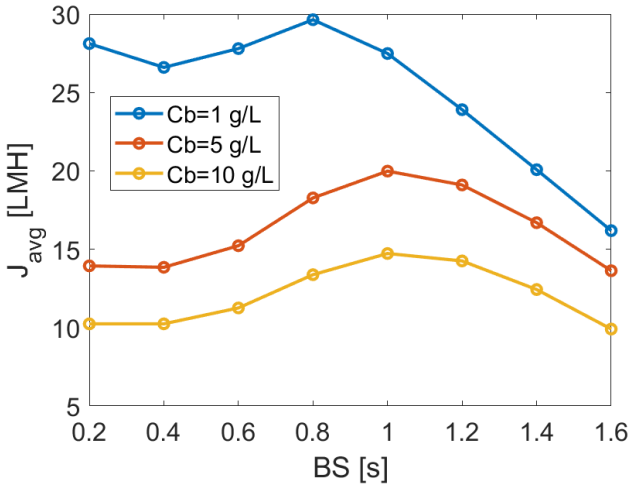

Figure 3-7.: Average flux under different backshock time values (TMP=0.85 bar, C_b=10 g/L, TBBS=5 s).

concentration polarization is mitigated and the flux is restored. Nevertheless, if BS is further increased, it uses more permeate than required and average flux declines again. It seems that the mitigating effect of BS on polarization effect is stronger at $C_b = 5$ g/L and $C_b = 10$ g/L, since the flux can be increased up to a 43.8 % (from 10.24 to 14.73 LMH for $C_b = 10$ g/L) at BS = 1 s. Vinther et al. (2014b) found through CFD that BS close to 1 s can generate the maximum average flux in dynamic UF of dextran T500 under TMP = 2 bar and TBBS = 5 s. For $C_b = 1$ g/L something particular occurs at BS between 0.2 and 0.8 s. It seems that increasing BS from 0.2 to 0.4 s is only wasting permeate as concentration polarization is not mitigated (flux slightly decreases). However, between 0.4 s and 0.8 s, BS is capable to reduce concentration polarization and average flux is increased up to 30 LMH. After 0.8 s, BS uses more permeate than required and flux declines again. Considering that there is a region where BS can obtain maximum fluxes, optimizations can be formulated in order to maximize flux according to input conditions. Additionally, this result indicates that variations in C_b can move the maximum, so the optimum is not defined at certain operating conditions but it must be found dynamically according to input disturbances.

In Figure **3-8**, high TBBS values allow $C_{m,max}$ to rise (from 43.4 to 123.5 g/L) along with the concentration polarization modulus (from 43.4 to 123.5) and, hence, the observed rejection slightly decreases from 94.03 to 90.85 %. Regarding flux behavior, two influences have to be considered: the use of permeate during backshock and the osmotic pressure. These two variables affect directly the average flux. For $C_{m,max}$ of 43.4 and 123.5 g/L, the osmotic pressures are 0.0167 and 0.2253 bar, respectively. The increase in osmotic pressure is compensated with less permeate wasted in backshock, hence, more permeate is passing through the membrane in average (an increment from 22.96 LMH to 34.48), with the corresponding consequence of obtaining a lower rejection.

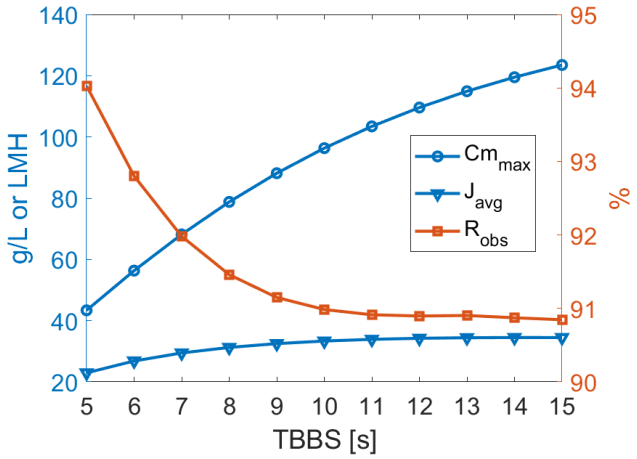

Figure 3-8.: Maximum dextran concentration on the membrane surface, average flux and molecular weight cut off under different time between backshocks values (TMP=0.85 bar, C_b=1 g/L, BS=1.25 s).

The effect of different TMP values between 1 and 3 bar are depicted in Figure **3-9**. As higher TMP values are imposed, more fluid is forced to cross the membrane. This fact increases the rate at which membrane performs the filtration, as can be observed with the increment in average flux from 29.03 to 92.6 LMH. Besides, since convective and diffusive transport terms tend to be balanced according to Equation 3-1, more flux (convective term) implies a higher solute concentration at the membrane surface. Consistently, $C_{m,max}$ arises 3.45 times from 59.6 to 205.8 g/L. According to Wijmans et al. (1985), $C_{m,max}$ for UF of dextran T70 is estimated in 177 g/L at $C_b = 0.935$ g/L, $V_{cross} = 1.06$ m/s and TMP = 2 bar, which is close to the value of 153.3 g/L from Figure **3-9**. Such difference is about 13.4 % and can be attributed to the distinct diffusivities associated to the dextrans T70 and T500, differences in membrane properties, different cross-flow velocity used, and dynamic operation applied in this research. Fluxes values in Wijmans et al. (1985) ranges between $1.78 \cdot 10^{-5}$ and $5.56 \cdot 10^{-5}$ m/s, which corresponds to 64.08 and 200.16 LMH, respectively. Herein, flux includes values lower than reported in Wijmans et al. (1985) due to the applied dynamic operation uses lower TPM (1 - 3 bar), while Wijmans et al. (1985) uses 2, 4 and 6 bar, in conventional cross-flow operation. If concentration polarization modulus is considered, it is evident that observed rejection must decline as the modulus increments from 59.6 to 205.8. Observed rejection falls from 91.46 % to 58.3 %. In general terms, higher TMP values improves average flux J_v but at the cost of reducing selectivity.

From this viewpoint, it is clear that a robust mathematical model for UF and MF is required in order to implement PSE strategies that allow intensification of such membrane technologies. Additionally, optimal design and operation can be found by using this PSE approach.

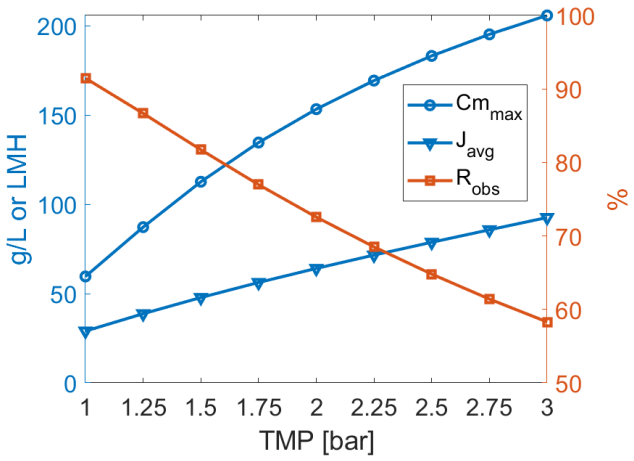

Figure 3-9.: Maximum dextran concentration on the membrane surface, average flux and molecular weight cut off under different transmembrane pressure values (C_b = 1 g/L, BS = 1.25 s and TBBS = 5 s).

3.4.3. Comparative analysis for dextran separation

The mathematical relation for permeability as a function of Molecular Weight Cut-Off is obtained as: $L_p = 3.0327 \cdot (MWCO)^{0.5114}$ with L_p in LMH/bar and MWCO in kDa. With the aid of this relation and the tuning procedure explained in the methodology, the adjustment of membrane 2 provides the following values for L_p, "a" and "b", respectively, 27.11 LMH/bar, 23.8 and 0.

Average flux J_{avg} and total observed rejection R_{obs} are compared between membrane 1 and membrane 2 during concentration of a dextran aqueous solution. In the first simulation, different TMP values are tried out ranging from 1 to 3 bar (Figure **3-10**) while keeping the others in the nominal values (BS=1.25 s, TBBS=5 s, Cb=1 g/L). The flux of membrane 2 is 56.63 % of membrane 1 for a TMP of 1 bar, which means that the required area for a target permeate flow is 56.63 % less in membrane 1 than for membrane 2. Although flux is crucial for comparison, it is useless if the separation is poor. Therefore, rejection factor is considered as measure of the separation performance. For 1 bar in TMP, the rejection factor is bigger in membrane 2 than in membrane 1, nevertheless, both are above 91 %. As TMP increases, the flux in membrane 1 rises faster than in membrane 2, however, the rejection factor is heavily affected in membrane 1. This result is expected since larger TMP values force more liquid to flow through the membrane, thus allowing the dextran to cross the pores of membrane 1 (MWCO=3380 kDa under conventional cross-flow operation) which are larger than pores of membrane 2 (MWCO=72 kDa under conventional cross-flow operation).

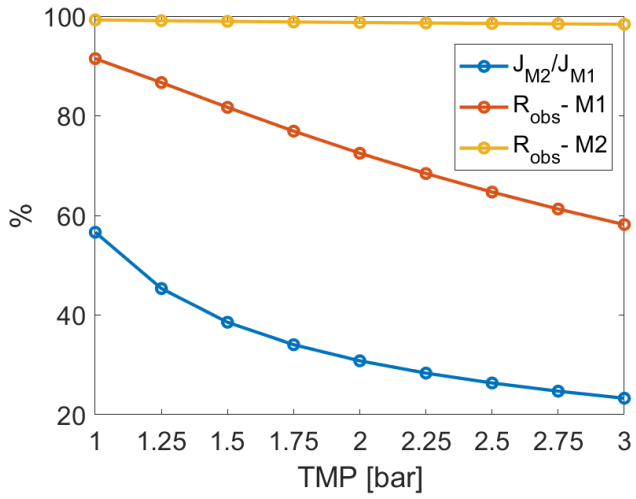

Figure 3-10.: Flux and observed rejection for two membranes under different TMP values with Cb=1 g/L. Membrane 1: MWCO=3380 kDa, under dynamic conditions (BS = 1.25 s and TBBS = 5 s). Membrane 2: MWCO=72 kDa, under conventional cross-flow operation (BS = 0).

The influence of different bulk concentrations are depicted in Figure **3-11**. Membrane 1 improves its rejection factor from 91.49 % to 96.89 %, with increasing C_b values due to the dynamic membrane effect, while it is still showing savings in the required area compared to membrane 2 in the range of 45.74 % and 56.63 %. An interesting trend is captured in the flux ratio from Figure **3-11**: a minimum is present, which implies that $C_{m,max}$ rises at different rate for both membranes as C_b increments.

Once identified that other C_b values enhance observed rejection of membrane 1, different TMP values are tested under $C_b = 10$ g/L (Figure **3-12**). From this plot, membrane 1 has comparable separation performance as membrane 2 (with observed rejections avobe 93 %), in addition to providing higher fluxes with the corresponding saving in the required area.

This result suggests that a membrane operated under dynamic conditions can save costs while keeping good separation performance under some regions of TMP and C_b with respect to a membrane with a lower MWCO operated under conventional cross-flow conditions. For example, if a minimum rejection of 93 % is accepted for a dextran concentration process, it can be concluded that membrane 1 allows saving required area in all the range of TMP between 1 and 3 bar, while satisfying rejection threshold (Figure **3-12**). Since normally MWCO corresponds to 90 % rejection, a 93 % is higher than expected. Higher TMP also affects the capital and operational costs, since more powerful pumps are required. Thus it is better to select the lower TMP values of the range.

Considering the process design of Figure **3-1**, membrane cost for concentrating a dextran

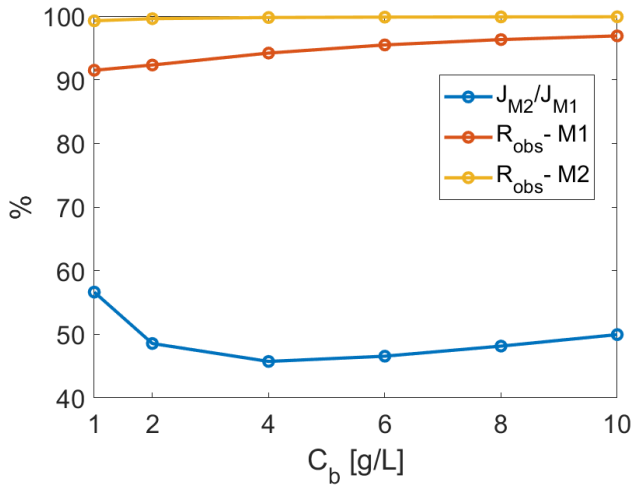

Figure 3-11.: Flux and observed rejection for two membranes under different Cb values with TMP=1 bar. Membrane 1: MWCO=3380 kDa, under dynamic conditions (BS = 1.25 s and TBBS = 5 s). Membrane 2: MWCO=72 kDa, under conventional cross-flow operation (BS = 0).

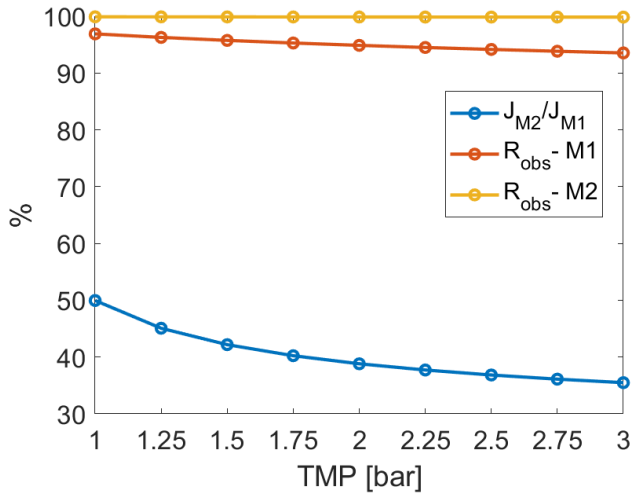

Figure 3-12.: Flux and observed rejection for two membranes under different TMP values with Cb=10 g/L. Membrane 1: MWCO=3380 kDa, under dynamic conditions (BS = 1.25 s and TBBS = 5 s). Membrane 2: MWCO=72 kDa, under conventional cross-flow operation (BS = 0).

solution of 4 g/L is dependent on the target concentration. This relation is depicted in Figure **3-13** for a F_o = 10 000 L/h and TMP = 1 bar. When the target concentration is 6, 8 and 10 g/L, the cost for membrane 1 is 48.7 %, 49.9 % and 51.5 % of the cost for membrane 2 at the same target concentrations, respectively (which is in accordance with the estimated economic savings in Figure **3-11**). On the other hand, the retentate flow is computed for both membranes. Since, membrane 1 presents lower observed rejections than membrane 2 (Figure

3-11), it is expected that more of the dextran is lost in the permeate flow for membrane 1. According to Equation 3-16, the F_b decreases as C_p increases, since its derivative is always negative (Equation 3-17). Therefore, dextran loss through permeate stream implies that less retentate can be obtained at the target concentration C_b, which is confirmed as retentate flow is less for membrane 1 than for membrane 2 in Figure **3-13**. Retentate flow for membrane 1 is 97.7 %, 96.3 % and 95.3 % of that of membrane 2 at C_b of 6, 8 and 10 g/L, respectively. Using membrane 1, instead of membrane 2, implies economic savings in the order of 50 % as less area is required. However, there is a slight reduction of the retentate flow of 3.6 % in average.

$$\frac{dF_b}{dC_p} = F_o \cdot \frac{C_o - C_b}{(C_b - C_p)^2} < 0, \ \forall \ C_p \tag{3-17}$$

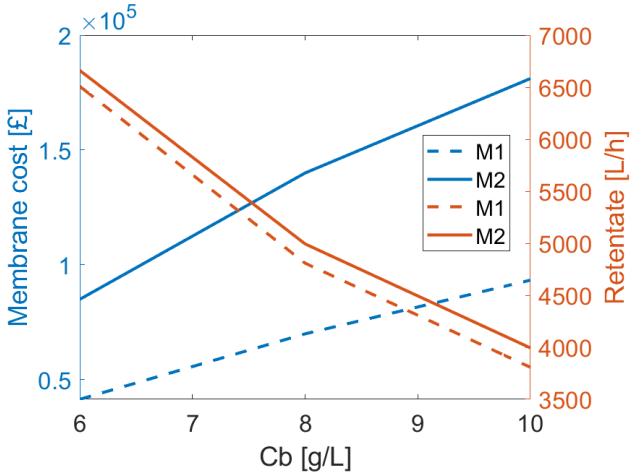

Figure 3-13.: Membrane cost and retentate flow for target concentration ranging from 6 to 10 g/L. Membrane 1 is under dynamic operation with BS = 1.25 s, TBBS = 5 s, TMP = 1 bar and F_o = 10 000 L/h. Membrane 2 is under conventional cross-flow operation.

Increasing the feed flow from 4 000 to 10 000 L/h, membrane costs and retentate flow are calculated for membrane 1 and membrane 2 considering a TMP = 1 bar and a target concentration of C_b = 10 g/L (Figure **3-14**). Figure **3-14** depicts a linear relation between membrane cost and feed flow F_o, expected from the Equation 3-15. Exploiting such linear relationship, the slope is analyzed instead. For membrane 1 the slope of membrane cost is 9.33 and for membrane 2 is 18.11. Then, increasing F_o increments the membrane cost at a higher rate (almost twice) for membrane 2 than for membrane 1. Therefore, the economic saving by using membrane 1 instead of membrane 2 is 51.5 % in all the range of F_o. The retentate flow for membrane 1 has a slope of 0.381, being 95.5 % of the slope for membrane

2, which is 0.399. This result implies that the membrane 1 yield a retentate flow of 95.5 % of that of membrane 2 in all the range of F_o.

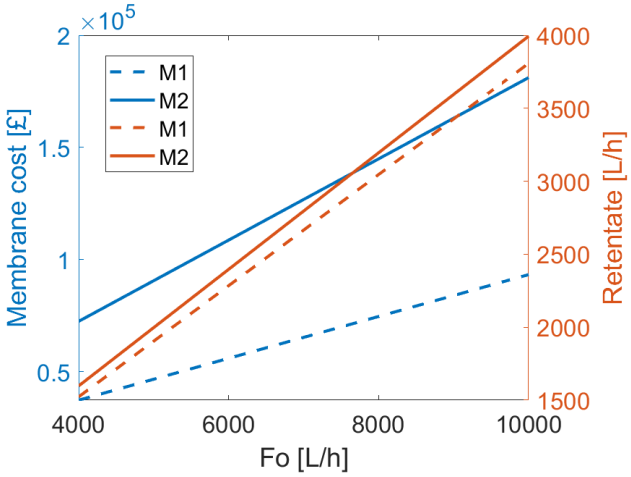

Figure 3-14.: Membrane cost and retentate flow for feed flow ranging from 4000 to 10 000 L/h. Membrane 1 is under dynamic operation with BS = 1.25 s, TBBS = 5 s, TMP = 1 bar and F_o = 10 000 L/h. Membrane 2 is under conventional cross-flow operation.

Evaluating membrane cost and retentate flow under different transmembrane pressures yields the Figure **3-15**, considering a F_o = 10 000 L/h and a target concentration of C_b = 10 g/L. Increasing the TMP from 1 to 3 bar, the membrane cost is reduced from 51.5 % to 37.9 %. Nevertheless, the retentate flow for membrane 1 is 95.3 % of the retentate flow for membrane 2 at TMP = 1 bar, and decreases to 89.8 % at TMP = 3 bar. The retentate flow decline is explained since observed rejection for membrane 1 is diminished at high TMP (Figure **3-12**). Thus, the dextran lost in permeate stream implies that less retentate flow can be obtained.

3.5. Conclusions

Mathematical modeling of dynamic operation in dextran ultrafiltration is a key tool, from a process system engineering perspective, in order to evaluate the separation performance under different operating conditions. In this sense, a previously developed hybrid model is exploited to perform a sensitivity analysis. The average flux (J_{avg}), the observed rejection (R_{obs}) and the maximum dextran concentration ($C_{m,max}$) at the membrane surface are computed as a function of bulk dextran concentration (C_b), backshock time (BS), time between backshock (TBBS) and transmembrane pressure (TMP). According to the results, concentration polarization is well diagnosed by concentration polarization modulus. Values for this

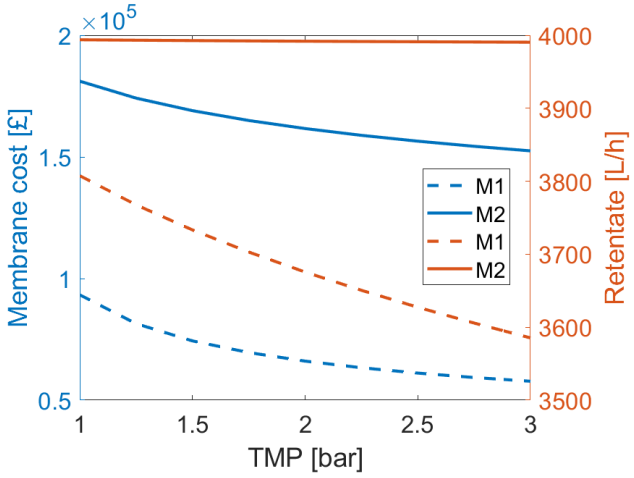

Figure 3-15.: Membrane cost and retentate flow for transmembrane pressure ranging from 1 to 3 bar. Membrane 1 is under dynamic operation with BS = 1.25 s, TBBS = 5 s, TMP = 1 bar and F_o = 10 000 L/h. Membrane 2 is under conventional cross-flow operation.

modulus as high as 160 have a negative impact on observed rejection, while values close or lower than 34 improve selectivity due to the dynamic boundary layer formation. BS values close to 1 s improve average flux up to 43.8 % under C_b of 5 and 10 g/L. BS = 0.8 s improves J_{avg} just 7 % for C_b of 1 g/L. Increasing TBBS higher than 5 s, keeping fixed BS = 1.25 s, improves J_{avg} in 50.2 % but gives up some of the rejection (from 94.03 to 90.85 %). A similar behavior is found when analyzing the effect of TMP. Increasing TMP, from 1 to 3 bar, improves J_{avg} in a factor of 3.2, but it generates a drastic reduction in selectivity: R_{obs} falls from 91.46 % to 58.3 %.

In addition to the sensitivity analysis, a comparative analysis is accomplished. A membrane of high MWCO, 3380 kDa (membrane 1), under dynamic operation (BS = 1.25 s and TBBS = 5 s) is compared to a membrane of low MWCO, 72 kDa (membrane 2), under conventional cross-flow operation. The membrane cost is determined during concentration of a dextran solution of 4 g/L to 6, 8 and 10 g/L. Membrane cost savings can achieve values around 50 % by using membrane 1 instead of membrane 2 at the expense of obtaining slightly less retentate flow. The reduction in retentate flow ranges from 3.6 % to 10.2 %. These losses in retentate flow are acceptable or not according to a further economic analysis where revenues are considered. Profits determine if the economic saving in area exceeds the loss in retentate flow.

Given these results, it is clear that the developed hybrid mathematical model allows optimization of operation through sensitivity analysis, and allows designing of the separation process given a definite concentration target, in the context of dextran ultrafiltration.

Table 3-3.: Nomenclature.

	List of symbols
A_1, A_2, A_3	Polinomial coefficients in osmotic pressure expression
A_m	Membrane area (m^2)
a, b, P_1, P_2, P_3, P_4	Parameters for intrinsic rejection expression
BS	Backshock duration time (s)
C	Dextran concentration (kg/m^3 or g/L)
D_i	Dextran diffusion coefficient (m^2/s)
F	Cross-flow (L/h)
J_s	Dextran flux ($kg/(m^2 \cdot s)$)
J_v	flux through the membrane ($m^3/(m^2 \cdot s)$)
k_1	Coefficients for flux through small pores (-)
k_2	Coefficients for flux through large pores (-)
L_p	Membrane permeability (LMH/bar)
R_{int}	Intrinsic rejection (-)
R_{obs}	Observed rejection (-)
t	time (s)
v	Volume level in the permeate tank (m^3)
v_{out}	Flow from the permeate tank (m^3/s)
x	Spatial coordinate in the boundary layer (m)
	Greek letters
α	Coefficient in diffusivity expression (m^2/s)
β	Exponent in diffusivity epression (-)
δ	Boundary layer thickness (μm)
ΔP_{BS}	Transmembrane pressure during BS (bar)
$\epsilon_1, \epsilon_2, \sigma_1, \sigma_2$	Parameters for intrinsic rejection expression
π	Osmotic pressure (bar)
	Subscripts
i	i^{th} molecular weight interval
p	Permeate
b	Bulk
T	Tank
m	Membrane
	Acronyms
M_W	Molecular weight (kDa)
MWCO	Molecular weight cut off (-)
RT	Retention time in SE-HPLC (min)
TBBS	Time between backshocks (s)
TMP	Transmembrane pressure (bar)

References

Abels, C., Carstensen, F., and Wessling, M. (2013). Membrane processes in biorefinery applications. *Journal of Membrane Science*, 444:285–317.

Baker, R. W. (2012). *Membrane Technology and Applications*. John Wiley & Sons, 3 edition.

Bakhshayeshi, M., Kanani, D. M., Mehta, A., van Reis, R., Kuriyel, R., Jackson, N., and Zydney, A. L. (2011). Dextran sieving test for characterization of virus filtration membranes. *Journal of Membrane Science*, 379:239–248.

Charcosset, C. (2006). Membrane processes in biotechnology: An overview. *Biotechnology Advances*, 24:482–492.

Chhaya, Sharma, C., Mondal, S., Majumdar, G., and De, S. (2012). Clarification of stevia extract by ultrafiltration: Selection criteria of the membrane and effects of operating conditions. *Food and Bioproducts Processing*, 90:525–532.

Díaz-Montes, E., Yáñez-Fernández, J., and Castro-Muñoz, R. (2020). Microfiltration-mediated extraction of dextran produced by leuconostoc mesenteroides sf3. *Food and Bioproducts Processing*, 119:317–328.

Gaspar, V. M., Moreira, A. F., de Melo-Diogo, D., Costa, E. C., Queiroz, J. A., Sousa, F., Pichon, C., and Correia, I. J. (2016). Multifunctional nanocarriers for codelivery of nucleic acids and chemotherapeutics to cancer cells.

Jonsson, G. E. and Prado-Rubio, O. A. (2011). Modeling and operation of dynamic membrane processes. International Congress on Membranes and Membrane Processes : ICOM 2011 ; Conference date: 01-01-2011.

KWON, B., MOLEK, J., and ZYDNEY, A. (2008). Ultrafiltration of pegylated proteins: Fouling and concentration polarization effects. *Journal of Membrane Science*, 319:206–213.

López-Murillo, L. H., Grisales-Díaz, V. H., Pinelo, M., and Prado-Rubio, O. A. (2021). Ultrafiltration intensification by dynamic operation: Insights from hybrid modeling. *Chemical Engineering and Processing - Process Intensification*, 169:108618.

Macedo, A., Duarte, E., and Pinho, M. (2011). The role of concentration polarization in ultrafiltration of ovine cheese whey. *Journal of Membrane Science*, 381:34–40.

Mach, O. and Lacko, L. (1968). Density gradient in a dextran medium. *Analytical Biochemistry*, 22:393–397.

Mountzouris, K., Gilmour, S., Grandison, A., and Rastall, R. (1999). Modeling of oligodextran production in an ultrafiltration stirred-cell membrane reactor. *Enzyme and Microbial Technology*, 24:75–85.

Mountzouris, K., Gilmour, S., and Rastall, R. (2002). Continuous production of oligodextrans via controlled hydrolysis of dextran in an enzyme membrane reactor. *Journal of Food Science*, 67:1767–1771.

Neggaz, Y., Vargas, M. L., Dris, A. O., Riera, F., and Alvarez, R. (2007). A combination of serial resistances and concentration polarization models along the membrane in ultrafiltration of pectin and albumin solutions. *Separation and Purification Technology*, 54:18–27.

Peinemann, K.-V. and Nunes, S. P. (2010). *Membranes for water treatment*. John Wiley & Sons.

Pinelo, M., Jonsson, G., and Meyer, A. S. (2009). Membrane technology for purification of enzymatically produced oligosaccharides: Molecular and operational features affecting performance. *Separation and Purification Technology*, 70:1–11.

Prado-Rubio, O. A., Morales-Rodríguez, R., Andrade-Santacoloma, P., and Hernández-Escoto, H. (2016). Process intensification in biotechnology applications.

Pu, Y., Zou, Q., Liu, L., Han, Z., Wang, X., Wang, Q., and Chen, S. (2012). Clinical dextran purified by fractional ultrafiltration coupled with water washing. *Carbohydrate Polymers*, 87:1257–1260.

Qi, T., Da, X., Zhang, Y., Chen, X., Cui, Z., Qiu, M., and Fan, Y. (2020). Modeling and optimal operation of intermittent feed diafiltration for refining oligodextran using nanoporous ceramic membranes. *Separation and Purification Technology*, 253:117491.

Rosinha, I. P. (2011). High frequency backshock effect on ultrafiltration of selected polysaccharides. master thesis. universidade técnica de lisboa & technical university of denmark.

Su, Z., Luo, J., Pinelo, M., and Wan, Y. (2018). Directing filtration to narrow molecular weight distribution of oligodextran in an enzymatic membrane reactor. *Journal of Membrane Science*, 555:268–279.

Torras, C., Nabarlatz, D., Vallot, G., Montané, D., and Garcia-Valls, R. (2008). Composite polymeric membranes for process intensification: Enzymatic hydrolysis of oligodextrans. *Chemical Engineering Journal*, 144:259–266.

Vinther, F. and Jönsson, A.-S. (2016a). Modelling of optimal back-shock frequency in hollow fibre ultrafiltration membranes i: Computational fluid dynamics. *Journal of Membrane Science*, 506:130–136.

Vinther, F. and Jönsson, A.-S. (2016b). Modelling of optimal back-shock frequency in hollow-fibre ultrafiltration membranes ii: Semi-analytical mathematical model. *Journal of Membrane Science*, 506:137–143.

Vinther, F., Pinelo, M., Brøns, M., Jonsson, G., and Meyer, A. S. (2014a). Mathematical modelling of dextran filtration through hollow fibre membranes. *Separation and Purification Technology*, 125:21–36.

Vinther, F., Pinelo, M., Brøns, M., Jonsson, G., and Meyer, A. S. (2014b). Predicting optimal back-shock times in ultrafiltration hollow fibre modules through path-lines. *Journal of Membrane Science*, 470:275–293.

Vinther, F., Pinelo, M., Brøns, M., Jonsson, G., and Meyer, A. S. (2015). Predicting optimal back-shock times in ultrafiltration hollow fiber modules ii: Effect of inlet flow and concentration dependent viscosity. *Journal of Membrane Science*, 493:486–495.

Wei, P., Cheng, L.-H., Zhang, L., Xu, X.-H., lin Chen, H., and jie Gao, C. (2014). A review of membrane technology for bioethanol production. *Renewable and Sustainable Energy Reviews*, 30:388–400.

Wijmans, J., Nakao, S., Berg, J. V. D., Troelstra, F., and Smolders, C. (1985). Hydrodynamic resistance of concentration polarization boundary layers in ultrafiltration. *Journal of Membrane Science*, 22:117–135.

Yehl, C. J. and Zydney, A. L. (2021). Characterization of dextran transport and molecular weight cutoff (mwco) of large pore size hollow fiber ultrafiltration membranes. *Journal of Membrane Science*, 622:119025.

Zarrintaj, P., Saeb, M. R., Jafari, S. H., and Mozafari, M. (2020). Application of compatibilized polymer blends in biomedical fields.

Zeynali, R., Ghasemzadeh, K., Jalilnejad, E., and Basile, A. (2020). Economic evaluation of wastewater and water treatment technologies.

Zuriaga-Agustí, E., Alventosa-deLara, E., Barredo-Damas, S., Alcaina-Miranda, M., Iborra-Clar, M., and Mendoza-Roca, J. (2014). Performance of ceramic ultrafiltration membranes and fouling behavior of a dye-polysaccharide binary system. *Water Research*, 54:199–210.

Appendix A

Chemical Engineering & Processing: Process Intensification 169 (2021) 108618

Contents lists available at ScienceDirect

Chemical Engineering and Processing - Process Intensification

journal homepage: www.elsevier.com/locate/cep

Ultrafiltration intensification by dynamic operation: Insights from hybrid modeling

Luis Humberto López-Murillo [a], Víctor Hugo Grisales-Díaz [b], Manuel Pinelo [c], Oscar Andrés Prado-Rubio [a,*]

[a] Departamento de Ingeniería Química, Universidad Nacional de Colombia, Grupo de Investigación en Aplicación de Nuevas Tecnologías (GIANT), Manizales, Colombia
[b] Departamento de Microbiología, Universidad Libre de Colombia Seccional Pereira, Microbiotec, Pereira, Colombia
[c] Department of Chemical and Biochemical Engineering, Technical University of Denmark, PROSYS - Process and Systems Engineering Centre, DK-2800 Kgs. Lyngby, Denmark

ARTICLE INFO

Keywords:
Dynamic ultrafiltration
Membrane intensification
MWCO tuning
Hybrid modeling

ABSTRACT

Concentration polarization and fouling are the most important issues to be addressed when designing ultrafiltration (UF) and microfiltration (MF) units for a specific application. Dynamic operation in UF and MF, such as backshock, is a method that allows mitigating adverse effects of polarization and fouling thus enhancing the separation performance. However, there is a trade-off between operational conditions (i.e. backshock duration time BS, the time between backshock TBBS, and flux) to achieve the desired effects. Herein, two hybrid mathematical models are developed and tuned to predict the behavior of the polarization layer in dynamic UF (R^2_{adj} of 0.9185 and 0.9626, respectively). Both hybrid models can estimate the concentration on the membrane surface (e.g. 27 g/L when BS is 1.25 s and TBBS is 5 s). The results illustrate the intensifying effect of dynamic operation by decreasing the Molecular Weight Cut-off up to 74 times without decreasing the membrane flux. The performed experiments and developed models provide system insights for membrane systems design where the rejection could be enhanced and tunned according to operating conditions rather than the membrane pore size.

1. Introduction

Ultrafiltration (UF) and microfiltration (MF) are separation technologies widely used in industrial fields such as water treatment [1–7], food [8], beverage [9], pharmaceutical [10–12] and biotechnology due to their good performance and selectivity under moderate conditions. Nevertheless, filtration membrane technologies have some drawbacks that limit their performance and efficiency, namely concentration polarization and fouling [13,14]. These phenomena affect membrane performance by reducing the flux and decreasing selectivity (or rejection factor).

Due to the adverse impact of the aforementioned phenomena, there have been efforts to develop several methods to reduce, control, avoid and correct the effects of concentration polarization and fouling by mechanical, hydraulic, chemical means or their combination [13,14]. Some examples are: turbulence promoters, pulsed or reverse flow (dynamic operation), rotating or vibrating membranes, stirred cells with rotating blades close to the membrane, ultrasonic enhancement, periodic maintenance cleaning, periodic backwash with permeate gas (dynamic operation), generation of a dynamic membrane layer, pretreatment by filtration, membrane surface treatment, preparation of more hydrophilic membranes, appropriated operating mode selection.

Among the mentioned methods to control concentration polarization and fouling, some could be grouped into the general term "dynamic operation". Particularly, there is a technique in which, every period of time, the flux is reversed across the membrane during a specified amount of time. Then, pressure is applied in the permeate side and the flux crosses from permeate to the retentate side. Such reversed flux can remove some of the internal and external fouling while disrupting the concentration profile in the boundary layer. There are several variations of this technique with different names: backshock, backpulse and backflush, only differentiating in frequency and duration [29]. The dynamic operation can be considered as part of process – intensifying methods [30] since overall performance can be improved significantly by reverting flux in a periodic way [31–34]. Nevertheless, further intensification by using dynamic operation only can be achieved for

* Corresponding author.
E-mail addresses: lhlopezm@unal.edu.co (L.H. López-Murillo), vhgrisalesd@unal.edu.co (V.H. Grisales-Díaz), mp@kt.dtu.dk (M. Pinelo), oaprador@unal.edu.co (O.A. Prado-Rubio).

https://doi.org/10.1016/j.cep.2021.108618
Received 17 June 2021; Received in revised form 4 August 2021; Accepted 30 August 2021
Available online 9 September 2021

Table 1
List of models used for predicting ultrafiltration process behavior.

System	Model type	Model use	Ref
Whey separation process with UF	It includes mass balances and a black box model to predict fouling.	The model is evaluated under different feed stream concentrations and is used for control purposes.	[15]
Crossflow membrane filtration of colloidal suspension	It is an artificial neural network with a radial basis function.	It is used to predict the flux decline under different conditions: particle size, solution pH, ionic strength and transmembrane pressure.	[16]
Crossflow membrane filtration of colloidal suspension	It is based on Darcy's law integrated with a feedforward artificial neural network	It is used to predict flux and flux resistances.	[17]
Soy protein production from extracts of defatted soybean flour by using tubular and spiral wound ultrafiltration modules	Darcy's law and film theory.	Flux prediction	[18]
Cross flow membrane filtration of colloidal suspension	Feedforward back-propagation neural network and a radial basis function network. The architectures of these are found by genetic algorithms.	Flux prediction	[19]
Whey UF process	A data driven differential equation (empiric model).	Flux prediction	[20]
Water treatment plant	A hybrid model integrating Darcy's law and artificial neural networks.	Flux prediction in dead-end ultrafiltration process.	[21]
Wastewater treatment application	Single Input–Single Output structures and Multiple Input–Single Output structures were evaluated by using system identification techniques.	Flux prediction	[22]
Wastewater treatment of a petrochemical process	A hybrid model coupling Darcy's law and artificial neural networks.	Flux prediction	[23]
Dynamic UF of dextran	Computational fluid dynamics and semi-analytical models	Flux and observed rejection prediction	[24–28]

UF and MF if it is performed at the appropriate operating conditions. The appropriate selection of operating conditions is not an easy task for a particular application. Therefore, it is interesting to use a process system engineering approach where mathematical models are used for process design and operation.

In literature, different models have been developed for predicting ultrafiltration processes behavior. Some of the latest models are summarized in Table 1. In general, the proposed models have the following limitations to be applied for process intensification:

- Those models based on solution diffusion approach do not include the real phenomena that occur in UF and MF: the sieving mechanism. Mostly, they are limited to static operation and not dynamic operation.
- Black box models, such as autoregressive models, artificial neural networks, among others, only predict flux and not the permeate concentration, rejection neither selectivity. Additionally, they need extensive experimental data to calibrate the models, and results are particular for the investigated application limiting their use in other fields. Besides, noise from experimental data tends to be captured by the model.
- Development of pure deterministic models is difficult because the phenomena involved are nonlinear and time variant, and there is insufficient process understanding of the mechanistic underneath.
- Recent models using computational fluid dynamics have not been validated with experimental data [25–28].

Therefore, the aim of this research is to analyze the intensifying effect of the dynamic operation on UF separation performance, thus develop and tune two hybrid models with different complexity levels. Both are intended to predict flux and observed rejection in dynamic UF considering concentration polarization, vital for optimizing process design and operation. The proposed hybrid models merge the flexibility of black box approaches with the interpretability of first principles models, thus they have good extrapolation capabilities and low data requirements [29, 23]. Their structure allows having insights into the phenomena underneath, so they can be used for UF and MF process design and optimization of operating conditions. Compared to previously developed models depicted in Table 2, the novel hybrid models proposed in this work are aimed to increase prediction power while providing insights into the dynamic phenomena underneath. Thus, they have enhanced extrapolation capabilities than previous efforts modeling similar systems. Finally, hybrid models can serve as a building block for developing models with phenomena more complicated than concentration polarization.

The paper is structured as follows: the methodology presents the experimental setup, model development, the methods for data treatment and model tuning. The results section shows the models prediction capabilities and the effects of the dynamic operation on UF performance. Finally the conclusions are drawn.

2. Methodology

All abbreviations and nomenclature used throughout this paper are summarized in Table 2.

2.1. Experimental set up

Experiments for conventional and dynamic operation of UF membrane were performed using Dextran T500 [35]. Dextrans are commonly used in dextran sieving tests as a standard method for characterizing the pore size distribution of ultrafiltration membranes [36]. Additionally, dextrans have very important applications in clinical, pharmaceutical and biomedical field [37–39].

The experiments are carried out in an ultrafiltration system used to test crossflow filtration with hollow fibers in continuous, diafiltration or high frequency backshock operation mode. Such equipment is conformed by eight components (see Fig. 1): hollow fiber module

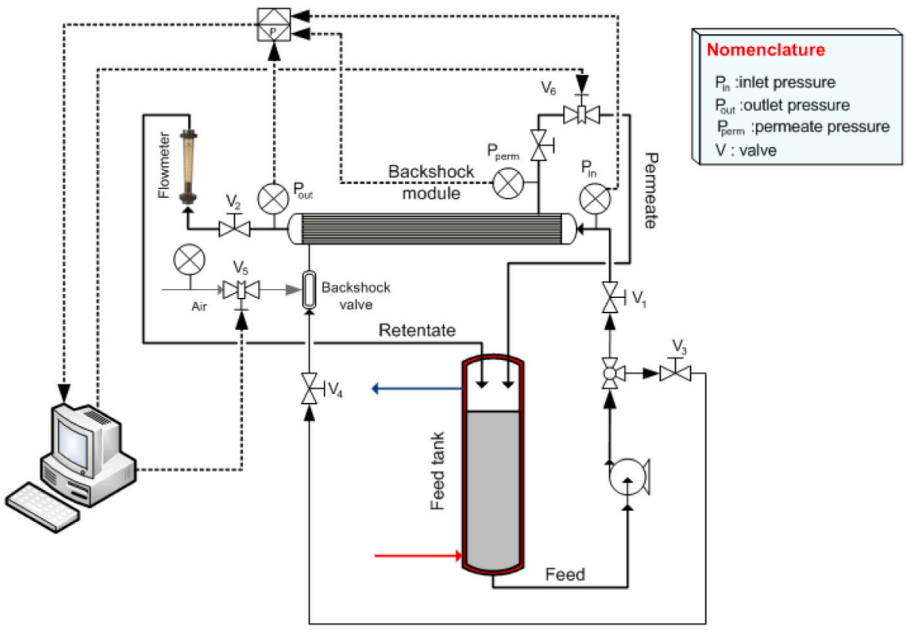

Fig. 1. Ultrafiltration system used to test cross flow filtration with hollow fibers in continuous, diafiltration or high frequency backshock operation mode.

Table 2
Nomenclature.

	List of symbols
A_m	Membrane area (m^2)
BS	Backshock duration time (s)
c	Total dextran concentration (g/ml)
C	Dextran concentration (kg/m^3 or g/L)
D_i	Dextran diffusion coefficient (m^2/s)
F	Crossflow (L/h)
J_s	Dextran flux ($kg/(m^2\ s)$)
J_v	flux through the membrane ($m^3/(m^2\ s)$)
k_1	Coefficients for flux through small pores (–)
k_2	Coefficients for flux through large pores (–)
L_p	Membrane permeability ($m^3/(m^2\ s\ bar)$)
M_W	Molecular weight (kDa)
MWCO	Molecular weight cut off (–)
R_{int}	Intrinsic rejection (–)
R_{obs}	Observed rejection (–)
RT	Retention time in SE-HPLC (min)
t	time (s)
TBBS	Time between backshocks (s)
TMP	Transmembrane pressure (bar)
v	Volume level in the permeate tank (m^3)
v_{out}	Flow from the permeate tank (m^3/s)
x	Spatial coordinate in the boundary layer (m)
	Greek letters
α	Coefficient in diffusivity expression (m^2/s)
β	Exponent in diffusivity expression (–)
δ	Boundary layer thickness (μ m)
ΔP_{BS}	Transmembrane pressure during BS (bar)
π	Osmotic pressure (bar)
	Subscripts
i	ith molecular weight interval
p	Permeate
b	Bulk
T	Tank
m	Membrane

(bore-side feed), pump, feed tank, permeate hold up tank, flowmeter, thermostat, backshock system and a computer.

The feed solution is dextran T500 (Amersham Pharmacia Biotech AB) in an aqueous solution at 1 g/L. Dextran T500 has an average molecular weight of 500 kDa. The feed tank contains the aqueous solution and is pumped to the membrane module where the stream is divided in two: the retentate and the permeate. The flowmeter is placed in the retentate stream. Both permeate and retentate are returned to the feed tank, closing the system. The permeate stream passes through a tank of 2 L (where samples are taken) before returning to the feed tank. Dextran concentrations are measured by size exclusion high performance liquid chromatography (SE-HPLC) coupled to a refractive index detector as indicated in literature for dextran quantification [36,40–42]. A high frequency backshock system is installed to apply pressure in the permeate side to reverse the flow during a time specified by the user in the computer.

The membrane module is a hollow fiber system with poly-ether sulfone (PES) membrane from X-flow Membranes (The Netherland). The module has 54 cm in length, 2.4 cm in shell diameter, 50 tubes and 1.5 mm in tubes diameter corresponding to 0.1 m^2 of membrane area. The operational conditions of the experiment are summarized in Table 3. The dextran solution is fed to the membrane and different backshock times (BS) and times between backshock (TBBS) are evaluated. The reverse flux in dynamic operation allows disruption of the concentration profile at the boundary layer. This strongly modifies the concentration polarization phenomenon as the concentration at the membrane surface is diluted after each disruption. As consequence, there is a lower probability that solute crosses the membrane through the pores, creating the intensifying effect on membrane rejection (selectivity).

From the experimental perspective, it is necessary to assess which values of BS and TBBS are the best for intensifying the system performance. A total of 9 dynamic experiments are carried out plus a conventional crossflow filtration (without BS). Average permeate and feed concentrations are measured by SE-HPLC, and average flux is also monitored. Chromatograms are mathematically processed to extract the concentration of six molecular weight intervals using an experimental correlation to transform retention time to molecular weight. So, from one single experiment, it can be obtained seven experimental data points: six concentrations (one for each molecular weight interval) and one average flux. Hence, 7 data points per experiment (10 experiments) give a total of 70 experimental data to perform the model tuning.

2.2. SE-HPLC data treatment

Dextran T500 not only contains molecules with 500 kDa, but it presents a molecular weight distribution being 500 kDa the average.

Table 3
Operating conditions for the experimental tests in the dynamic ultrafiltration system.

Variable	Value
Transmembrane pressure (TMP)	0.85 bar
Cross flow (F)	162 L/h
Backshock time (BS)	0.25, 0.75, 1.25 s
Time between backshock (TBBS)	5, 10, 15 s

Hence, a mathematical procedure is needed to estimate the concentration of each molecular weight interval from the chromatograms. Eight intervals are constructed but the first and the last are discarded as they do not contribute significantly to the total concentration, so only six intervals are used. To do so, first, a logarithmic relation between retention time and molecular weight is built by analyzing chromatograms from dextran samples of different average molecular weights (dextran T500, T229, T110, T70, T40 and T10). Then, a linear regression between the area under the curve and concentration is developed by performing a calibration curve with samples of dextran T500 at six different concentrations. So, with the logarithmic relation, the elution time is converted to molecular weight and, with the linear regression, the chromatogram signal is divided into intervals and their corresponding areas are transformed to concentration. Thus, the concentration of each molecular weight interval can be computed.

In a previous work, multiple experiments were performed to tune the dynamic operating system, including replicates [35]. The best operation performance was selected to investigate in this contribution. The concentration measurements from retentate, permeate and feed streams were made in duplicate. The heights of the replicated chromatograms are averaged before extracting the area under the curve. Once the concentration of each molecular weight interval is computed, the observed rejection factor is calculated (Eq. (1)) [14].

$$R_{obs} = 1 - \frac{C_{Ti}}{C_{ib}} \tag{1}$$

where C_{Ti} is dextran concentration of ith molecular weight interval in the permeate tank, and C_{ib} is dextran concentration of ith molecular weight interval in feed stream. The observed rejections and fluxes are average quantities since permeate concentrations and fluxes are measured from the permeate tank (which holds up the permeate until sampling) in each experiment.

2.3. Model development

Unlike the models reviewed in Table 2, the models developed here allow prediction of observed rejection and flux in dynamic ultrafiltration by considering BS and TBBS values.

The models are intended to describe dynamically the phenomena inside the boundary layer formed over the membrane surface in the retentate side (Fig. 2). So, mass balances are developed for dextran at the boundary layer where diffusive and convective transport are present. Diffusion is modeled by Fick's law and convection is modeled by Darcy's law. Solutes are retained by a membrane sieving action, that is, solutes only can cross the membrane if they pass through larger pores. High dextran concentrations produce osmotic pressures that must be considered in the model. In addition, periodic backshocks are performed, so reverse flux must be part of the model.

The assumptions to be considered in the model construction are:

- There are not chemical reactions at the membrane surface.
- Physicochemical properties in the boundary layer are constant.
- There are not velocity components in directions different from the perpendicular one to the membrane surface at the boundary layer.
- The diffusivity coefficients are only dependent on molecular weight and not on the concentration. Interactions between different molecular weight dextrans are ignored. Fick's law is a good representation for describing diffusion of dextrans.

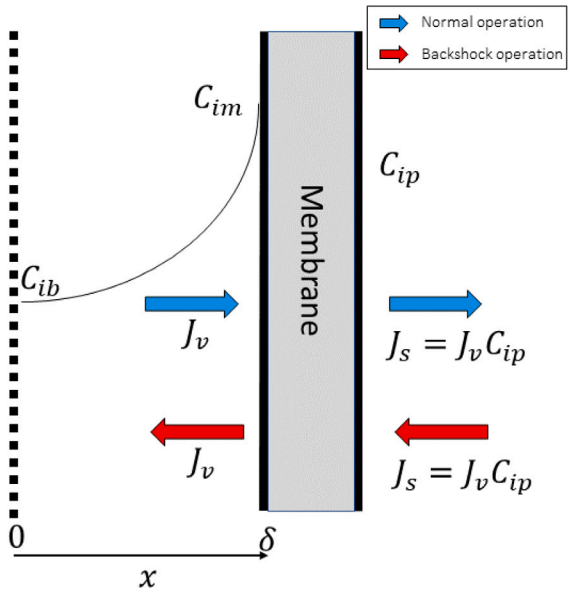

Fig. 2. Boundary layer diagram where concentration polarization takes place after achieving steady state. The left side corresponds to feed and the right side to permeate. *Source:* Adapted from [14].

- The thickness of the boundary layer is constant when defining the crossflow velocity. This parameter is estimated using a correlation based on the dimensionless numbers Reynolds and Schmidt [43].
- The osmotic pressure generated by high dextran concentration can be modeled by a third degree polynomial [44].
- The concentration in permeate is much less than in the feed side, so polarization and osmotic pressure is neglected on the permeate side.

A mass balance is performed for each molecular weight interval of dextran over the boundary layer on the membrane surface. Additionally, at the exit of permeate stream, there is a small tank holding up 2 L of retentate from which the samples were taken. For this tank, a simple mass balance is performed to predict its volume and concentration over time.

Both hybrid models share the same phenomena and the same assumptions, only differing in the black box section.

Hybrid model 1

The mass balance for the boundary layer is represented by Eq. (2) [45].

$$\frac{\partial C_i}{\partial t} = D_i \frac{\partial^2 C_i}{\partial x^2} - J_v \frac{\partial C_i}{\partial x} \tag{2}$$

where C_i is the solute concentration in the boundary layer, D_i is the solute diffusion coefficient, J_v is the flux trough the membrane and x is the perpendicular direction to the membrane surface. D_i is modeled by Eq. (3) [24].

$$D = \alpha \cdot (M_W)^{\beta} \tag{3}$$

where α is $2.6804 \cdot 10^{-10}$ and β is -0.4754. The diffusivity expression is considered part of the black box model inside the hybrid model 1.

The partial differential equation (Eq. (2)) is coupled with the following boundary condition [14].

$$J_v C_i - D_i \left.\frac{\partial C_i}{\partial x}\right|_{x=\delta} = J_s \tag{4}$$

The solute flux through the membrane, J_s, is also expressed as $J_s = J_v C_{ip}$. The flux J_v can be calculated by the Darcy's law (Eq. (5)) [14]. It is worth mentioning that the flux through the membrane changes when

the backshock is taking place, since the inversion of the driving force implies a reverse flux. So, positive transmembrane pressure drives a forward flux during TBBS and negative transmembrane pressure drives a backward flux during BS.

$$\begin{cases} J_v = L_p(TMP - \Delta\pi) & Forward\ flux \\ J_v = -L_p \cdot \Delta P_{BS} & Backward\ flux \end{cases} \quad (5)$$

where, L_p is the membrane permeability, TMP is the transmembrane pressure, $\Delta\pi$ is the osmotic pressure difference across the membrane, ΔP_{BS} is the transmembrane pressure made by the backshock system (being $\Delta P_{BS} = 0.9$ bar from experiments). The second expression in Eq. (5) has a negative sign because, during backshock, the flux is reverted going backwards from permeate to the retentate side. It is important to note that BS, TBBS and ΔP_{BS} have to be carefully chosen for simulations, since the average flux can yield negative values if enough flux is reversed during backshock operation compared to forward operation. BS indicates how long the second expression in Eq. (5) holds, while TBBS–BS indicates how long the first expression in Eq. (5) holds.

The osmotic pressure for dextran is computed by Eq. (6) [44].

$$\pi = A_1 \cdot c + A_2 \cdot c^2 + A_3 \cdot c^3 \quad (6)$$

where, $A_1 = 0.0867$, $A_2 = 2.98$, $A_3 = 89.8$. Eq. (5) is required in Eq. (2) but it still lacks of information: the boundary condition needs the solute flux, J_s, and therefore the permeate concentration, C_{ip}. The calculation of J_s has already been described for membranes where the solution-diffusion model applies [24,46], e.g. in reverse osmosis (see Eq. (7)).

$$J_s = B(C_{im} - C_{ip}) \quad (7)$$

where, B is the solute permeability through the membrane and C_{im} is the concentration at the membrane surface. Nonetheless, the solution diffusion model does not describe appropriately the separation mechanism that occurs in ultrafiltration and microfiltration. Hence, it is necessary to develop a more appropriate expression for computing J_s. According to the pore flow model, which is more appropriate for ultrafiltration and microfiltration, the solute retention is carried out by the sieving action. It means that the membrane has a pore size distribution, that is, there are pores smaller than the solute size and also pores bigger than solute size. Therefore, the Eqs. (8) and (9) are used instead [47].

$$J_v = k_1(TMP - \Delta\pi) + k_2(TMP - \Delta\pi) \quad (8)$$

$$J_s = k_2(TMP - \Delta\pi)C_{im} \quad (9)$$

The total flux through the membrane is conformed of two contributions. The first term of Eq. (8) corresponds to the flux through the pores smaller than the solute size, and the second term corresponds to the flux through the pores bigger than the solute size. In Eq. (9) the solute flux is expressed as the flux through the large pores multiplied by the concentration at the membrane surface.

The permeate concentration can be computed with the aid of Eqs. (8) and (9), as follows.

$$C_{ip} = \frac{J_s}{J_v} = \frac{k_2}{k_1 + k_2} C_{im} \quad (10)$$

Recalling the definition of intrinsic rejection [24].

$$R_{int} = 1 - \frac{C_{ip}}{C_{im}} = 1 - \frac{k_2}{k_1 + k_2} \quad (11)$$

So, the permeate concentration can be expressed as a function of the intrinsic rejection and the concentration at the membrane surface (see Eq. (12)). Note that R_{int} is specific to the pairing membrane and solute, since k_1 and k_2 are related to the membrane pore size distribution relative to the solute size. It implies that R_{int} is independent of pressure and concentration and only depends on the solute size relative to the pore size distribution of the membrane (sieving action). The expression for C_{ip} as a function of R_{int} is considered part of the black box model inside the hybrid model 1.

$$C_{ip} = (1 - R_{int})C_{im} \quad (12)$$

The mass balance for the 2 L tank in the permeate stream is in Eqs. (13) and (14).

$$\frac{dv}{dt} = J_v \cdot A_m - v_{out} \quad (13)$$

$$\frac{dC_{Ti}}{dt} = \frac{J_v \cdot A_m \cdot C_{ip} - v_{out} \cdot C_{Ti} - C_{Ti} \cdot \frac{dv}{dt}}{v} \quad (14)$$

where v is the volume level inside the tank, A_m is the membrane area, v_{out} is the outlet flow, being zero when the tank is not full and the same value as the term $J_v \cdot A_m$ when the tank is full, C_{Ti} is the concentration inside the tank for the ith molecular weight interval.

The differential Eq. (2) is solved using the method of lines with 1000 nodes in the boundary layer and ode15s function from Matlab®. Ode15s function is chosen because of its ability and speed to solve stiff systems.

Hybrid model 2

From preliminary model tuning, it was noticed that still the variance of the experimental data is not fully represented by hybrid model 1. Therefore, an additional gray-box model is proposed to cover the remaining output variance.

If R_{int} from the first hybrid model is plotted against molecular weight, a monotonic ascending curve, that tends to one as molecular weight grows up, is observed. This kind of curve can be modeled by exponentials, sigmoids or rational functions. The latter was proper for modeling R_{int} (Eq. (15a)).

$$R_{int} = min\left(1 - \frac{1 + b \cdot (1 + a \cdot M_W)}{1 + a \cdot M_W}, 1\right) \quad (15a)$$

This function takes the minimum value between the expression and one, because the rational function can give values greater than one, which is not allowed for the physical interpretation of R_{int}. If a and b are estimated for each operating condition and their dependence on BS/TBBS are analyzed, a Lennard-Jones like function with two parameters could fit the data (Eqs. (15b) and (15c)). These last two parameters for a expression are left to depend linearly on TBBS (Eqs. (15d) and (15e)).

$$a = \epsilon_1 \cdot \left[\left(\frac{\sigma_1}{BS/TBBS + \sigma_1}\right)^{12} - \left(\frac{\sigma_1}{BS/TBBS + \sigma_1}\right)^{6}\right] + 1.63 \quad (15b)$$

$$b = \epsilon_2 \cdot \left[\left(\frac{\sigma_2}{BS/TBBS + \sigma_2}\right)^{12} - \left(\frac{\sigma_2}{BS/TBBS + \sigma_2}\right)^{6}\right] + 2.808 \cdot 10^{-3} \quad (15c)$$

$$\epsilon_1 = P_1 \cdot TBBS + P_2 \quad (15d)$$

$$\sigma_1 = P_3 \cdot TBBS + P_4 \quad (15e)$$

The independent terms in Eqs. (15b) and (15c) forces a and b to adopt certain values when there is no backshock. These values are found when a and b were estimated for operation with no backshock.

2.4. Parameter estimation and optimization problem

Concentration polarization model in hybrid model 1 (Eq. (2)) requires some parameters to be solved, such as intrinsic rejection R_{int} and permeability L_p. Therefore, a parameter estimation must be carried out by using the collected experimental data.

For parameter estimation the model outputs are: fluxes and observed rejection factors for each molecular weight interval, the inputs are: time between backshock (TBBS) and backshock time (BS), and the parameters to be estimated are: intrinsic rejection (R_{int}) and permeability (L_p).

For parameter estimation, a weighted sum of squared residuals is used as objective function (Eq. (16)).

$$L = \sum_{n=1}^{N} W_i \cdot (y_{sim} - y_{exp})^2 \tag{16}$$

where N is the total number of experimental data, W_i are the weights, y_{sim} are the simulated outputs and y_{exp} are the experimental outputs. Using the weight factor W_i, the observed rejections are scaled to percentages, that is, between 0 and 100 and not in the original range (0 to 1). This is done to provide analogous rejection and flux contributions to the objective function and have a better trade-off for the model predictions. The model tuning is a non-convex optimization problem, then, it presents multiple local minima, so gradient based algorithms get stuck in there. Thus, a global optimization algorithm is required to find the best parameters that fit the experimental data. The metaheuristic method referred to as particleswarm available in Matlab® is employed with the following parameters: SelfAdjustmentWeight = 1.1 and SocialAdjustmentWeight = 1.8. These values were tunned from preliminary simulation and have shown a faster convergence.

The workflow for the identification of the hybrid model 2 follows the next steps:

- a and b are estimated for each operating condition.
- $P_1, P_2, P_3, P_4, \epsilon_2, \sigma_2$ from Eq. (15) are estimated by using the values of a and b from the previous step. The Matlab function used to find these parameters was lsqcurvefit with the following options: 'StepTolerance' set to $1 \cdot 10^{-10}$ and 'FunctionTolerance' set to $1 \cdot 10^{-10}$.

The chosen statistical indexes for model performance are the adjusted determination coefficient R^2_{adj} plus the parameters and predictor confidence interval of 95%.

3. Results and discussion

3.1. SE-HPLC data treatment

The concentration of the permeate stream is measured for each operating condition. For establishing what percentage of the chromatogram is related to each molecular weight interval, the area under the curve is divided into eight regions. The retention time intervals are divided according to [8.3, 9.0, 9.8, 10.7, 11.5, 12.3, 13.2, 14.0, 15] minutes which, through the logarithmic relation, corresponds to [6705, 3636, 1755, 847, 409, 197, 95, 46, 19] kDa. The first and the last divisions are neglected in the analysis due to their relatively low contribution to the total concentration. The divisions between 9 and 14 min in retention time are equally spaced.

The experimental results at different BS and TBBS are depicted in Table 4. $R_{obs,1}$ corresponds to rejection of dextran with molecular weight between 3636 and 1755 kDa, $R_{obs,2}$ between 1755 and 847 kDa, $R_{obs,3}$ between 847 and 409 kDa, $R_{obs,4}$ between 409 and 197 kDa, $R_{obs,5}$ between 197 and 95 kDa, and $R_{obs,6}$ between 95 and 46 kDa.

If the absorbance in permeate and feed chromatograms is directly used to compute observed rejection [42,48], a continuum spectrum is obtained (Figs. 3–5). It is observed that increasing BS from 0 to 1.25 s, the rejection profiles are higher. It is explained from the fact that backshock system allows the disruption of the profile concentration on the feed side, since the reversed permeate stream dilutes the concentration on the boundary layer [25,27]. Dextran concentration at the membrane surface on the feed side is decreased as BS increases, so there is less probability that solute can cross the membrane and it causes the rejection values to be higher for all molecular weights with respect to static operation (no BS). So, longer times for backschock permit a larger impact on the boundary layer. This is further analyzed with the hybrid models developed in the following sections.

From (Figs. 3–5) the membrane molecular weight cut off (MWCO) is reduced substantially from 3380 kDa (without BS) by a factor of 74, 28 and 17, for TBBS of 5, 10 and 15 s, respectively. These results disagree with the traditional perspective that separation performance is only defined by the pore size distribution of the membrane, indicating that operating conditions (BS and TBBS) can also influence significantly the separation performance.

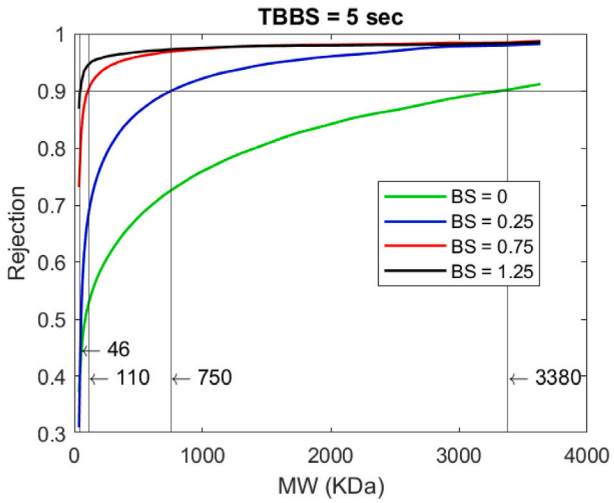

Fig. 3. Experimental observed rejection in a continuous spectrum under TBBS = 5 s for four values of BS: 0, 0.25, 0.75 and 1.25 s. The straight lines indicate MWCO in each operating condition.
Source: Adapted from [35].

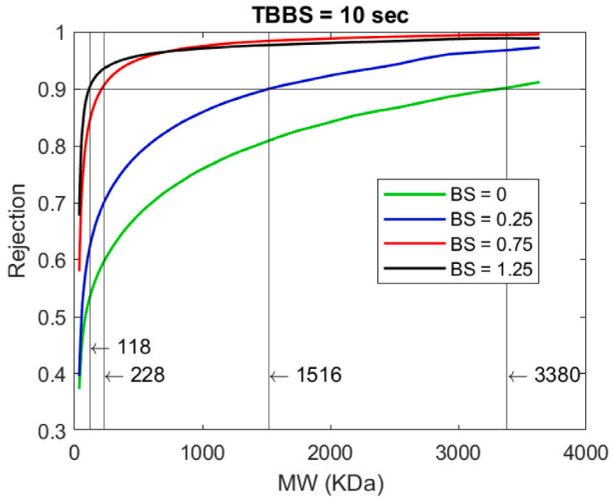

Fig. 4. Experimental observed rejection in a continuous spectrum under TBBS = 10 s for four values of BS: 0, 0.25, 0.75 and 1.25 s. The straight lines indicate MWCO in each operating condition.
Source: Adapted from [35].

Table 4
Experimental data where inputs are BS and TBBS, while outputs are the observed rejection for six molecular weight intervals and flux.

BS	TBBS	$R_{obs,1}$ 3636–1755 kDa	$R_{obs,2}$ 1755–847 kDa	$R_{obs,3}$ 847–409 kDa	$R_{obs,4}$ 409–197 kDa	$R_{obs,5}$ 197–95 kDa	$R_{obs,6}$ 95–46 kDa	Flux [LMH]
0	–	0.8600	0.7736	0.6885	0.6110	0.5439	0.4729	33.60
0.25	5	0.9646	0.9227	0.8603	0.7807	0.6877	0.5466	39.42
0.75	5	0.9734	0.9636	0.9447	0.9172	0.8760	0.7980	34.67
1.25	5	0.9670	0.9597	0.9477	0.9339	0.9170	0.8799	20.26
0.25	10	0.9363	0.8642	0.7852	0.7028	0.6175	0.5126	38.36
0.75	10	0.9876	0.9714	0.9422	0.8941	0.8189	0.6911	46.35
1.25	10	0.9766	0.9614	0.9437	0.9178	0.8769	0.7888	38.58
0.25	15	0.9323	0.8627	0.7821	0.6941	0.6028	0.4860	37.57
0.75	15	0.9646	0.9481	0.9140	0.8543	0.7592	0.5865	45.98
1.25	15	0.9755	0.9647	0.9407	0.8986	0.8263	0.6800	57.64

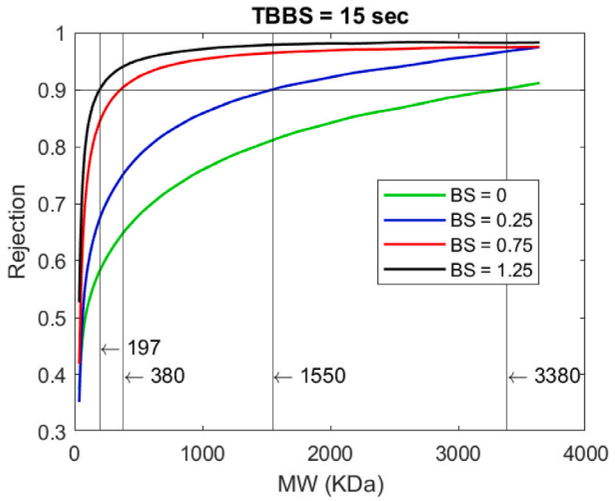

Fig. 5. Experimental observed rejection in a continuous spectrum under TBBS = 15 s for four values of BS: 0, 0.25, 0.75 and 1.25 s. The straight lines indicate MWCO in each operating condition.
Source: Adapted from [35].

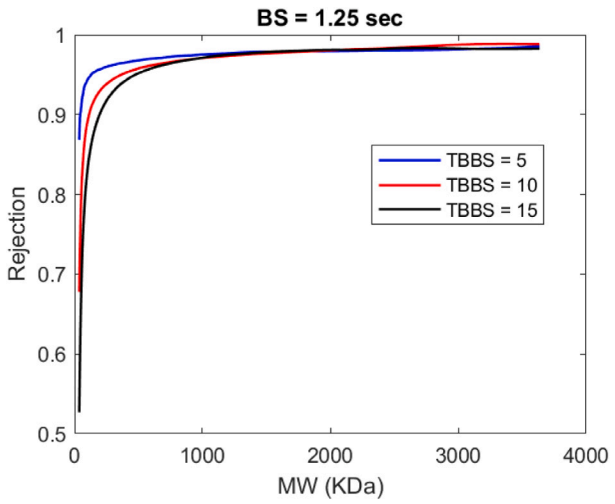

Fig. 6. Experimental observed rejection in a continuous spectrum under BS = 1.25 s for three values of TBBS: 5, 10 and 15 s.
Source: Adapted from [35].

Prior research had analogous results showing how operating conditions can affect directly the MWCO of a membrane by disrupting the concentration polarization in the boundary layer by different means [49]. Investigations on characterization of virus retentive membranes [50] have shown that the sieving curve (and therefore the MWCO) was highly correlated with important parameters such as stirring speed, TMP and flux. Zydney, A. L. and Xenopoulos, A. found that sieving coefficients and MWCO are highly influenced by changes in filtrate flux, particularly for membranes of high MWCO [42]. Wickramasinghe, S.R. and coworkers have stated that the MWCO of a membrane only applies under the test conditions specified by the manufacture, since MWCO is highly dependent on solute species and operating conditions [48]. Yehl, C.J. and Zydney, A.L. have investigated how operating conditions, such as effective wall shear rate and permeate flow rate can influence the MWCO of a hollow fiber membrane during dextran ultrafiltration [51]. The MWCO can vary from <200 kDa to more than 1200 kDa with effective wall shear rates ranging from 2000 s^{-1} to 11000 s^{-1}. Besides, the MWCO can vary between 190 kDa and 1280 kDa for permeate flow rates between 1.7 ml/min and 10 ml/min, respectively. Analogously to the mentioned research, herein it is demonstrated that using dynamic operation the separation is highly influenced by disrupting the boundary layer and even could be tuned.

From Figs. 3–5, it is interesting to notice the increase of observed rejection for larger dextran molecular weight. This is explained by the sieving mechanism that allows the UF membrane to separate solutes of different sizes. So, dextrans with high molecular weight are expected to be more retained than the smaller ones. The sieving mechanism can be related to the probability that a solute with a specified size finds a pore large enough to pass through it, considering that the membrane has a pore size distribution.

From Fig. 6 it is evident that lower TBBS values improve substantially the rejection factor, especially for low molecular weight range. When using low–frequency disruptions, polarization generates a reduction in solute rejection since high dextran concentrations are maintained longer on the membrane surface. Hence, high frequency of backshock allows keeping controlled polarization by reducing the average solute concentration on the membrane surface. The reason is that backshock times are in the same order of magnitude as the development of the polarization layer (this point is further discussed in the hybrid models section). Thus, lower TBBS values promote increasing rejection.

Nevertheless, increasing BS and reducing TBBS does not guarantee a better overall performance of the process, considering the trade-off between observed rejection and membrane flux. Table 4 indicates that increasing BS from 0.25 to 1.25 s, decreases the flux under TBBS of 5, however, increasing the BS under TBBS of 15 increases flux. This is clear evidence that the effect of BS over flux depends on TBBS value. The flux reduction is generated by two situations: if the BS is too large with respect to TBBS, most of the permeate is used to wash the membrane during backshock causing a decrease in the average flux over a period of time. On the other hand, if the BS is small compared to TBBS, concentration polarization fully develops and flux declines again. For example, the flux of 20.26 LMH in Table 4 is lower than that of static operation because in such an experiment BS represents the biggest proportion of the TBBS, which means that the combination of BS = 1.25 and TBBS = 5 wastes more permeate than the other experiments.

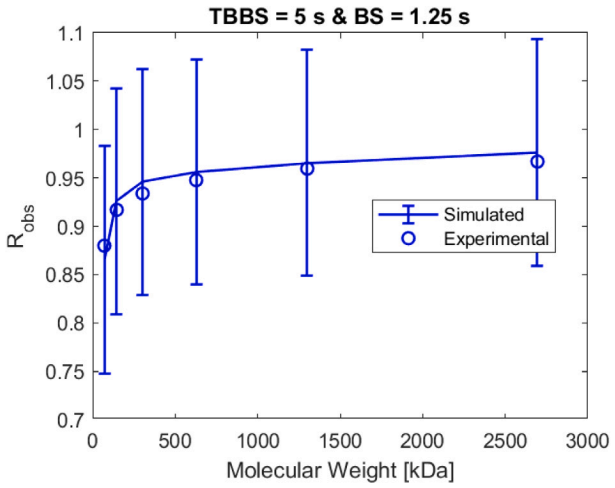

Fig. 7. Predictor confidence interval for hybrid model 1.

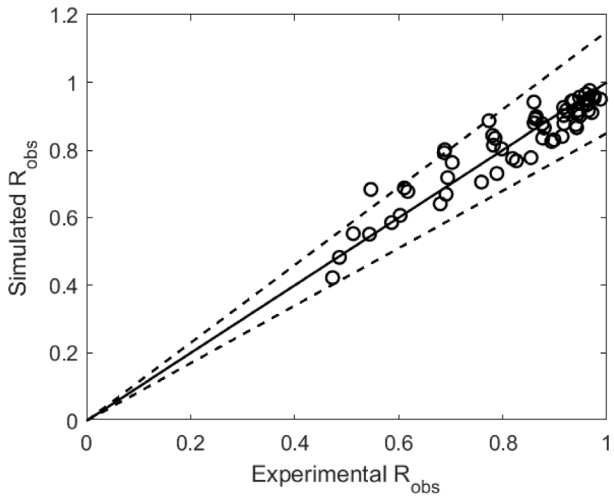

Fig. 8. Parity plot for observed rejections (Hybrid model 1). Dashed lines indicate ± 15%.

3.2. Model calibration and predictive power

Hybrid model 1

The results of the parameter estimation for hybrid model 1 are presented in Table 5. An adjusted determination coefficient is computed for the model yielding a value of 0.9185 which is an indicator of good performance for the model.

The values for $R_{int,i}$ are in agreement with their physical interpretation. Note that $R_{int,1}$ corresponds to the highest molecular weight and $R_{int,6}$ to the lowest molecular weight. It is expected that high molecular weight solutes are rejected by the membrane in a higher probability and this is confirmed in Table 5. In spite of the high values for the estimated intrinsic rejections, the concentration polarization has such a dramatic impact on the performance that observed rejection is much lower compared to the intrinsic rejections, achieving values of down to 47%.

The permeability obtained from parameter estimation (Table 5) is in agreement with values reported in the literature under similar conditions with a membrane made of poly-ether sulfone [52]. There, ultrafiltration of dextran with molecular weight between 36 and 44 kDa was carried out under 1 bar of TMP and a feed concentration of 1g/L. The permeability was found to be between 55 and 65 $L/(m^2 \cdot h \cdot bar)$ corresponding approximately to the confidence interval shown in Table 5.

Confidence intervals for each parameter do not include zero, hence it can be said that such parameters are statistically distinct from zero and contribute to the prediction capability of the model. In addition, the confidence intervals are narrow since their corresponding percentages with respect to the nominal values are below 15% as shown in the last column in Table 5.

Predictor confidence intervals are computed and illustrated in Fig. 7 for TBBS = 5 s and BS = 1.25 s, and it is observed that they include satisfactorily the experimental data. For the remaining operating conditions, the figures have similar behavior (results not shown). However, such intervals include values above 1 and this is not possible for the model since the observed rejections are always lower than the intrinsic rejections. So, although the predictor confidence intervals cover values above 1, the real model outputs for observed rejections are bounded up to the same values as intrinsic rejections.

From parity plots for rejection and flux in Figs. 8 and 9, it is clear that most of the points fall into the ± 15% , only 4 out of 70 points fall outside. Such differences between the simulated data and experimental data may be due to some assumptions made during model construction, for instance, the membrane is modeled as a barrier perpendicular to the flux and the axial geometry of the hollow fiber is not considered. There are some other factors that could also be influencing such as potential

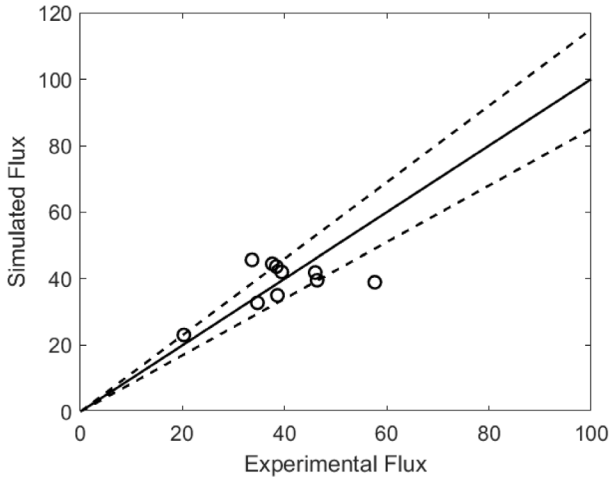

Fig. 9. Parity plot for fluxes in LMH (Hybrid model 1). Dashed lines indicate ± 15%.

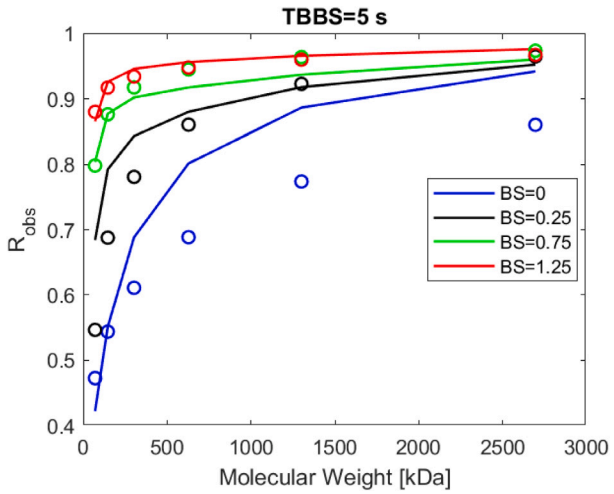

Fig. 10. Experimental and simulated observed rejection versus molecular weight under TBBS = 5 s for three values of BS: 0, 0.25, 0.75 and 1.25 s. (Hybrid model 1.)

Table 5
Estimated parameters and their confidence intervals for the first hybrid model: intrinsic rejections for six molecular weight intervals and permeability.

Parameter	Value	Confidence interval (at 95% confidence)	Confidence interval (%)
$R_{int,1}$	0.9990	0.9549–1.0431	±4.41%
$R_{int,2}$	0.9985	0.9603–1.0367	±3.83%
$R_{int,3}$	0.9977	0.9627–1.0327	±3.51%
$R_{int,4}$	0.9965	0.9581–1.0349	±3.85%
$R_{int,5}$	0.9938	0.9305–1.0571	±6.37%
$R_{int,6}$	0.9847	0.8435–1.1259	±14.34%
L_p $L/(m^2 \cdot h \cdot bar)$	56.2211	52.0216–60.4206	±7.47%

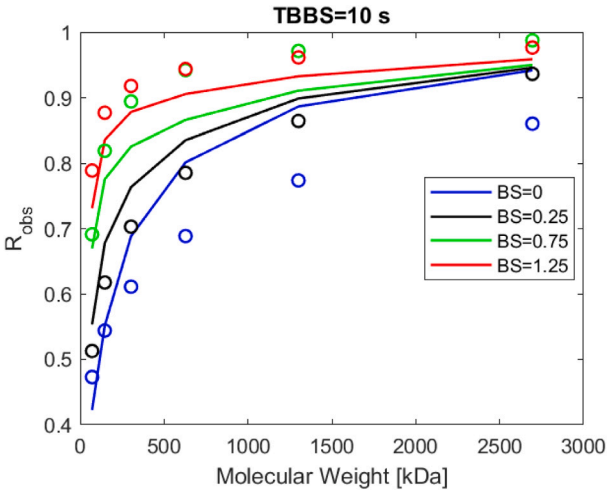

Fig. 11. Experimental and simulated observed rejection versus molecular weight under TBBS = 10 s for three values of BS: 0, 0.25, 0.75 and 1.25 s. (Hybrid model 1.)

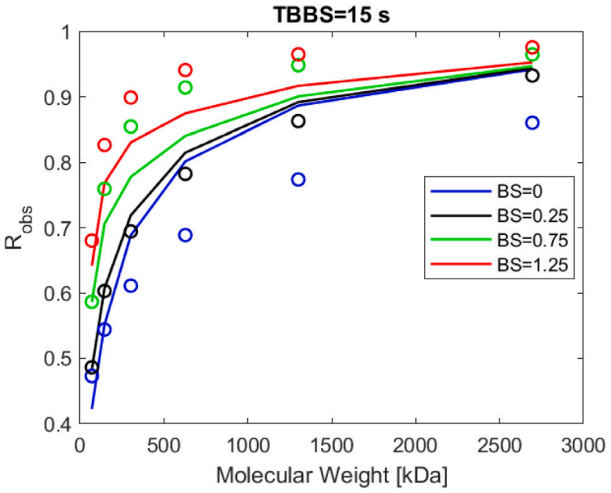

Fig. 12. Experimental and simulated observed rejection versus molecular weight under TBBS = 15 s for three values of BS: 0, 0.25, 0.75 and 1.25 s. (Hybrid model 1.)

fouling, the membrane asymmetry and changes in the hydrodynamic conditions of the boundary layer.

Although Figs. 8 and 9 seem to be a good indicator of model prediction, Figs. 10–12 clearly indicate that the hybrid model 1 have limitations to capture the variance in observed rejection for TBBS = 10 and TBBS = 15 (for all BS values). This shows the model flaws from a structural or phenomenological perspective. For this reason, a new hybrid model is proposed, intended to be able to predict better the observed rejections.

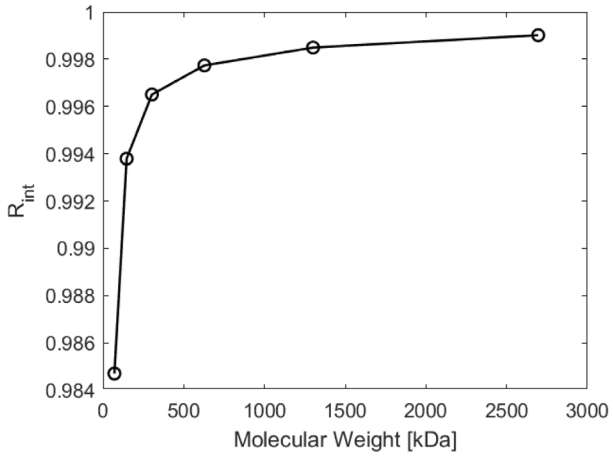

Fig. 13. Estimated intrinsic rejection versus molecular weight.

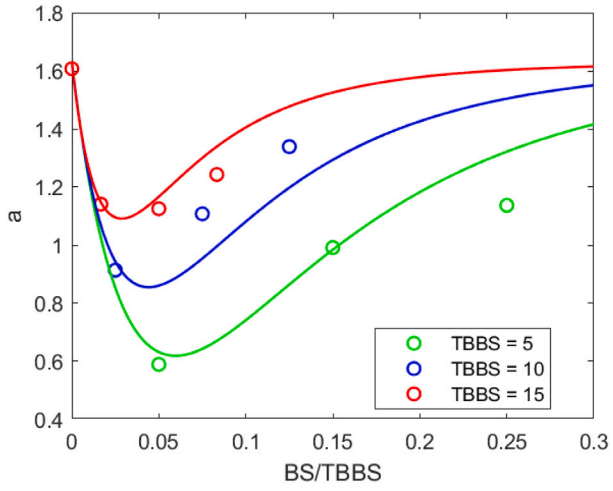

Fig. 14. Dependence of a parameter on BS/TBBS and TBBS. Circles represent values from estimation for each operating condition and line represents the fitted Eq. (15b).

Hybrid model 2

From the previous model, R_{int} can be plotted versus M_W (Fig. 13). Such a graph points out that R_{int} can be modeled by a rational function like Eq. (15a). The parameters a and b are estimated for each operation condition and they are depicted in Figs. 14 and 15. It is observed that a Lennard-Jones like function can fit the values for a and b. Hence, the black box model used to predict R_{int} is summarized in Eq. (15).

Eq. (15) have 6 parameters in total to be estimated $P_1, P_2, P_3, P_4, \epsilon_2$, σ_2. Table 6 summarizes the estimated parameters and their confidence intervals. Since these parameters do not have physical interpretation, they can take any value including negatives. Their confidence intervals show that many of them lie in a wide interval but all of them are

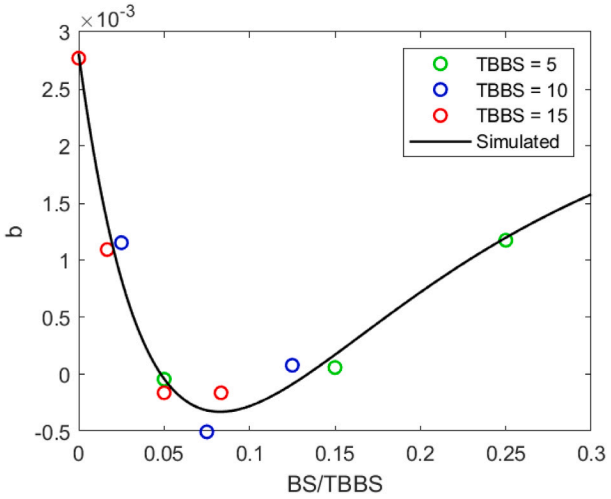

Fig. 15. Dependence of b parameter on BS/TBBS. Circles represent values from estimation for each operating condition and line represents the fitted Eq. (15c).

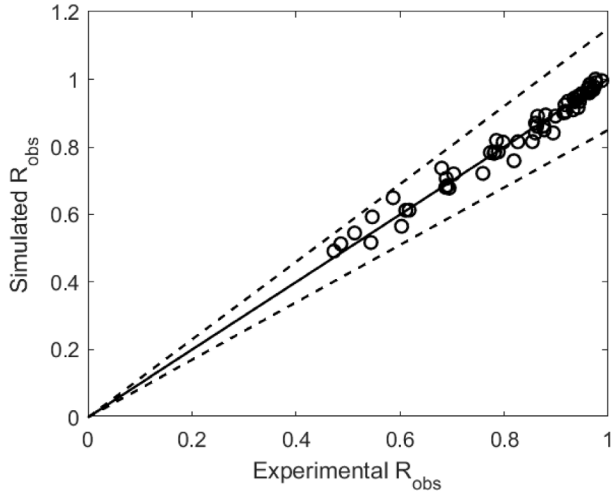

Fig. 17. Parity plot for observed rejections (Hybrid model 2). Dashed lines indicate ± 15%.

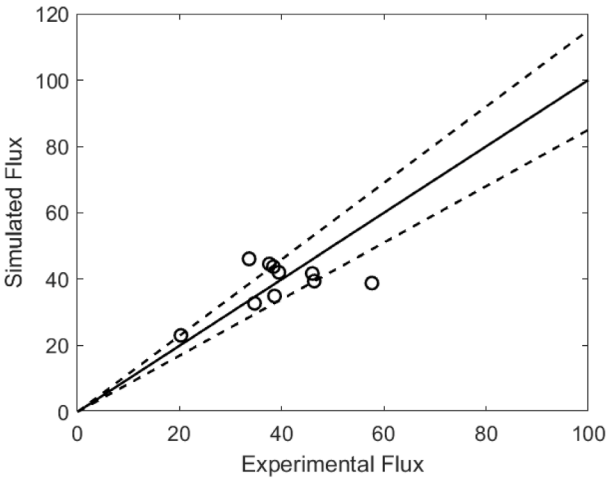

Fig. 16. Parity plot for fluxes (Hybrid model 2). Dashed lines indicate ± 15%.

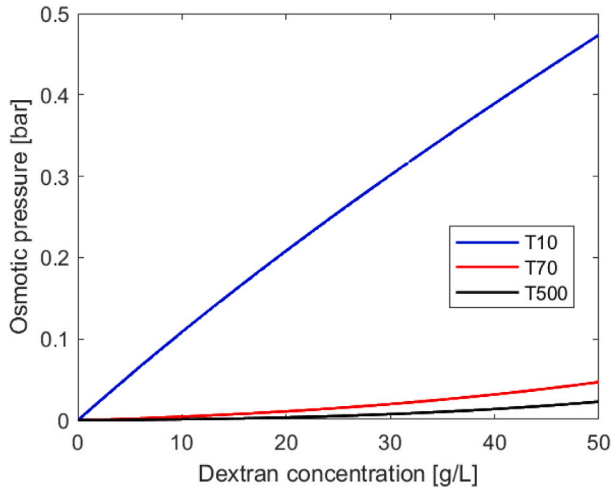

Fig. 18. Osmotic pressure for different dextrans: T500, T70 and T10 versus dextran concentration [43,44].

statistically different from zero, so they all contribute to the predictive capability of the hybrid model 2.

In Figs. 16 and 17 a parity plot for flux and observed rejection are plotted, respectively. The dots in Fig. 17 are more distributed over the 45° line indicating a better prediction for the hybrid model 2 compared to the hybrid model 1. The dots in Fig. 16 seem to be unchanged or the change was imperceptible. It points out that the black box model used to structure the intrinsic rejection in hybrid model 2 only influences the observed rejections and not the fluxes.

Considering that the maximum concentration on the membrane surface, predicted with the hybrid model 2, is almost 30 g/L (Fig. 23), the osmotic pressure for dextran T500 is negligible compared to the operating transmembrane pressure (TMP = 0.85 bar) for dextran concentration between 0 and 30 g/L (Fig. 18). Therefore, the flux variance in model predictions is not caused by osmotic pressures. Indeed, the flux variance predicted by the model is due to the different BS and TBBS values. So, the average flux depends on the duration and frequency of the backshock as longer BS durations imply wasting more permeate. This analysis conflicts with the analysis made in CFD modeling performed by Frank and co-workers [24–28] where it is stated that flux variance in UF of dextran T500 is caused by osmotic pressure. There is a subtlety in their analysis, they state that osmotic pressures do not change significantly with molecular weight and for that reason they used the correlation for the osmotic pressure of dextran T10. Using experimental data from the literature, it can be seen in Fig. 18 that there is a substantial difference between osmotic pressures for dextran T500 and dextran T10, therefore, their properties cannot be treated as if they were the same compound.

In Figs. 19–21, observed rejection are plotted against molecular weight as before. It is evident that the hybrid model 2 has better prediction capabilities than the hybrid model 1 analyzed in the previous section. This better overall performance is confirmed when calculating the adjusted determination coefficient yielding a value of $R^2_{adj} = 0.9626$.

Besides the confidence interval of parameters, the predictor confidence interval was calculated for TBBS = 5 s and BS = 1.25 s and it is illustrated in Fig. 22. Note that experimental data fall inside the predictor confidence interval which is narrower than the corresponding to hybrid model 1 in Fig. 7.

A dynamic simulation for dextran concentration profiles in the boundary layer was made by using the hybrid model 2 with BS = 1.25 s and TBBS = 5 s, because it provides an insight into the phenomena occurring there. This simulation allows to know the maximum concentration achieved on the membrane surface predicted by the model and understand the effect of the dynamic operation on the concentration

Table 6
Estimated parameters and their confidence intervals for the second hybrid model.

Parameter	Value	Confidence interval (at 95% confidence)	Confidence interval (%)
P_1	−0.1888	−0.2214 to −0.1562	±17.27%
P_2	4.9861	4.8085 to 5.1637	±3.56%
P_3	−0.0253	−0.0399 to −0.0106	±58.10%
P_4	0.6129	0.4861 to 0.7398	±20.69%
ϵ_2	0.0125	0.0110 to 0.0141	±12.60%
σ_2	0.6759	0.5629 to 0.7890	±16.73%
L_p L/(m^2 h bar)	56.2211	55.7808 to 56.6614	±0.78%

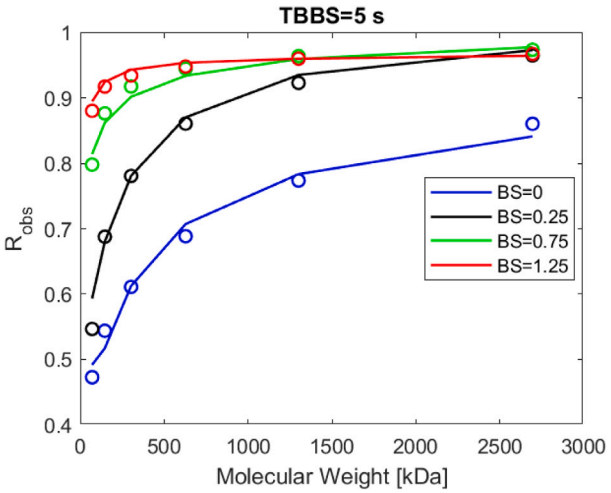

Fig. 19. Experimental and simulated (Hybrid model 2) observed rejection versus molecular weight under TBBS = 5 s for different BS = 0, 0.25, 0.75 and 1.25 s.

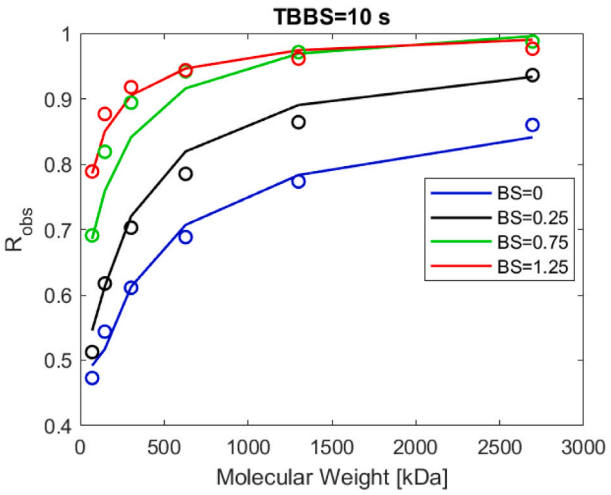

Fig. 20. Experimental and simulated (Hybrid model 2) observed rejection versus molecular weight under TBBS = 10 s for different BS = 0, 0.25, 0.75 and 1.25 s.

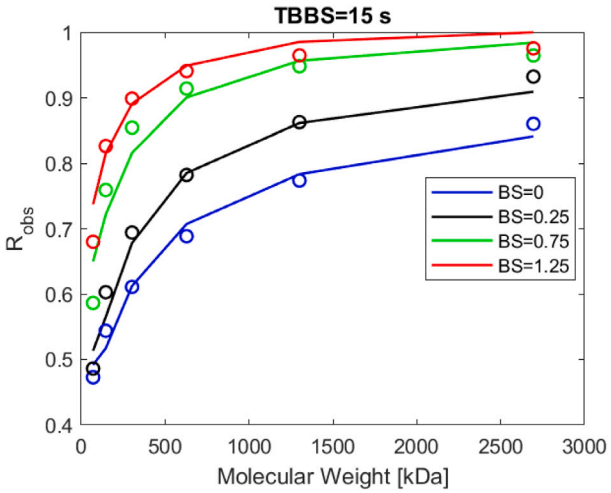

Fig. 21. Experimental and simulated (Hybrid model 2) observed rejection versus molecular weight under TBBS = 15 s for different BS = 0, 0.25, 0.75 and 1.25 s.

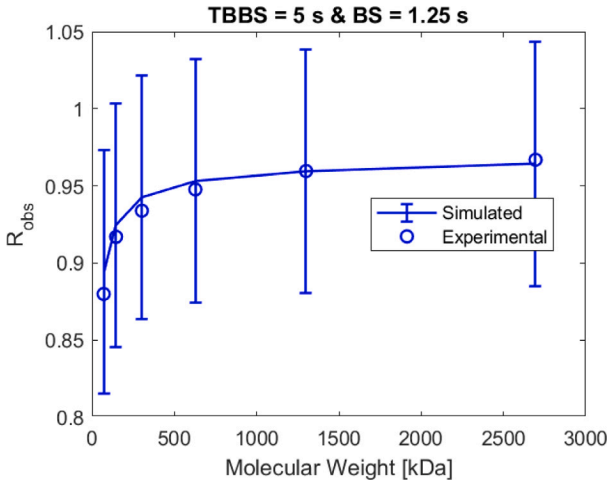

Fig. 22. Predictor confidence interval for hybrid model 2.

profiles over the boundary layer. The results are plotted in Figs. 23 and 24. In Fig. 23 the boundary layer is about 15 μm which is in agreement with the value of 20 μm reported in the literature as a typical number for many applications [14]. It can be observed that dextran concentration at the membrane surface can achieve values of almost 30 g/L (Fig. 23), that is, thirty times the feed concentration. This concentration polarization is mitigated by the backshock system as observed in Fig. 24. For TBBS of 10 and 15 s, this high concentration value is kept a longer time because the backshock is performed at a lower frequency. This result confirms that high dextran concentrations at the membrane surface affect strongly the rejection factors under different operation conditions and that dynamic operation is an efficient method to mitigate concentration polarization as seen before in Figs. 3–5.

Since static operation does not use permeate to wash the membrane and dextran T500 has negligible osmotic pressures for concentrations between 0 and 30 g/L, the hybrid model 2 predicts that the maximum flux corresponds to static operation. This fact leads to consider that the concentration on the membrane surface should achieve values higher than 30 g/L, so more significant osmotic pressures can be obtained and maximum flux can correspond to dynamic operation. In fact, it has been reported dextran concentrations (dextran T70) on the membrane surface as high as 177 g/L with a feed concentration of 0.935 g/L under TMP of 2 bar with no BS [44]. Since diffusivity is the main parameter

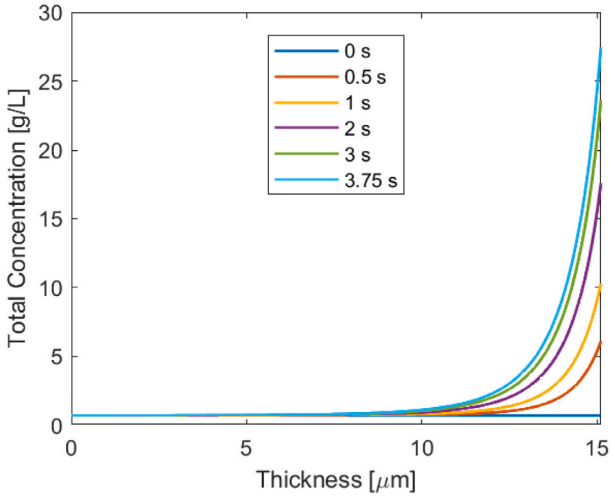

Fig. 23. Total dextran concentration in boundary layer during normal operation at 0, 1, 2, 3, 3.75 s.

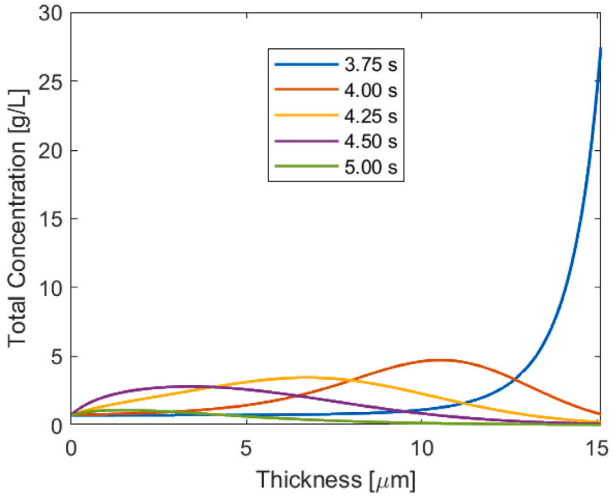

Fig. 24. Total dextran concentration in boundary layer during backshock operation at 3.75, 4, 4.25, 4.5, 5 s.

influencing the maximum concentration that dextran can achieve on the membrane surface, the assumption that dextran diffusivity does not depend on concentration is questionable or perhaps the correlation itself for diffusivity could be no appropriate for this application or maybe there could be extra phenomena not yet included in the model.

Despite the model limitations, it is evident that most of the variance in experimental data is explained by the model with a high degree of precision.

4. Conclusions

Dynamic operation in ultrafiltration, by means of a backshock, have a tremendous effect on the MWCO where it can be tuned from 3380 kDa to values between 46 and 197 kDa, corresponding to a separation intensification in factors of 74 and 17 times, respectively. Two hybrid models were developed with different degrees of hybridization. The first achieved an adjusted determination coefficient of 0.9185 while the second 0.9626. This indicates that the modifications introduced into the second hybrid model allow increasing the prediction power significantly.

The results of the present investigation reinforce that separation performance not only depends on the physical properties of the membrane and solute but it can also be directly manipulated by means of dynamic operation. The idea that operating conditions can modify the MWCO of a membrane has been recently mentioned in the literature but it is not very popularized, so it is necessary that this novel paradigm of separation performance in UF and MF must be spread out in membrane sciences since its applications allow intensifying the UF and MF processes.

The development of hybrid mathematical models for dynamic UF done in this paper opens new opportunities for optimization of process design and operation. Additionally, both hybrid models can be used to provide further process insights and can serve as building blocks for developing models including more phenomena beyond concentration polarization. By using the models developed here as building blocks, future research work could include precipitation, gel formation and fouling.

CRediT authorship contribution statement

Luis Humberto López-Murillo: Experimental data treatment, Development of hybrid models, Parameter estimation, Analysis, Writing. **Víctor Hugo Grisales-Díaz:** Black box modeling, Methodology. **Manuel Pinelo:** Supervision of experiments. **Oscar Andrés Prado-Rubio:** Conceptualization, Methodology, Experimental data, Experimental data treatment, Analysis, Wording correction.

Declaration of competing interest

The authors declare that they have no known competing financial interests or personal relationships that could have appeared to influence the work reported in this paper.

Acknowledgment

This work was supported by the Universidad Nacional de Colombia (Resolución C de 073 de 2018).

References

[1] H. Byhlin, A.-S. Jönsson, Influence of adsorption and concentration polarisation on membrane performance during ultrafiltration of a non-ionic surfactant, Desalination 151 (1) (2003) 21–31, http://dx.doi.org/10.1016/S0011-9164(02)00969-4.

[2] A.-S. Jönsson, B. Jönsson, H. Byhlin, A concentration polarization model for the ultrafiltration of nonionic surfactants, J. Colloid Interface Sci. 304 (1) (2006) 191–199, http://dx.doi.org/10.1016/j.jcis.2006.08.030.

[3] S.P. Verma, B. Sarkar, Rhamnolipid based micellar-enhanced ultrafiltration for simultaneous removal of Cd(II) and phenolic compound from wastewater, Chem. Eng. J. 319 (2017) 131–142, http://dx.doi.org/10.1016/j.cej.2017.03.009.

[4] S.P. Verma, B. Sarkar, Simultaneous removal of Cd (II) and p-cresol from wastewater by micellar-enhanced ultrafiltration using rhamnolipid: Flux decline, adsorption kinetics and isotherm studies, J. Environ. Manag. 213 (2018) 217–235, http://dx.doi.org/10.1016/j.jenvman.2018.02.069.

[5] M. Chen, K. Shafer-Peltier, S.J. Randtke, E. Peltier, Modeling arsenic (V) removal from water by micellar enhanced ultrafiltration in the presence of competing anions, Chemosphere 213 (2018) 285–294, http://dx.doi.org/10.1016/j.chemosphere.2018.09.046.

[6] M. Grzegorzek, K. Majewska-Nowak, The use of micellar-enhanced ultrafiltration (MEUF) for fluoride removal from aqueous solutions, Sep. Purif. Technol. 195 (2018) 1–11, http://dx.doi.org/10.1016/j.seppur.2017.11.022.

[7] L. Shi, J. Huang, L. Zhu, Y. Shi, K. Yi, X. Li, Role of concentration polarization in cross flow micellar enhanced ultrafiltration of cadmium with low surfactant concentration, Chemosphere 237 (2019) 124859, http://dx.doi.org/10.1016/j.chemosphere.2019.124859.

[8] Y. Neggaz, M.L. Vargas, A.O. Dris, F. Riera, R. Alvarez, A combination of serial resistances and concentration polarization models along the membrane in ultrafiltration of pectin and albumin solutions, Sep. Purif. Technol. 54 (1) (2007) 18–27, http://dx.doi.org/10.1016/j.seppur.2006.08.017.

[9] A. Macedo, E. Duarte, M. Pinho, The role of concentration polarization in ultrafiltration of ovine cheese whey, J. Memb. Sci. 381 (1–2) (2011) 34–40, http://dx.doi.org/10.1016/j.memsci.2011.07.012.

[10] S. Zaidi, A. Kumar, Experimental studies in the dead-end ultrafiltration of dextran: analysis of concentration polarization, Sep. Purif. Technol. 36 (2) (2004) 115–130, http://dx.doi.org/10.1016/S1383-5866(03)00207-7.
[11] B. Kwon, J. Molek, A. Zydney, Ultrafiltration of PEGylated proteins: Fouling and concentration polarization effects, J. Memb. Sci. 319 (1–2) (2008) 206–213, http://dx.doi.org/10.1016/j.memsci.2008.03.035.
[12] Y. Pu, Q. Zou, L. Liu, Z. Han, X. Wang, Q. Wang, S. Chen, Clinical dextran purified by fractional ultrafiltration coupled with water washing, Carbohydr. Polym. 87 (2) (2012) 1257–1260, http://dx.doi.org/10.1016/j.carbpol.2011.09.006.
[13] K.-V. Peinemann, S.P. Nunes, Membranes for Water Treatment, John Wiley & Sons, 2010.
[14] R.W. Baker, Membrane Technology and Applications, third ed., John Wiley & Sons, 2012, www.wiley.com.
[15] M.B. Saltık, L. Özkan, M. Jacobs, A. van der Padt, Dynamic modeling of ultrafiltration membranes for whey separation processes, Comput. Chem. Eng. 99 (2017) 280–295, http://dx.doi.org/10.1016/j.compchemeng.2017.01.035.
[16] H. Chen, A.S. Kim, Prediction of permeate flux decline in crossflow membrane filtration of colloidal suspension: a radial basis function neural network approach, Desalination 192 (1–3) (2006) 415–428, http://dx.doi.org/10.1016/j.desal.2005.07.045.
[17] C.R. Azevedo, V.G. Díaz, O.A. Prado-Rubio, M.J. Willis, V. Préat, R. Oliveira, M. Stosch, Hybrid semiparametric modeling: A modular process systems engineering approach for the integration of available knowledge sources, in: Syst. Eng. Fourth Ind. Revolut., (January 2020) Wiley, 2019, pp. 345–373, http://dx.doi.org/10.1002/9781119513957.ch14.
[18] N. Krishnakumar, M. Yea, M. Cheryan, Ultrafiltration of soy protein concentrate: performance and modelling of spiral and tubular polymeric modules, J. Memb. Sci. 244 (1–2) (2004) 235–242, http://dx.doi.org/10.1016/j.memsci.2004.06.056.
[19] G.B. Sahoo, C. Ray, Predicting flux decline in crossflow membranes using artificial neural networks and genetic algorithms, J. Memb. Sci. 283 (1–2) (2006) 147–157, http://dx.doi.org/10.1016/j.memsci.2006.06.019.
[20] K.W. Yee, D.E. Wiley, J. Bao, A unified model of the time dependence of flux decline for the long-term ultrafiltration of whey, J. Memb. Sci. 332 (1–2) (2009) 69–80, http://dx.doi.org/10.1016/j.memsci.2009.01.041.
[21] C.M. Chew, M. Aroua, M. Hussain, A practical hybrid modelling approach for the prediction of potential fouling parameters in ultrafiltration membrane water treatment plant, J. Ind. Eng. Chem. 45 (2017) 145–155, http://dx.doi.org/10.1016/j.jiec.2016.09.017.
[22] O.A. Prado-Rubio, M. von Stosch, Towards sustainable flux determination for dynamic ultrafiltration through multivariable system identification, in: 27th Eur. Symp. Comput. Aided Process Eng., vol. 3, 2017, pp. 2719–2724, http://dx.doi.org/10.1016/B978-0-444-63965-3.50455-4.
[23] V.H. Grisales Díaz, O.A. Prado-Rubio, M.J. Willis, M. von Stosch, Dynamic hybrid model for ultrafiltration membrane processes, 2017, pp. 193–198, http://dx.doi.org/10.1016/B978-0-444-63965-3.50034-9.
[24] F. Vinther, M. Pinelo, M. Brøns, G. Jonsson, A.S. Meyer, Mathematical modelling of dextran filtration through hollow fibre membranes, Sep. Purif. Technol. 125 (2014) 21–36, http://dx.doi.org/10.1016/j.seppur.2014.01.034.
[25] F. Vinther, M. Pinelo, M. Brøns, G. Jonsson, A.S. Meyer, Predicting optimal back-shock times in ultrafiltration hollow fibre modules through path-lines, J. Memb. Sci. 470 (2014) 275–293, http://dx.doi.org/10.1016/j.memsci.2014.07.031.
[26] F. Vinther, M. Pinelo, M. Brø ns, G. Jonsson, A.S. Meyer, Predicting optimal back-shock times in ultrafiltration hollow fiber modules II: Effect of inlet flow and concentration dependent viscosity, J. Memb. Sci. 493 (2015) 486–495, http://dx.doi.org/10.1016/j.memsci.2015.06.029.
[27] F. Vinther, A.-S. Jönsson, Modelling of optimal back-shock frequency in hollow fibre ultrafiltration membranes I: Computational fluid dynamics, J. Memb. Sci. 506 (2016) 130–136, http://dx.doi.org/10.1016/j.memsci.2015.12.061.
[28] F. Vinther, A.-S. Jönsson, Modelling of optimal back-shock frequency in hollow-fibre ultrafiltration membranes II: Semi-analytical mathematical model, J. Memb. Sci. 506 (2016) 137–143, http://dx.doi.org/10.1016/j.memsci.2016.01.040.
[29] Y. Gao, J. Qin, Z. Wang, S.W. Østerhus, Backpulsing technology applied in MF and UF processes for membrane fouling mitigation: A review, J. Memb. Sci. 587 (2019) 117136, http://dx.doi.org/10.1016/j.memsci.2019.05.060.
[30] A.I. Stankiewicz, J.A. Moulijn, Process intensification: transforming chemical engineering, Chem. Eng. Prog. 96 (1) (2000) 22–34.
[31] P. Srijaroonrat, E. Julien, Y. Aurelle, Unstable secondary oil/water emulsion treatment using ultrafiltration: fouling control by backflushing, J. Memb. Sci. 159 (1–2) (1999) 11–20, http://dx.doi.org/10.1016/S0376-7388(99)00044-7.
[32] A. Salladini, M. Prisciandaro, D. Barba, Ultrafiltration of biologically treated wastewater by using backflushing, Desalination 207 (1–3) (2007) 24–34, http://dx.doi.org/10.1016/j.desal.2006.02.078.
[33] M. Bakhshayeshi, H. Zhou, C. Olsen, W. Yuan, A.L. Zydney, Understanding dextran retention data for hollow fiber ultrafiltration membranes, J. Memb. Sci. 385–386 (2011) 243–250, http://dx.doi.org/10.1016/j.memsci.2011.09.047.
[34] E.E. Borujeni, Y. Li, A.L. Zydney, Application of periodic backpulsing to reduce membrane fouling during ultrafiltration of plasmid DNA, J. Memb. Sci. 473 (2015) 102–108, http://dx.doi.org/10.1016/j.memsci.2014.08.059.
[35] I.P. Rosinha, High frequency backshock effect on ultrafiltration of selected polysaccharides (Master thesis), Universidade Técnica de Lisboa & Technical University of Denmark, 2011, p. 148.
[36] M. Bakhshayeshi, D.M. Kanani, A. Mehta, R. van Reis, R. Kuriyel, N. Jackson, A.L. Zydney, Dextran sieving test for characterization of virus filtration membranes, J. Memb. Sci. 379 (1–2) (2011) 239–248, http://dx.doi.org/10.1016/j.memsci.2011.05.067.
[37] E.-H. Song, J. Shang, D. Ratner, Polysaccharides, in: Polym. Sci. a Compr. Ref., Elsevier, 2012, pp. 137–155, http://dx.doi.org/10.1016/B978-0-444-53349-4.00246-6.
[38] V.M. Gaspar, A.F. Moreira, D. de Melo-Diogo, E.C. Costa, J.a.A. Queiroz, F. Sousa, C. Pichon, I.J. Correia, Multifunctional nanocarriers for codelivery of nucleic acids and chemotherapeutics to cancer cells, in: Nanobiomaterials Med. Imaging, Elsevier, 2016, pp. 163–207, http://dx.doi.org/10.1016/B978-0-323-41736-5.00006-6.
[39] P. Zarrintaj, M.R. Saeb, S.H. Jafari, M. Mozafari, Application of compatibilized polymer blends in biomedical fields, in: Compat. Polym. Blends, Elsevier, 2020, pp. 511–537, http://dx.doi.org/10.1016/B978-0-12-816006-0.00018-9.
[40] A.M. Basedow, K.H. Ebert, Production, characterization, and solution properties of dextran fractions of narrow molecular weight distributions, J. Polym. Sci. Polym. Symp. 66 (1) (1979) 101–115, http://dx.doi.org/10.1002/polc.5070660113.
[41] G. Tkacik, S. Michaels, A rejection profile test for ultrafiltration membranes & devices, Bio/Technology 9 (10) (1991) 941–946, http://dx.doi.org/10.1038/nbt1091-941.
[42] A.L. Zydney, A. Xenopoulos, Improving dextran tests for ultrafiltration membranes: Effect of device format, J. Memb. Sci. 291 (1–2) (2007) 180–190, http://dx.doi.org/10.1016/j.memsci.2007.01.006.
[43] G. Jonsson, Boundary layer phenomena during ultrafiltration of dextran and whey protein solutions, Desalination 51 (1) (1984) 61–77, http://dx.doi.org/10.1016/0011-9164(84)85053-5.
[44] J. Wijmans, S. Nakao, J. Van Den Berg, F. Troelstra, C. Smolders, Hydrodynamic resistance of concentration polarization boundary layers in ultrafiltration, J. Memb. Sci. 22 (1) (1985) 117–135, http://dx.doi.org/10.1016/S0376-7388(00)80534-7.
[45] R.B. Bird, W.E. Stewart, E.N. Lightfoot, Transport Phenomena, 2nd, Wiley, J. Wiley, 2002.
[46] K. Scott, Handbook of Industrial Membranes, first ed., Elsevier Science, 1996.
[47] G. Jonsson, Overview of theories for water and solute transport in9 UF/RO membranes, Desalination 35 (1980) 21–38, http://dx.doi.org/10.1016/S0011-9164(00)88602-6.
[48] S.R. Wickramasinghe, S.E. Bower, Z. Chen, A. Mukherjee, S.M. Husson, Relating the pore size distribution of ultrafiltration membranes to dextran rejection, J. Memb. Sci. 340 (1–2) (2009) 1–8, http://dx.doi.org/10.1016/j.memsci.2009.04.056.
[49] G. Jonsson, Tuning of the cut-off curves by dynamic ultrafiltration, in: Proc. Int. Conf. Membr. Membr. Process. ICOM2008, Hawaii, 2008.
[50] G. Grznárová, M. Viktorin, A. Lang, Characterization of virus retentive membranes by a tailor-made dextran method, Desalination 200 (1–3) (2006) 297–298, http://dx.doi.org/10.1016/j.desal.2006.03.331.
[51] C.J. Yehl, A.L. Zydney, Characterization of dextran transport and molecular weight cutoff (MWCO) of large pore size hollow fiber ultrafiltration membranes, J. Memb. Sci. 622 (2021) 119025, http://dx.doi.org/10.1016/j.memsci.2020.119025.
[52] V. García-Molina, S. Esplugas, T. Wintgens, T. Melin, Ultrafiltration of aqueous solutions containing dextran, Desalination 188 (1–3) (2006) 217–227, http://dx.doi.org/10.1016/j.desal.2005.04.120.